Fundulus grandis otolith microchemistry as a metric of estuarine discrimination and environmental conditions in the northern Gulf of Mexico

By

Thomas Reid Nelson

A thesis submitted to the Graduate Faculty of
Auburn University in partial fulfillment of the requirements for the Degree of
Master of Science

Auburn Alabama
August 2, 2014

Copyright 2014 by Thomas Reid Nelson

Approved By

Dennis DeVries, Co-chair, Professor of Fisheries
Russell Wright, Co-chair, Associate Professor of Fisheries
Ash Bullard, Member, Associate Professor of Fisheries
Joel Gagnon, Member, Associate Professor of Earth and Environmental Sciences

Abstract

The Gulf Killifish *Fundulus grandis* is an important component of saltmarsh ecosystems and is an ideal choice as an indicator species for environmental changes, given that it remains near the same marsh throughout its life. Also, their otoliths may provide a record of environmental conditions experienced by a given fish, because they are metabolically inert, grow continuously with fish growth, and incorporate trace elements from the environment. In this study, I used laser ablation inductively coupled plasma mass spectrometry (LA-ICPMS) to asses whether the otoliths of *F. grandis* along the N. Gulf of Mexico coast that were exposed to oil as a result of the 2010 Deepwater Horizon oil spill and as a result of being in close proximity to an oil refinery, contained trace elemental markers that could be attributed to oil exposure. Paired oiled and non-oiled sites did not differ in trace metals shown to be associated with oil. However, concentrations of Mn^{55}, Sr^{86}, Sr^{88}, and Ba^{137} varied among sites and allowed for discrimination of estuaries in Louisiana and the west side of Mobile Bay Alabama from other regions when sites were combined. Sites in Mississippi, Florida, and the east side of Alabama were unable to be separated from one another, given that concentrations of these three elements and two Sr isotopes were similar among these regions. Mn^{55} was indicative of Alabama sites on the west side of Mobile Bay, especially the Fowl River site, and Ba^{137} was shown to be an effective marker for *F. grandis* collected from Louisiana. Salinity and temperature also had significant effects on Sr and Ba incorporation into otoliths.

Acknowledgements

I would like to thank all of the people who helped me in the field collecting these fish, Adrian Stanfill, Emily DeVries, Brooke Merrill, Carl Klimah, Jenny Herbig, Danielle Horn, Jay Foster, and Kyle Gallagher, without their help fish collections would have been impossible. Special thanks go to Tammy DeVries for spending countless hours pulling miniscule otoliths out of Killifish, and having to deal with strong H_2O_2 for cleaning purposes. I would also like to thank Ash Bullard for help with sampling design and methods of collection for Gulf Killifish. I would like to thank Mohamed Shaheen and Joel Gagnon for all of the help with the LA-ICPMS and being readily available to answer my numerous questions regarding all of the chemical aspects of this project. My two advisors Dennis DeVries and Russell Wright deserve special thanks for allowing me the freedom to develop a project beyond the scope of originally proposed work and to explore some of my own ideas. I would also like to thank them for all of the guidance and help along the way especially when obstacles were encountered.

Formatting and Software

Thesis formatted following journal guidelines for Estuaries and Coasts.

Statistical Analyses were performed using R version 3.0.3 (2014-03-06) coupled with R-Studio, and SAS 9.3.

Figures were generated in R version 3.0.3 and Sigmaplot 12.0.

Table of Contents

Abstract ii

Acknowledgments iii

Formatting and Software iv

List of Tables viii

List of Figures ix

Introduction 1

Methods 5

Field Collection 5

Lab Processing 6

Otolith Microchemistry 7

Limits of Detection 8

Standardization 9

Water Chemistry 10

Statistical Analysis 11

Sample Data Contamination 11

Whole Otolith Analysis 13

Otolith Edge and Core Analysis 14

Salinity and Temperature 15

Water Chemical Analysis 15

Relative Condition 16

Results 17
Field Collection 17
Detectable Isotopes 18
Whole Otolith Analysis 18
Whole Otolith Comparisons 18
Discrimination Among Sites and Regions 21
Otolith Edge and Core Analysis 22
Core Verses Edge 22
Core Comparisons 23
Edge Comparisons 25
Salinity and Temperature 26
Isotope Correlation with Salinity and Temperature 27
Water Chemistry 28
Variation Among Sites and Seasons 28
Correlation with Salinity and Temperature 29
Otolith and Water Correlation 30
Relative Condition 31
Discussion 32
Oil Indicators 32
Differences Among Sites 33
Salinity and Temperature Effects on Otoliths 38
Conclusions 43
Literature Cited 45
Tables 52

Figures.....64

List of Tables

Table 1.....52

Table 2.....53

Table 3.....54

Table 4.....55

Table 5.....56

Table 6.....57

Table 7.....58

Table 8.....59

Table 9.....60

Table 10.....61

Table 11.....62

Table 12.....63

List of Figures

Figure 1. Sample sites in the northern Gulf of Mexico. Boxes on the map at the top of the figure correspond to sample areas that are indicated by numbers below the boxes. Enlarged panels of each sample area are shown and denoted with the corresponding number and name of the area in the bottom right of each panel. Within each panel sites are labeled and denoted with an oiled or non-oiled symbol. 64

Figure 2. Mean (± 1 SE) *F. grandis* length collected during each season; bars with different letters indicate significant differences among seasons based on Tukey pairwise comparisons (A) and mean *F. grandis* length collected at each site during each season (B). Lines connecting points in panel B help to visualize patterns and separate seasons. They do not depict a linear relationship between sites 65

Figure 3. Mean whole otolith Sr^{86} concentrations (ppm) as a function of mean Sr^{88} concentrations (ppm). Notice that all points are not on top of one another and do not cluster on the 1 to 1 line, indicating that these two isotopes of Sr do not show an exact correlation with one another 66

Figure 4. Mean (± 1 SE) whole otolith Mn^{55} concentrations (ppm) across sites, where bars with different letters indicate significant differences among sites based on Tukey pairwise comparisons (A). Mean whole otolith Mn^{55} concentrations across sites by season, where letters beside season in the legend correspond to significant differences among seasons, based on Tukey pairwise comparisons (B). Mean whole otolith Mn^{55} concentrations across sites by fish length class (C) and across fish length classes by season (D). Lines connecting points in panels B-D help to visualize patterns and separate seasons and lengths; they do not depict relationships between sites or length classes 67

Figure 5. Mean (± 1 SE) whole otolith Fe^{57} concentrations (ppm) across sites, where bars with different letters indicate significant differences among sites based on Tukey pairwise comparisons (A). Mean whole otolith Fe^{57} concentrations across sites by seasons, where letters beside season in the legend correspond to significant differences among seasons based on Tukey pairwise comparisons (B). Mean whole otolith Fe^{57} concentrations across fish length classes for each season (C). Lines connecting points in panels B-C help to visualize patterns and separate seasons; they do not depict relationships between sites or length classes 68

Figure 6. Mean (± 1 SE) whole otolith Rb^{85} concentrations (ppm) across sites, where bars with different letters indicate significant differences among sites based on Tukey pairwise comparisons (A). Mean whole otolith Rb^{85} concentrations across sites by seasons, where letters beside season in the legend correspond to significant differences among seasons based on Tukey pairwise comparisons (B). Lines connecting points in panel B help to visualize patterns and separate seasons; they do not depict relationships between sites.....69

Figure 7. Mean (± 1 SE) whole otolith Sr^{86} concentrations (ppm) across sites, where bars with different letters indicate significant differences among sites based on Tukey pairwise comparisons (A). Mean whole otolith Sr^{86} concentrations across sites by seasons, where letters beside season in the legend correspond to significant differences among seasons based on Tukey pairwise comparisons (B). Mean whole otolith Sr^{86} concentrations across sites for each fish length class (C) and across fish length classes for each season (D). Lines connecting points in panels B-D help to visualize patterns and separate seasons and lengths; they do not depict relationships between sites or length classes 70

Figure 8. Mean (± 1 SE) whole otolith Sr^{88} concentrations (ppm) across sites, where bars with different letters indicate significant differences among sites based on Tukey pairwise comparisons (A). Mean whole otolith Sr^{88} concentrations across sites by seasons, where letters beside season in the legend correspond to significant differences among seasons based on Tukey pairwise comparisons (B). Mean whole otolith Sr^{88} concentrations across sites for each fish length class (C) and across fish length classes for each season (D). Lines connecting points in panels B-D help to visualize patterns and separate seasons and lengths; they do not depict relationships between sites or length classes 71

Figure 9. Mean (± 1 SE) whole otolith Ba^{137} concentrations (ppm) across sites, where bars with different letters indicate significant differences among sites based on Tukey pairwise comparisons (A). Mean whole otolith Ba^{137} concentrations across sites by seasons, where letters beside season in the legend correspond to significant differences among seasons (B). Mean whole otolith Ba^{137} concentrations across fish length classes for each season (C). Lines connecting points in panels B-C help to visualize patterns and separate seasons and lengths; they do not depict relationships between sites or length classes.....72

Figure 10. Mean (± 1 SE) whole otolith Pb^{208} concentrations (ppm) across sites (A) and mean of whole otolith Pb^{208} across sites for each fish length class (B). Mean whole otolith Pb^{208} concentrations across fish length classes for each season where letters beside seasons in the legend correspond to significant differences among seasons based on Tukey pairwise comparisons (C). Lines connecting points in panels B-C help to visualize patterns and separate seasons and length classes; they do not depict relationships between sites or length classes..73

Figure 11. Mean (± 1 SE) whole otolith U^{238} concentrations (ppm) across sites, where bars with different letters indicate significant differences among sites based on Tukey pairwise comparisons (A). Mean whole otolith U^{238} concentrations across sites by seasons, where letters beside season in the legend correspond to significant differences among seasons based on Tukey pairwise comparisons (B). Lines connecting points in panel B help to visualize patterns and separate seasons; they do not depict relationships between sites.....74

Figure 12. Hierarchical clustering of individual sites, where the y-axis is distance between clusters based on Ward's method of clustering 75

Figure 13. Mean (± 1 SE) otolith region (i.e., core and edge) Mn^{55} concentrations (ppm) across sites (A) and seasons (B) 76

Figure 14. An example from each site of an individual sample Mn^{55} concentration (ppm) for the entire otolith ablation from edge to edge, with the core marked by the arrow on each plot....77

Figure 15. Mean (± 1 SE) otolith region (i.e., core and edge) Fe^{57} concentrations (ppm) across seasons.....78

Figure 16. Mean (± 1 SE) otolith region (i.e., core and edge) Cu^{63} concentrations (ppm) across seasons.....79

Figure 17. An example from each site of an individual sample Cu^{63} concentration (ppm) for the entire otolith ablation from edge to edge, with the core marked by the arrow on each plot....80

Figure 18. Mean (± 1 SE) otolith region (i.e., core and edge) Sn^{118} concentrations (ppm) across seasons.....81

Figure 19. Mean (± 1 SE) otolith region (i.e., core and edge) Ba^{137} concentrations (ppm) across sites (A) and seasons (B) 82

Figure 20. Mean (± 1 SE) otolith core Mn^{55} concentrations (ppm) across sites, where letters above bars correspond to significant differences among sites based on Tukey pairwise comparisons.....83

Figure 21. Mean (± 1 SE) otolith core Fe^{57} concentrations (ppm) across sites, where letters above bars correspond to significant differences among sites based on Tukey pairwise comparisons (A). Mean otolith core Fe^{57} concentrations across sites by seasons where letters beside season in the legend correspond to significant differences among seasons based on Tukey pairwise comparisons (B). Lines connecting points in panel B help to visualize patterns and separate seasons; they do not depict relationships between sites.....84

Figure 22. Mean (± 1 SE) otolith core Rb^{85} concentrations (ppm) across seasons, where letters above bars indicate significant differences among seasons based on Tukey pairwise comparisons.....85

Figure 23. Mean (± 1 SE) otolith core Sr^{86} concentrations (ppm) across sites, where letters above bars correspond to significant differences among sites based on Tukey pairwise comparisons (A). Mean otolith core Sr^{86} concentrations across seasons, where letters above bars indicate significant differences among seasons based on Tukey pairwise comparisons (B) 86

Figure 24. Mean (± 1 SE) otolith core Sr^{88} concentrations (ppm) across sites, where letters above bars correspond to significant differences among sites based on Tukey pairwise comparisons (A). Mean otolith core Sr^{88} concentrations across sites by seasons (B). Lines connecting points in panel B help to visualize patterns and separate seasons; they do not depict relationships between sites.....87

Figure 25. Mean (± 1 SE) otolith core Ba^{137} concentrations (ppm) across sites, where letters above bars correspond to significant differences among sites based on Tukey pairwise comparisons (A). Mean otolith core Ba^{137} concentrations across sites by seasons, where letters beside seasons in the legend correspond to significant differences among seasons based on Tukey pairwise comparisons (B). Lines connecting points in panel B help to visualize patterns and separate seasons; they do not depict relationships between sites.....88

Figure 26. Mean (± 1 SE) otolith edge Fe^{57} concentrations (ppm) across sites, where letters above bars correspond to significant differences among sites based on Tukey pairwise comparisons (A). Mean of otolith edge Fe^{57} concentrations across sites by seasons, where letters beside seasons in the legend correspond to significant differences among seasons based on Tukey pairwise comparisons (B). Lines connecting points in panel B help to visualize patterns and separate seasons; they do not depict relationships between sites.....89

Figure 27. Mean (± 1 SE) otolith edge Sr^{86} concentrations (ppm) across sites, where letters above bars correspond to significant differences among sites based on Tukey pairwise comparisons (A). Mean otolith edge Sr^{86} concentrations across sites by seasons, where letters beside seasons in the legend indicate significant differences among seasons based on Tukey pairwise comparisons (B). Lines connecting points in panel B help to visualize patterns and separate seasons; they do not depict relationships between sites.....90

Figure 28. Mean (± 1 SE) otolith edge Sr^{88} concentrations (ppm) across sites, where letters above bars correspond to significant differences among sites based on Tukey pairwise comparisons (A). Mean otolith edge Sr^{88} concentrations across sites by seasons, where letters beside seasons in the legend indicate significant differences among seasons based on Tukey pairwise comparisons (B). Lines connecting points in panel B help to visualize patterns and separate seasons; they do not depict relationships between sites.....91

Figure 29. Mean (± 1 SE) of otolith edge Ba^{137} concentrations (ppm) across sites, where letters above bars correspond to significant differences among sites based on Tukey pairwise comparisons (A). Mean otolith edge Ba^{137} concentrations across sites by seasons, where letters beside seasons in the legend indicate significant differences among seasons based on Tukey pairwise comparisons (B). Lines connecting points in panel B help to visualize patterns and separate seasons; they do not depict relationships between sites.....92

Figure 30. Mean (± 1 SE) salinity (ppt) across sites, where letters above bars correspond to significant differences among sites based on Tukey pairwise comparisons (A) and the salinity observed at each site for each season (B). Lines connecting points in panel B help to visualize patterns and separate seasons; they do not depict relationships between sites 93

Figure 31. Mean (± 1 SE) water temperature across seasons, where letters above bars correspond to significant differences among seasons based on Tukey pairwise comparisons (A) and the temperature observed at each site for seasons (B). Lines connecting points in panel B help to visualize patterns and separate seasons; they do not depict relationships between sites 94

Figure 32. Plot of salinity (ppt) as a function of water temperature (°C) for all sampling events.....95

Figure 33. Elements and Sr isotopes above detection limits > 50% of the time in otolith edges (Mg^{25}, Al^{27}, Mn^{55}, Fe^{57}, Cu^{63}, Zn^{66}, Rb^{85}, Sr^{86}, Sr^{88}, Sn^{118}, Ba^{137}, Pb^{208}) as a function of salinity (ppt) at time of collection. The modeled relationships of Sr^{86} and Ba^{137} concentrations as a function of salinity are shown 96

Figure 34. Elements and Sr isotopes above detection limits > 50% of the time in otolith edges (Mg^{25}, Al^{27}, Mn^{55}, Fe^{57}, Cu^{63}, Zn^{66}, Rb^{85}, Sr^{86}, Sr^{88}, Sn^{118}, Ba^{137}, Pb^{208}) as a function of water temperature (°C) at time of collection. The modeled relationships of Sr^{88} and Ba^{137} concentrations as a function of temperature are shown 97

Figure 35. The relationship of otolith edge Sr^{88} concentrations (ppm) as a function of water temperature (°C) at time of collection across various salinities (ppt) (0, 5, 10, 15, 20, 25) (A). 3-D representation of otolith edge Sr^{88} concentrations as a function of salinity and temperature at time of collection (B). Data for the 3-D representation were smoothed using a running-average with a 0.6 sampling proportion 98

Figure 36. The relationship of otolith edge Ba^{137} concentrations (ppm) as a function of salinity (ppt) at time of collection across various temperatures (°C) (10, 15, 20, 25, 30, 35) (A). 3-D representation of otolith edge Ba^{137} concentrations as a function of salinity and temperature at time of collection (B). Data for the 3-D representation were smoothed using a running-average with a 0.6 sampling proportion 99

Figure 37. Element:Ca ratios of water chemistry samples across sites (A,B,C,E) and seasons (D). Letters above bars indicate significant different among sites (A,B,C,E) and seasons (D) based on Tukey pairwise comparisons.....100

Figure 38. Element:Ca ratios (element mmol mol^{-1} Ca_{water} [Mg mol $mol^{-1}Ca_{water}$]) above detection limits > 50% of the time in water chemical samples (Mg:Ca, Mn:Ca, Fe:Ca, Zn:Ca, Sr:Ca, and Ba:Ca) as a function of salinity (ppt) at time of collection. The modeled relationships of Mg:Ca, Fe:Ca, Sr:Ca, and Ba:Ca concentrations as a function of salinity are shown.....101

Figure 39. Element:Ca ratios (mmol mol^{-1} [Mg mol mol^{-1}]) above detection limits > 50% of the time in water chemical samples (Mg:Ca, Mn:Ca, Fe:Ca, Zn:Ca, Sr:Ca, and Ba:Ca) as a function of water temperature (ppt) at time of collection.....102

Figure 40. Otolith edge element:Ca ratios (µmol mol^{-1}) as a function of water element:Ca ratios (mmol mol^{-1} [Mg:Ca mol mol^{-1}]) for elements that were greater than detection limits in at least 50% of the water samples. The modeled relationship of otolith Sr^{86}:Ca as a function of water Sr:Ca is shown.....103

Figure 41. Otolith edge Sr^{88}:Ca (µmol mol^{-1}) as a function of water temperature at time of collection across various Sr:Ca (mmol mol^{-1}) water concentrations (4, 6, 8, 10).....104

Figure 42. *F. grandis* relative condition (mean [± 1 SE]) across sites, with letters above bars corresponding to significant differences among sites based on results of Tukey pairwise comparisons (A). Mean relative condition across sites by seasons, with letters beside seasons in the legend corresponding to significant differences among seasons based on results of Tukey pairwise comparisons (B) and mean relative condition across fish length classes by seasons (C). Lines connecting points in panels B-C help to visualize patterns and separate seasons and length classes; they do not depict relationships between sites or length classes.....105

Introduction

The Gulf Killifish, *Fundulus grandis* is an important component of saltmarsh ecosystems along the US. Gulf of Mexico coast. This fish is one of the most abundant nekton species found in saltmarshes and provides an important prey resource for many piscivores, including commercially valuable fishes (Rozas and Reed 1993, Rozas and Zimmerman 2000). Studies of toxicology (Weis and Khan 1990, Smith and Weis 1997), movement (Lotrich 1975, Teo and Able 2003b, Skinner et al. 2005), growth (Kneib and Stiven 1978, Teo and Able 2003a), spawning (Kneib and Stiven 1978, Petersen et al. 2010), and environmental impacts (Courtenay et al. 2002, Finley et al. 2009) all have been conducted with the Atlantic killifish, *Fundulus heteroclitus* (Mummichog). A congener to *F. grandis*, *F. heteroclitus*, is similarly an important link in Atlantic coast saltmarsh food web, transferring energy from the marsh surface to the open estuary (Kneib 1986). Compared to the volume of literature available for *F. heteroclitus*, research on *F. grandis* is sparse. These two species are thought to be very similar, sharing a recent ancestry in the family Fundulidae (Whitehead 2010), and they have even been shown to hybridize with one another when ranges overlap (Gonzalez et al. 2009). It is also generally accepted that these fishes share similar life history patterns, movement patterns, and habitat requirements (Kneib and Stiven 1978, Kneib 1986, Rozas and LaSalle 1990, Rozas and Reed 1993, Kneib and Wagner 1994, Whitehead et al. 2012).

Fundulus heteroclitus is an obligate marsh resident that uses the marsh for spawning, to find prey, and for refuge (Kneib and Stiven 1978, Kneib and Wagner 1994). Individuals move within the tidal cycle onto the marsh at high tide to forage and seek refuge from predation, and then back into tidal creeks and deeper refuges as tides recede (Teo and Able 2003b). Although they exhibit these types of tidal movements, they still occupy small home ranges and remain around the same marsh throughout their life (Lotrich 1975, Teo and Able 2003b, Skinner et al.

2005, Able et al. 2006, Able et al. 2012). This marsh residency, along with ubiquitous marsh distribution (Rozas and Reed 1993, Kneib and Wagner 1994) and susceptibility to pollutants (Weis and Khan 1990, Smith et al. 1995, Weis et al. 2001), are cited as reasons why both *F.heteroclitus* and *F. grandis* have been used as indicators of environmental health for marsh ecosystems (Courtenay et al. 2002, Whitehead et al. 2012). Small home ranges have been documented numerous times for *F. heteroclitus* (see above), and just recently for *F. grandis* (Nelson et al. 2014).

Otoliths provide a good structure for assessing many aspects of fish biology because they are present in all teleost fishes, are metabolically inert, grow continuously with the fish providing records of fish growth, and may contain environmental markers (Campana and Neilson 1985, Campana 1999, Campana and Thorrold 2001, Sturrock et al. 2012). Trace elements in surrounding water chemistries (Farrell and Campana 1996, Walther and Thorrold 2006) and diet items (Kennedy et al. 2000, Buckel et al. 2004) can be incorporated into the structure of the otolith usually through substitution with Ca in the $CaCO_3$ aragonite otolith matrix (Doubleday et al. 2014). However, elemental composition of water has been shown to be the major contributor to otolith microchemical signatures (Walther and Thorrold 2006, Doubleday et al. 2013).

Variation in otolith chemistry has been used to answer a variety of questions pertinent to fish ecology in marine, estuarine, and freshwater systems and the numbers of studies using this approach has grown quite rapidly since its introduction. Separation of fish stocks (Campana et al. 2000, Sohn et al. 2005, Niklitschek et al. 2010), retrospective tracking of fish movements (Walther et al. 2011, Albuquerque et al. 2012, Muhlfeld et al. 2012, Farmer et al. 2013), identification and discrimination of estuarine nursery habitat (Thorrold et al. 1998, Gillanders and Kingsford 2003, Vasconcelos et al. 2007, Tanner et al. 2011), and determination of past

environmental conditions experienced by fish (Lowe et al. 2009, 2011, Farmer et al. 2013) have all been achieved using otolith microchemical analysis.

Many studies have found significant differences in otolith microchemical signatures of fishes collected from different areas in estuarine (Vasconcelos et al. 2007, Bradbury et al. 2008, Tanner et al. 2011), marine (Ashford and Jones 2007, Longmore et al. 2010, Ferguson et al. 2011), and freshwater systems (Brazner et al. 2004, Zeigler and Whitledge 2010, Wolff et al. 2012). Open water marine systems can prove to be difficult when trying to identify distinct spatial signatures because of the uniform distributions of elements in offshore waters that can be incorporated into the otolith (Sturrock et al. 2012). Estuarine systems on the other hand have greater environmental variability in water chemistries than open marine areas (Tanner et al. 2011), due to varying amounts of chemical inputs across estuaries (Oros et al. 2007, Reay 2009, Statham 2012, Wang et al. 2012), variable salinity, and variation in fresh water input (Rooker et al. 2004, Lowe et al. 2011).

Variability in salinity can greatly affect strontium concentrations in fish otoliths; more specifically it has been documented that Sr concentrations increase with increasing salinity (Bath et al. 2000, Lowe et al. 2009, Albuquerque et al. 2012), and this relationship occurs because seawater typically has a higher concentration of Sr than freshwater (de Villiers 1999). However, this relationship can be effected by temperature (Martin et al. 2004, Rooker et al. 2004, Reis-Santos et al. 2013), physiological processes (Kalish 1991), and surrounding freshwater concentrations of Sr (Kraus and Secor 2004).

Barium (Ba) is another common element used in otolith studies that has a relationship with salinity, given that the majority of Ba enters estuaries through suspended particulate matter (SPM) in river outflows (Hanor and Chan 1977, Coffey et al. 1997). Therefore, Ba should have a negative relationship with salinity, because as salinity increases the amount of

freshwater contributions should in general decrease. Also saline waters have been shown to have a direct effect on Ba concentrations by causing desorption from water (Coffey et al. 1997). Similarly, salinity has been shown to have a negative relationship with Ba in fish otoliths (Martin and Thorrold 2005, Reis-Santos et al. 2013), although this relationship can be complicated by temperature (Elsdon and Gillanders 2002, Reis-Santos et al. 2013).

Because otolith microchemical signatures may provide a record of environmental conditions experienced throughout the life of a fish, otolith microchemistry can be a useful tool in environmental impact studies. Elements (Na, Mg, Cr, and Sr) found in crude oil from the 2002 *Prestige* oil spill in Northwestern Spain, were incorporated in otoliths of juvenile turbot (*Scophthalmus maximus*), a benthic inshore fish, in the laboratory (Morales-Nin et al. 2007). The *Deepwater Horizon* oil spill (referred to hereafter as DHOS) in the Gulf of Mexico was the largest oil spill in U.S. history (Abbriano et al. 2011) and possibly the largest offshore spill to have ever occurred (Camilli et al. 2010). It released 4 million barrels of Louisiana crude oil into the northern Gulf of Mexico (NGOM) during summer 2010 (Camilli et al. 2010).

Analysis of DHOS oil using ICP-MS found Al, V, Cr, Co, Ni, Cu, Zn, Se, and Sn in the oil, and a lack of heavier metals suggesting that it was lighter than other oils (Grosser et al. 2012). Additionally, Se, Ni, and V have been found in other crude oils and refinery effluents (Miekeley et al. 2005, De Almeida et al. 2009, Ellis et al. 2011). Initial studies on environmental impacts of the DHOS spill suggest that nearshore (Fodrie and Heck 2011, Moody et al. 2013) and offshore fishes (Rooker et al. 2013, Szedlmayer and Mudrak 2014) have been relatively resilient to adverse effects of oiling in the NGOM. However, detection of small genetic differences in Gulf Killifish in Barataria Bay LA, were presumed to be an effect of the DHOS oil (Whitehead et al. 2012).

The objectives of this study were to first determine if oil exposure changed the detectable elemental compositions of *F. grandis* otoliths, which was accomplished by comparing the otoliths of fish collected from paired oiled and un-oiled marshes. Secondly, I determined if the elemental composition of otoliths of *F. grandis* differed across the broader Northern Gulf of Mexico, both on small and large spatial scales. Lastly, using the elemental composition of otolith edges, I determined the effects of salinity, temperature, and water elemental composition on element incorporation into *F. grandis* otoliths.

Methods

Field Collection

Collection of *F. grandis* occurred at a total of 10 sites (Table 1, Figure 1). The amount of DHOS oiling at sites was assessed using the NOAA Environmental Response Management Application (ERMA) (gomex.erma.noaa.gov) and oiled sites were paired with non-oiled ones. Louisiana sites were located in Barataria Bay near Grand Isle, LA and were saltmarshes dominated by *Spartina alterniflora*, interspersed with small tidal creeks. The sites included one that was heavily oiled from the DHOS oil spill (Barataria A, BA) and one that did not receive DHOS oil (Barataria B, BB). Sites in Mississippi were both near Pascagoula and were also dominated by *S. alterniflora*. The refinery site (RF) was a fringing marsh along a dredge ditch adjacent to an oil refinery (likely to have been exposed regularly to non-DHOS oil) and the Crooked Creek site (CK) was a large marsh interspersed with shallow tidal creeks, adjacent to a deep tidal creek in the Grand Bay National Wildlife Refuge (and not regularly exposed to oil). Three sites were located in Alabama west of Mobile Bay: Fowl B (FB) was a fringing *S. alterniflora* marsh located on a tidal creek on the north shore of Fowl River Bay. Fowl A (FA) was a large *S. alterniflora* marsh that had received light oiling from the DHOS spill located on the

south point of Fowl River Bay interspersed with shallow tidal creeks. The Fowl River (FR) site was located in a *Juncus roemerianus* marsh along a bend in Fowl River and had tidal creeks running throughout it. Two more Alabama sites were located east of Mobile Bay near Orange Beach, AL. Wolf (WF) was located in a large tidal creek in the Wolf Bay watershed and consisted of a *J. roemerianus* marsh fringed with *S. alterniflora*. Perdido (PD) was a *J. roemerianus* marsh with shallow tidal creeks, on a small island situated near the mouth of Perdido Pass and also received light oiling from the DHOS spill. In Florida, Hogtown Bayou (HT) was a shallow tidal creek surrounded by a *J. roemerianus* marsh fringed with *S. alterniflora* on the south shoreline of Hogtown Bayou located near Santa Rosa Beach, FL; this bayou is a part of the larger Choctawhatchee Bay.

Fish were collected in fall 2012, winter 2013, spring 2013, and summer 2013 from all sites using minnow traps baited with cut menhaden (*Brevoortia* sp.). At each site, eight traps were placed in saltmarsh habitat and left for a soak time of 1 – 1.5 hours. All *F. grandis* in traps were euthanized, stored on ice, and returned to the lab. During each fish collection trip temperature and salinity were measured using a YSI 30 model. Water samples (for water chemistry analysis) were collected during the winter, spring, and summer sampling trips. Each water sample was filtered through a 0.45 µm filter, fixed with 125 µL nitric acid, stored in 125 ml acid washed polypropylene bottles, and refrigerated until processing.

Lab Processing

Fish were either processed immediately after returning from the field or were frozen for later processing. Up to twenty *F. grandis* were selected from each site for otolith analysis. These 20 fish consisted of four fish from each of five different size ranges (50-59mm, 60-69mm, 70-79mm, 80-89mm, 90-100+mm), if present. If all size ranges were not represented then the numbers selected were chosen equally from represented classes to reach a total of 20

individuals. Lengths and weights of the selected fish were recorded and their sagittal otoliths were removed. These otoliths were then rinsed in 30% H_20_2 to clean off any residual tissue and stored dry in vials until preparation for microchemistry.

For each fish, one of the sagittal otoliths was prepared for microchemistry analysis. First the otolith was re-washed in 30% H_20_2 and rinsed with triple distilled ultra-filtered water (DIUF). The otolith was then inspected under a dissecting scope to look for remaining tissue; if present, it was removed with forceps and the otolith was rinsed again with DIUF. After cleaning, otoliths were polished until a smooth surface was reached using a range of 3M lapping film (grit size 30 µm to 0.3 µm), working from the coarsest grit to the finest (where the coarsest grit was chosen depending on the size of the otolith). After polishing, otoliths were mounted to petrographic slides using Weldbond glue and stored until microchemical analysis.

Otolith Microchemistry

Otolith microchemical analyses were conducted at the University of Windsor, Great Lakes Institute for Environmental Research (GLIER), Windsor, Canada. Trace element composition of otoliths from *F. grandis* were quantified using a laser ablation inductively-coupled plasma mass spectrometry (LA-ICP-MS) system comprising a high energy, ultrafast femtosecond laser (Integra-C® by Quantronics®, East Setauket, New York;) and a Thermo-Electron® X7-II® ICP-MS. Straight line laser ablations were run from one edge of the otolith to the other through the core. Ablation speed for all otoliths was set at 5 µm/s using a computer controlled stage with a spot size of 20 µm. Ablated material was carried to the ICP-MS using Ar gas. For ablations the laser energy was 27µJ after a 2.5 mm pinhole, the repetition rate was 100Hz, with a pulse width of 130 fs and a 785 nm wavelength. The ICP-MS was operated with 1200 W RF power, a nebulizer gas flow rate of 1.01L/min, coolant gas rate of 14L/min, and a sampling depth of 120 mm. The concentrations (count per second [cps]) of 33 isotopes (Li^7,

Mg^{25}, Al^{27}, Ca^{43}, Ca^{44}, V^{51}, Cr^{53}, Mn^{55}, Fe^{57}, Co^{59}, Ni^{60}, Ni^{62}, Cu^{63}, Zn^{66}, Zn^{67}, Se^{77}, Se^{78}, Rb^{85}, Sr^{86}, Sr^{88}, Y^{89}, Cd^{111}, Sn^{118}, Sn^{120}, Cs^{133}, Ba^{137}, Ba^{138}, La^{139}, Ce^{140}, Pb^{206}, Pb^{207}, Pb^{208}, U^{238}) were quantified, and given the speed of the ablation and the number of elements tested, elemental concentrations were output roughly every 0.4 seconds of the ablation.

Limits of Detection

Two runs of a glass reference standard (National Institute of Standards and Technology [NIST] 610) with known concentrations of isotopes were analyzed both before and after approximately 16 otolith samples. These standard runs allowed me to quantify and correct for instrumental drift, determine the precision (CV) of elemental concentrations, and served as external calibration standards. Estimates of background levels of isotopes in the Ar carrier gas were analyzed for 60 seconds before every otolith analysis, which allowed limits of detection (LODs) to be calculated based on the following formula from Ludsin et al. (2006):

$$\mathrm{LOD} = \frac{3 \cdot \sigma_{\mathrm{bgd}}}{\mathrm{S} \cdot \mathrm{Y}} \cdot \sqrt{\frac{1}{\mathrm{N_{bgd}}} + \frac{1}{\mathrm{N_{pk}}}}$$

where σ_{bgd} equals the standard deviation (SD) of the pre-ablation background determination of isotopes, N_{bgd} and N_{pk} are replicate determinations used in the integration of the background and ablation signal, respectively, S is mean sensitivity (counts/s per unit concentration) for the NIST reference standard, and Y is the ablation yield relative to the NIST reference standard, determined from the measured count rates and known concentrations of the internal standard (Longerich et al. 1996). Based on this formula an isotopes's concentration had to be greater than 3 SDs above background levels to be considered greater than detection limits. If an isotope was greater than the detection limit in at least 50% of my otolith samples then it was included in analysis; if isotopes were below detection limits, a zero was used as the element concentration for that sample in whole otolith average concentrations.

Standardization

In order to correct for differences in mass of ablated material, to convert raw isotope concentrations from cps to ppm, and to adjust isotope concentrations to a ratio with calcium, Ca^{43} was used as an internal standard held constant at 400432 ppm for samples and the published 81830 ppm for the NIST standard (Longerich et al. 1996, Ludsin et al. 2006, Lowe et al. 2011). Counts per second were transformed to ppm using the following equation (Ludden et al. 1995):

$$[C_x]_{samp} = \frac{\left[\frac{CPS_x}{CPS_{Is}}\right]_{samp} \cdot (C_{Is})_{samp} \cdot (C_x)_{std}}{\left[\frac{CPS_x}{CPS_{Is}}\right]_{std} \cdot (C_{Is})_{std}}$$

where C_x is the concentration of the isotope of interest, C_{ls} is the concentration of the internal standard (Ca^{43}), CPS_x is the count per seconds of the element being investigated, and CPS_{ls} is the count per seconds of the internal standard. The subscripts samp and std refer to the sample and the standard (NIST 610) respectively.

Ca^{43} was used instead of Ca^{44} because Ca^{43} was measured on the same scale as all other isotopes during ablation, the digital mode (cps), while Ca^{44} was sometimes measured in a less precise analogue mode. This standardization is appropriate given that calcium carbonate is close to pure composition in minerals (Deer et al. 1962) and otolith composition is also mainly pure calcium carbonate ($CaCO_3$) (Campana 1999, Thresher 1999, Ludsin et al. 2006) with substitutions occurring at a rate of < 1% (Campana 1999). Given this, the stoichiometric equation for amount of Ca in $CaCO_3$, demonstrates that Ca represents 400432.02 ppm (≈ 40%) of otoliths.

$$\frac{\text{Ca } (40.078)}{\text{Ca}(40.078) + \text{C}(12.0107) + \text{O}_3(3 * 15.9994)} = .40043202 = 400432.02\text{ppm}$$

The unit used to report otolith elemental concentrations varies across the literature, with concentrations either being reported in ppm (Ludsin et al. 2006, Ranaldi and Gagnon 2008), µg

g^{-1} (Albuquerque et al. 2012), mmol mol^{-1} (Lowe et al. 2009), or µmol mol^{-1} (Sohn et al. 2005). Given that µg g^{-1} is equivalent to ppm and µmol mol^{-1} can be easily converted to mmol mol^{-1} and easily derived from µg g^{-1} using the following equation (X=isotope):

$$\frac{\text{ppm}(\text{ug g}^{-1})\text{X} \Big/ \text{Mass X(g)}}{1 \Big/ \text{Mass of CaCO}_3(100.0869\text{g})} = \text{µmol mol}^{-1}\text{X},$$

I chose to report otolith elemental concentrations in ppm, except for analyses where water concentrations were compared with otolith concentrations. In this case, otolith concentrations were reported in element:Ca µmol mol-1 for ease of comparisons to other studies.

Water Chemistry

Water samples were analyzed using solution-mode inductively-coupled plasma mass spectrometry (ICPMS), after 100 fold dilution with an internal standard solution of 1% HNO_3 with Be, In, and Tl to correct for matrix and drift effects on an individual sample basis.

Water sample concentrations were output in µg kg^{-1}, which is equivalent to ng g^{-1}. A molar element:Ca ratio for water was derived In order to compare concentrations of elements in water to concentrations in otoliths using the following formulas where X equals element of interest.

$$\frac{\text{ng g}^{-1}\text{X} \Big/ \text{Mass X(g)}}{1 \Big/ \text{Mass H}_2\text{0 (18g)}} = \text{nmol mol}^{-1}\text{X} \Big/ 1000 = \text{µmol mol}^{-1}\text{X} \Big/ 1000 = \text{mmol mol}^{-1}\text{X}$$

$$\frac{\text{ng g}^{-1}\text{Ca} \Big/ \text{Mass Ca}(40.078\text{g})}{1 \Big/ \text{Mass H}_2\text{0 (18g)}} = \text{nmol mol}^{-1}\text{Ca} \Big/ 10^9 = \text{mol Ca}$$

Molar element:Ca ratios in water for Sr, Ba, Mn, Zn, and Fe were reported using the units from the formulas above. Given this, concentrations of these elements in water are reported in

element mmol (with the exception of Mg) for every mol of calcium in water (element:Ca mmol mol^{-1}_{water}). Magnesium (Mg) concentrations were on the same magnitude of Ca concentrations therefore they are reported as mol Mg for every mol of Ca (Mg:Ca mol mol^{-1}_{water}).

Statistical Analysis

Sample Data Contamination

After ablation, subsequent examination and measurement of the ablation tracks indicated that some otoliths were contaminated with residue from the lapping film and this residue had been ablated. This was especially noticeable in samples from Mississippi during the winter collection that were extremely small (approx. 1.3 mm in diameter). This residue was not noticed prior to ablation due to the much lower magnification of the dissecting scope that was used to inspect otoliths after cleaning and polishing, compared with the image analysis system used for otolith measurements. After ablating a sample of the lapping film using the LA-ICPMS, I determined the films were composed primarily of Al, with low concentrations of other elements, causing elevated concentrations of Al where residue was present.

To reduce bias in isotopic concentration due to contamination, the isotopic compositions for the entire ablation were output for every otolith in which the concentration of Al was greater than or equal to 1000 ppm (n=33, with 18 from the winter collection in Mississippi), which is well above the reported 6.36 – 104.07 ppm (Sohn et al. 2005) and 0.0099 - 0.0156 ppm (Geffen et al. 2003) for otolith compositions. The entire abaltion output for these samples was checked and anywhere that Al rose in hump shaped patterns mimicked by other elements and when areas reached well above the rest of the Al levels in the abaltion (>200 ppm above rest of clean areas of ablation) all data in the rows were deleted. After the compromised rows were deleted a new average concentration for each isotope was calculated using the remaining portion of the abaltion and these data were used in the whole otolith analysis. This

ensured that true isotopic concentrations in otoliths were not deleted while data biased by the lapping film were revised. Also the subset of otoliths that were used for the comparisons of otolith cores verses edges, as well as any analysis using the core or edge data, consisted of otoliths without any contamination.

Whole Otolith Analysis

To determine if elemental and isotopic concentrations differed among sites for each isotope that was above LOD at least 50% of the time and to account for collection season and fish length (TL) effects on site differences, a two-way ANOVA with length included as covariate was used. First a full model with all interactions between main effects (i.e., site and season) and length was run and the most parsimonious model was chosen by removing insignificant main effects (except for site) and interactions from the model and re-running until only significant variables remained. If the main effects of season or length were not significant, but an interaction term using one of these effects was, then they were retained in the final model. All ANOVA tests were run using type III sums of squares (Speed et al. 1978, Shaw and Mitchellolds 1993). Final model ANOVAs were tested for normality of the residuals using the Shapiro Wilks test and for homogeneity of variance using Levene's test. If length remained in the final model, than a Levene's test was performed on the model without length, because this test cannot run with a covariate. Although the majority of ANOVAs failed these tests and appropriate data transformations did not help, the ANOVA test is robust to violations in these assumptions and has greater power than the similar non-parametric Kruskal-Wallace, or rank-sum approaches (Brownie and Boos 1994, Kahn and Rayner 2003); as such I continued to use ANOVAs with my data. Tukey HSD tests were run on ANOVA models that showed significant differences between sites and seasons in order to determine which sites and seasons differed from one another.

These Tukey tests were run on pairwise comparisons between variables obtained from the final most parsimonious ANOVA model.

Isotopes that showed significant differences between sites in the Tukey tests were used in a linear discriminant function analysis (LDFA) with leave one out cross validation, to determine if fish could be correctly classified to site of collection (prior probabilities set at 0.1 for each site given the ten sites) and then region of collection (prior probabilities set at 0.25 for each region) based on the otolith chemical signatures. Before LDFA was performed, all chemical data were scaled using z-scores:

$$X_{is} = \frac{X_i - \overline{X}}{SD\ (\overline{X})}$$

Where X_i is the concentration of isotope X for the i^{th} sample, $\overline{X}$ equals the mean of all samples of isotope X, SD $(\overline{X})$ is the standard deviation of the mean and X_{is} equals the scaled concentration of isotope X for the i^{th} sample.

Using the same scaled data from the LDFA, a hierarchical cluster analysis was performed based on a Euclidean distance matrix and Ward's method of cluster classification (Ward 1963, Wishart 1969). This cluster analysis was performed for all sites to see how sites were grouped, and to see if classification of fish to states or some other regional scheme was most appropriate.

Otolith Edge and Core Analysis

To compare elemental and isotopic concentrations in the core verses the edge of otoliths, the incremental output for the ablation was obtained for a subsample of 200 otoliths. This subsample consisted of one fish from each size class (if present) for each site and season (n=50/season, total n=200). If all size classes were not represented in a collection then the 5 fish were chosen from size classes that were present. Given that the LA-ICPMS slide stage moved at a consistent speed of 5μm/s, the ablation time in seconds was converted to μm for each otolith using the following formula:

$$\frac{\text{abaltion time (increments of 402)}}{\text{1000 seconds}} \cdot \frac{\text{5µm}}{\text{1 second}} = \text{ abaltion distance (µm)}$$

where isotope concentrations were output every 0.402 seconds, which resulted in concentration output roughly every 2 µm.

A standard distance of 113 µm was chosen to represent both the edge and core signatures. This value is the distance equal to 10% of the ablation when averaged across all of the smallest fish (50 – 59 mm) in the edge/core subsample. Therefore each edge chemical signature was measured by averaging 113 µm at the end of the ablation, and each core sample was measured by averaging 113 µm, where the center of the core was at 56.5 µm such that there was an equal distance of ablation area on either side of the core. Otolith cores were defined as the small, round opaque section in the center of the otoliths. The center of the core was determined by either recording the ablation time when the laser hit the center of the core during ablation (spring and summer samples), or was measured in µm using an image analysis system (fall and winter samples). If either the core and/or edge average isotopic concentrations were below the LOD determined for the entire ablation, then a zero was used to represent the concentration for that isotpe and region.

Split-plot ANOVA (SP-ANOVA) with individual fish as the whole plot and otolith region as the split plot was performed to see if otolith region (core and edge) chemical signatures differed within otoliths. The interactions of season, site, and length with otolith region, were used in the SP-ANOVA to determine if differences between the core and the edge were consistent across these effects. The most parsimonious model was chosen by removing insignificant ($p > 0.05$) interactions or main effects, with the exception of otolith region and re-running the model until only significant variables remained. If an interaction term was significant and one of the main effects in the interaction term was not, the insignificant main effect was included in the model.

Differences in detectable isotope (>50% LOD) concentrations among sites and seasons at both cores and edges of otoliths were analyzed with two-way ANOVAs. The main effect of site, season, and the interaction of these two terms were used in the first model and if the interaction was significant ($p < 0.05$) then no main effects could be removed and this was the best model. If the interaction was not significant ($p > 0.05$), the remaining significant main effects were used in the final model. If either site or season was shown to be significant then Tukey HSD tests were performed to clarify differences between sites and seasons and the pairwise comparisons were obtained from the best fitting model.

Salinity and Temperature

Differences in salinity and water temperature across sites and seasons were analyzed using a one-way ANOVA. If the site or season ANOVA was significant a Tukey HSD test was used to find differences among sites and/or seasons. Also, to determine if salinity was correlated with water temperature, a linear regression was used. Plots were generated using the average element concentrations from otolith edges to determine if any relationship between isotope concentration, salinity, and/or temperature existed. For plots that suggested concentration relationships with salinity and/or temperature, these relationships were modeled using multiple equations and the best model to describe the relationship was chosen with the lowest Akaike information criterion (AIC).

Water Chemical Analysis

A one-way ANOVA for each site and season was run to compare elemental concentrations in water samples among sites and seasons. If either the site or season ANOVA was significant a Tukey HSD test was used to identify differences between sites and seasons. For an element to be included in water chemistry analysis, it first had to be one of the elements that

met inclusion criteria (above LOD in >50% of samples) in otolith analysis, and it had to be above LOD in >50% of water chemistry samples as well.

To investigate how elemental concentrations for analyzed elements in water were affected by temperature and salinity, plots were first generated to visualize relationships. Elements that visually suggested relationships were modeled and the best model was chosen by selecting the model with the lowest AIC. Relationships between water chemistry and otolith edge isotopic concentrations were investigated using the otolith edge data and elements from water chemistry that met LOD criteria. Plots were generated to visualize relationships between water element concentration and otolith edge isotope concentration and if any relationships were suggested then they were modeled and the best model was chosen by selecting the one with the lowest AIC.

Relative Condition

Relative condition is a useful way to compare populations when a published standard weight equation does not exist (Neumann et al. 2012), as is the case for the Gulf Killifish. In order to calculate relative condition for all fish used in otolith analysis, a regression of the natural log of fish weight (g) versus the natural log of fish length (TL mm) was generated, which resulted in the following model:

$$\ln(W_p) = 3.298(\ln[L]) - 12.419$$

where W_p is the predicted weight for a fish based on the observed length (L). This model was used to generate predicted weights for each fish in the sample and the relative condition for each fish was determined using:

$$W_r = \left(\frac{W}{W_p}\right) \cdot 100$$

in which W_r is the relative condition, W is the observed weight of the fish, and W_p is the predicted weight.

Relative condition was compared across sites, seasons, and lengths using a two-way ANOVA with the main effects of site and season, and the covariate length, as well as the interaction between site and season, site and length, and length and season. Differences between sites and seasons were compared using Tukey pairwise comparisons, obtained from the most parsimonious model, which was chosen by removing insignificant main effects (main effects were only removed if a significant interaction did not include the main effect) and interactions from the model until only significant ones remained.

Results

Field Collections

Gulf Killifish were successfully captured from every sample site during each collection event. It was not always possible to collect 4 fish in each of the 5 size classes (≤59, 60-69, 70-79, 80-89, ≥90 mm) as per design (Table 2). I had 18-20 otoliths from each site on each sample date for OMC analysis, except for winter samples from BB and FR, which had 11 and 13 otoliths respectively. This was due to difficulty in sampling *F. grandis* during this time. This resulted in a final sample size of 773 total otoliths (180-200 per season; Table 2). Fish lengths did not vary across sites (ANOVA: $F_{9,733} = 1.330$, $p = 0.217$), but were significantly smaller in winter than any other season (ANOVA: $F_{3,733} = 5.491$, $p < 0.001$) (Figure 2A). Also the interaction of site and season was significant (ANOVA: $F_{27,733} = 4.069$, $p < 0.001$) (Figure 2B), given that lengths were quite variable across sites in the winter and summer.

Detectable Isotopes

Out of the 33 isotopes used in OMC analysis, 20 (Mg^{25}, Al^{27}, Ca^{43}, Ca^{44}, Mn^{55}, Fe^{57}, Cu^{63}, Zn^{66}, Zn^{67}, Rb^{85}, Sr^{86}, Sr^{88}, Sn^{118}, Sn^{120}, Ba^{137}, Ba^{138}, Pb^{206}, Pb^{207}, Pb^{208}, U^{238}) met the criteria (>50% LOD) to be used in whole otolith comparisons. For elements where more than one isotope met inclusion criteria (Zn, Sr, Sn, Ba, Pb) the isotopes were regressed against one another and if regressions varied too far from the 1:1 slope line (R^2<0.90), then both isotopes were used. Only Sr (R^2 = 0.361) and Zn (R^2 = 0.878) differed from the 1:1 relationship. The number of samples above LOD for Zn^{67} was less than Zn^{66}, which resulted in observations of zero for Zn^{67}, but not Zn^{66} when concentrations were low causing deviation from the 1:1 line. Therefore Zn^{66} was the only Zn isotope used in analysis. The low correlation for the Sr isotopes suggested these isotopes responded differently to external variables, either in concentration or availability. This plot identified two separate clusters of points (Figure 3) so both Sr^{86} and Sr^{88} were used in analysis. Given that Ca was used as an internal standard neither isotope was used for otolith analysis. Therefore 13 isotopes (Table 3) were used for whole otolith comparisons.

Whole Otolith Analysis

Whole Otolith Comparisons

Entire otolith average concentrations of Mn^{55}, Fe^{57}, Rb^{85}, Sr^{86}, Sr^{88}, Ba^{137}, Pb^{208}, and U^{238} differed significantly across sites. Manganese Mn^{55} differed across sites (ANOVA: $F_{9,720} = 8.841$, $p < 0.001$) and collection seasons (ANOVA: $F_{3,720} = 7.995$, $p < 0.001$) but length alone did not have a significant effect (ANOVA: $F_{1,720}$, $p = 0.060$). All three interaction terms were significant for Mn^{55}, site by length (ANOVA: $F_{9,720} = 5.223$, $p < 0.001$), site by season (ANOVA: $F_{27,720} = 3.11$ $p < 0.001$), and length by season (ANOVA: $F_{3,720} = 8.357$ $p < 0.001$). The FR and FA sites had significantly higher mean values of Mn^{55} than other sites, while FB and BB composed the next

highest group. (Table 4, Figure 4A). Despite these statistical interactions, the patterns of Mn^{55} concentrations were consistent across sites (Figure 4 B-D).

Iron (Fe^{57}) differed across sites (ANOVA: $F_{9,729} = 21.812$, $p < 0.001$) and seasons (ANOVA: $F_{3,729} = 9.421$, $p < 0.001$), but length (ANOVA: $F_{1,729} = 3.708$, $p = 0.055$) alone was not related. The interactions of site and season (ANOVA: $F_{27,729} = 18.979$, $p < 0.001$), and season and length (ANOVA: $F_{3,729} = 4.140$, $p = 0.006$) were both significant as well. The FB site had significantly higher mean Fe^{57} concentrations than other sites, with FA having the second highest concentrations. (Table 4, Figure 5A). No clear pattern existed relative to the significant interactions, although concentrations in the fall were lower than other seasons (Table 4, Figure 5B-C).

The Florida site, Hogtown Bayou (HT), had significantly lower mean rubidium concentrations than FB and WF and other sites were similar to one another (ANOVA: $F_{9,733} = 21.812$, $p < 0.001$) (Table 4, Figure 6A). Also, mean Rb whole otolith concentrations were less in the fall than the three other seasons (ANOVA: $F_{3,733} = 9.421$, $p < 0.001$) and the interaction between these two main effects (ANOVA: $F_{27,733}$, $p < 0.001$) was significant (Table 4, Figure 6B).

Mean strontium 86 (Sr^{86}) concentrations differed among sites (ANOVA: $F_{9,720} = 3.425$, $p < 0.001$) and seasons (ANOVA: $F_{3,720} = 41.1627$, $p < 0.001$) being highest in the fall (Table 4, Figure 7 A,B). All interaction terms, site by season (ANOVA: $F_{27,720} = 5.586$, $p < 0.001$), site by length (ANOVA: $F_{9,720} = 2.276$, $p = 0.016$), and season by length (ANOVA: $F_{3,720} = 20.524$, $p < 0.001$) were significant, but the covariate length was not (ANOVA: $F_{1,720} = 0.192$, $p = 0.661$). BB had the lowest mean Sr^{86} out of all sites, followed by BA and FR, which did not differ. CK and PD had the highest mean Sr^{86} concentrations and also did not differ (Table 4, Figure 7A). Although present, significant interactions did not affect overall patterns across sites (Figure 7B-D).

Sr^{88} concentrations also differed among sites (ANOVA: $F_{9,720}$=2.774, p = 0.003) and seasons (ANOVA: $F_{3,720}$ = 49.674, p < 0.001) (Table 4, Figure 8 A, B). Length (ANOVA: $F_{1,720}$ = 0.400, p = 0.527) alone was not significant, but the interactions of site by length (ANOVA: $F_{9,720}$ = 2.045, p = 0.032) and season by length (ANOVA: $F_{3,720}$ = 20.515, p < 0.001) were. The interaction of site and season (ANOVA: $F_{27,720}$ = 8.031, p < 0.001) was also significant. As with Sr^{86}, BB had the lowest mean Sr^{88}concentration followed by BA which did not differ from FR. CK and PD had the highest Sr^{88} concentrations for all sites and they did not differ (Table 4, Figure 8A). Winter samples had a lower mean Sr^{88} concentration than other seasons, fall and spring did not differ, and summer had the highest concentration (Table 4, Figure 8B). Even given the significant interaction terms, the general patterns of concentrations across sites were consistent (Figure 8B - C).

Barium concentrations (Ba^{137}) differed across sites (ANOVA: $F_{9,729}$ = 227.113, p < 0.001) and seasons (ANOVA: $F_{3,729}$ = 39.786, p < 0.001), and were negatively related to fish length (ANOVA: $F_{1,729}$ = 7.595, p = 0.006) (Table 4, Figure 9 A-C). The interactions of site by season (ANOVA: $F_{27,729}$ = 12.417, p < 0.001) and season by length (ANOVA: $F_{3,729}$ = 7.935, p < 0.001) were also both significant. Ba^{137} showed an interesting pattern across sites; concentrations were highest at BB and BA and BB even had a concentration significantly higher than BA. FR had the closest mean concentration to the Louisiana sites and was also higher than all remaining sites (Table 4, Figure 9A). All Ba concentrations generally decreased with fish length across seasons (Table 4, Figure 9B). Also, for the majority of seasons (winter, spring, summer) there was a decrease of Ba concentrations with fish size (Figure 9C).

Although there was a significant effect of site (ANOVA: $F_{9,747}$ = 2.315, p = 0.014) lead (Pb^{208}) concentrations did not differ across sites in pairwise comparisons (Table 4, Figure 10A). Concentrations differed among seasons (ANOVA: $F_{3,747}$ = 6.446, p < 0.001), but not fish length

(ANOVA: $F_{1,747} = 2.563$, $p = 0.110$). The site by length (ANOVA: $F_{9,747} = 2.776$, $p = 0.003$) and season by length interactions (ANOVA: $F_{3,747} = 6.439$, $p < 0.001$) were both significant and driven by one large fish collected in the fall at the HT site (Figure 10B, C).

Uranium (U^{238}) concentrations differed among sites (ANOVA: $F_{9,733} = 2.776$, $p = 0.003$), with BA higher than HT (Table 4, Figure 11A). Fall and winter samples had higher concentrations than spring and summer samples (ANOVA: $F_{3,733} = 7.206$, $p < 0.001$) and the significant site by season interaction (ANOVA: $F_{27,733} = 1.920$, $p = 0.004$) was driven by different patterns across sites during the fall and winter seasons (Table 4, Figure 11B).

Discrimination Among Sites and Regions

I included Mn^{55}, Fe^{57}, Rb^{85}, Sr^{86}, Sr^{88}, Ba^{137}, and U^{238} in the linear discriminant function analysis (LDFA) because the whole otolith concentration of these isotopes differed among sites. This analysis, where each site was used as a group in the function assigned fish to the correct collection sites with a low degree of accuracy. FR had the highest classification percentage (86 %), followed by BB (68 %) and BA (64 %). Also when misclassifications for BB and BA occurred, these two sites were classified as the other most of the time. Classification was poorest at CK (13 %) and HT (14 %) followed by PD, WF, FA, and FB (all around 40%, Table 5). When looking at which isotopes contributed most to the discriminators reasons for site misclassifications become clear, given that the main discriminators were Ba^{137}, Sr^{86}, Sr^{88}, Fe^{57}, and Mn^{55} (decreasing importance respectively, Table 6) and sites that were misclassified to one another had similar concentrations of these isotopes. The hierarchical cluster analysis also had similar results to the LDFA, with BB and BA making a discrete cluster and FR, FA, and FB being grouped together (Figure 12). After these the MS sites, sites on the east side of AL, and FL sites were clustered without geographical distinction.

To look for broader regional patterns that might be related to water chemistry, sites were grouped into four collection regions and another LDFA was performed. These four regions consisted of LA sites (BB, BA) MS sites (RF, CK), AL sites on the west side of Mobile Bay (FB, FA, and FR) and AL sites on the east side of Mobile Bay combined with FL sites (WF, PD, HT). Classification rates for these collection regions were better than for individual sites especially in the LA sampling region (97% classification success, Table 7). The MS and AL east +FL regions were misclassified to each other resulting in the low classification percentages for these groups (46% and 58% respectively) and the AL west grouping (67% successful) was misclassified to both MS and AL east + FL 15% of the time. The main isotopes contributing to discrimination were similar as in the LDFA above with Ba^{137} having the most influence followed by Sr^{86}, Sr^{88}, and Mn^{55} respectively (Table 8).

Otolith Edge and Core Analysis

Isotopes that met inclusion for whole otolith analysis also had to be above detection limits at least 50% of the time in either the core or edge of the subsample otoliths to be included in otolith region (i.e., edge, core) analysis. Out of the 13 elements (Mg^{25}, Al^{27}, Mn^{55}, Fe^{57}, Cu^{63}, Zn^{66}, Rb^{85}, Sr^{86}, Sr^{88}, Sn^{118}, Ba^{137} Pb^{208}, and U^{238}) used for whole otolith comparisons, all but U^{238} were >50% LOD in either the core or the edge samples, with Al^{27} and Sn^{118} only being detectable in edge samples. Given this, 12 elements were used in the within-otolith comparisons and edge comparisons, while Al and Sn were excluded from among site core comparisons.

<u>Core Versus Edge</u>

Out of the 12 isotopes tested, manganese (Mn^{57}), iron (Fe^{57}), copper (Cu^{63}), tin (Sn^{118}), and barium (Ba^{137}) showed significantly different concentrations between the core and edge regions of otoliths. Manganese core concentrations were higher than edges (SP-ANOVA: $F_{1, 175}$ = 156.53, $p < 0.001$). The magnitude of these differences varied across sites and seasons (Figure

13A, B) leading to the significant otolith region by site (SP-ANOVA $F_{18, 175} = 5.43$, $p < 0.001$), and otolith region by season (SP-ANOVA: $F_{6, 175} = 2.44$, $p = 0.027$) interactions. However, the core versus edge comparisons were consistent (Figure 13). Time series plots also show higher levels of Mn^{55} in the core verses the edges (Figure 14). Otolith cores generally had higher iron (Fe^{57}) concentrations than the edges (Figure 15; SP-ANOVA: $F_{1, 193} = 7.67$, $p = 0.006$), although edge and core concentrations were similar in the spring, leading to a significant otolith region by season interaction (SP-ANOVA: $F_{6, 193} = 19.06$, $p < 0.001$).

Copper (Cu^{63}) had a similar pattern of incorporation as Mn^{55} and Fe^{57} into the otolith with higher concentrations in the core versus the edge (SP-ANOVA: $F_{1, 193} = 10.45$ $p = 0.001$). The otolith region by season interaction was significant as well (SP-ANOVA: $F_{6, 193} = 2.21$, $p = 0.044$), although concentrations in the core were always higher (Figure 16). Time series plots also indicated higher levels in the core than on the edges of otoliths, though the patterns were not as clear as for Mn^{55} (Figure 17). Otolith edges had higher tin (Sn^{118}) concentrations than cores (SP-ANOVA: $F_{1, 193} = 5.31$, $p = 0.022$), although only significantly so in the fall, leading to the significant otolith region and season interaction (SP-ANOVA: $F_{1, 193} = 4.34$, $p < 0.001$) (Figure 18).

Barium concentrations differed between otolith cores and edges (SP-ANOVA: $F_{1, 175} = 17.65$, $p < 0.001$), and the interactions of otolith region by site (SP-ANOVA: $F_{18, 175} = 49.660$, $p < 0.001$), and otolith region by season (SP-ANOVA: $F_{6, 175} = 9.61$, $p < 0.001$) were significant. The model predicted that Ba concentratpions tended to be higher in the otolith core than the edge, but given the significant interactions this pattern was variable and was not consistent across all sites and seasons (Figure 19A, B).

Core comparisons

Of the 13 isotopes used in whole otolith comparisons Al, Sn, and U were below detection limits more than 50% of the time in the core; therefore 10 isotopes (Mg^{25}, Mn^{55}, Fe^{57},

Cu^{63}, Zn^{66}, Rb^{85}, Sr^{86}, Sr^{88}, Ba^{137} Pb^{208}) were used for comparisons of otolith cores across sites and seasons . Mn^{55}, Fe^{57}, Sr^{86}, Sr^{88}, and Ba^{137} exhibited significant differences across sites, and $Fe^{57,}$ Rb^{85}, Sr^{86}, and Ba^{137} had significant different concentrations across seasons. Core Mn^{55} concentrations differed across sites (ANOVA: $F_{9, \mathbf{190}} = 6.856$, $p < 0.001$) and the concentration patterns were similar to those seen in whole otolith analysis (Table 9, Figure20; c.f. Figure 4A).

Iron (Fe^{57}) concentration differences across sites (ANOVA: $F_{9, 160} = 5.532$, $p < 0.001$) were similar to whole otolith comparisons and differed across seasons (ANOVA: $F_{3, 160} = 5.069$, $p = 0.002$). The interaction of site and season (ANOVA: $F_{27, 160} = 6.823$, $p < 0.001$) was also significant (Table 9, Figure 21A). Fall had the lowest concentration of Fe^{57}, just as in whole otolith comparisons (Table 9, Figure 21B). The interaction of site and season seems to be driven by differences in concentrations of Fe in the core at HT between fall and summer similar to whole otolith comparisons (Figure 21B). Unlike in whole otolith comparisons, rubidium concentrations did not differ among sites and the only difference observed was among seasons (ANOVA: $F_{3, 196} = 5.006$, $p = 0.002$). Concentrations in winter and summer did not differ, but were higher in winter than the fall and spring (Table 9, Figure 22).

Strontium 86 (Sr^{86}) exhibited a significant difference in core concentrations across sites (ANOVA: $F_{9, 187} = 10.738$, $p < 0.001$) and seasons (ANOVA: $F_{3, 187} = 34.438$, $p < 0.001$). The concentration pattern observed across sites was similar to the whole otolith pattern, but more sites had concentrations similar to one another than in whole otolith comparisons (Table 9, Figure 23A). Otolith core concentrations were highest in the fall, followed by winter, spring, and summer (Table 9, Figure 23B). Strontium 88 (Sr^{88}) differed among sites (ANOVA: $F_{9, 160} = 5.239$, $p < 0.001$), but not seasons (ANOVA: $F_{3, 160} = 2.104$, $p = 0.102$) and these site differences resembled those seen in whole otolith comparisons (Table 9, Figure 24A). The season by site

interaction (ANOVA: $F_{27, 160} = 2.041$, $p = 0.004$) was significant because there was a low amount of core Sr^{88} in winter samples at many sites (Table 9, Figure 24B).

Core concentrations of barium (Ba^{137}) differed among sites (ANOVA: $F_{9, 160} = 24.760$, $p < 0.001$) and seasons (ANOVA: $F_{3, 160} = 6.644$, $p < 0.001$), and the site by season interaction was retained in the model (ANOVA: $F_{27, 160} = 2.146$, $p = 0.002$). BB and BA had the highest concentrations, similar to whole otolith concentrations, but interestingly FR and PD had the second highest core concentrations and were similar to RF and CK (Table 9, Figure 25A). Core concentrations were highest in the fall, while all other seasons did not differ, and PD had high core concentrations in the spring, driving the significant interaction (Table 9, Figure 25B).

Edge Comparisons

Out of the 13 isotopes used in whole otolith comparisons only U^{238} was below detection limits more than 50% of the time, so 12 isotopes (Mg^{25}, Al^{27}, Mn^{55}, Fe^{57}, Cu^{63}, Zn^{66}, Rb^{85}, Sr^{86}, Sr^{88}, Sn^{118}, Ba^{137}, Pb^{208}) were used for comparisons of otolith edges across sites and seasons. Only Fe^{57}, Sr^{86}, Sr^{88}, and Ba^{137} had significant differences across both sites and seasons.

Iron (Fe^{57}) edge concentrations differed among sites (ANOVA: $F_{9, 160} = 4.750$, $p < 0.001$) and seasons (ANOVA: $F_{3, 160} = 3.438$, $p = 0.02$), and the site by season interaction was also significant (ANOVA: $F_{27, 160} = 6.070$, $p < 0.001$). Iron had similar patterns across sites and seasons as in both the core and whole otolith analyses (Table 10, Figure 26A). Seasonal variation in the edge exhibited the same pattern as in the core, with fall having the lowest concentrations (Table 10, Figure 26B) and the significant interaction was driven by a notable difference between HT during fall and summer (Figure 26B).

Sr^{86} edge concentrations differed among sites (ANOVA: $F_{9, 160} = 7.623$, $p < 0.001$) and seasons (ANOVA: $F_{3, 160} = 8.162$, $p < 0.001$), and the site by season interaction (ANOVA: $F_{27, 160} = 2.635$, $p < 0.001$) was important. Patterns of Sr^{86} edge concentrations resembled both whole

otolith and core concentration patterns, but differences between sites were more distinct (Table 10, Figure 27A). The fall samples had the highest concentration of edge Sr^{86} and spring was lower than summer (Table 10, Figure 27B).

Strontium 88 (Sr^{88}) edge concentrations differed among sites (ANOVA: $F_{9, 160} = 7.779$, $p < 0.001$) and seasons (ANOVA: $F_{3, 160} = 15.364$, $p < 0.001$), and the site by season interaction term was significant(ANOVA: $F_{27, 160} = 3.477$, $p < 0.001$). Patterns of Sr^{88} edge concentrations across sites were similar to Sr^{88} whole and core comparisons, but concentration differences between sites were not as distinct as in whole otolith comparisons (Table 10, Figure 28A). Edge concentration was lowest in winter and highest in the summer (Table 10, Figure 28B); this combined with different concentration patterns across sites for each season, drove the interaction (Figure 28B).

Edge concentrations of barium (Ba^{137}) were significantly different across sites (ANOVA: $F_{9, 160} = 66.413$, $p < 0.001$) and seasons (ANOVA: $F_{3, 160} = 31.187$, $p < 0.001$) and the site by season interaction was significant (ANOVA: $F_{27, 160} = 4.808$, $p < 0.001$). Patterns across sites of edge Ba^{137} were similar to both core and whole otolith comparisons, with the notable exception that PD had much lower edge concentrations than core concentrations, which was also seen when investigating within otolith core and edge concentrations (Table 10, Figure 29A; c.f. Figure 19B). Edge Ba^{137} concentrations were highest in fall and lowest in winter and spring (Table 10, Figure 29B). Although there is a significant site by season interaction term, the overall pattern across sites remained consistent for all seasons (Figure 29B).

Salinity and Temperature

Each site experienced varying salinities and temperatures throughout the study (Table 11, Figure 30, Figure 31). Salinity differed significantly across sites (ANOVA: $F_{9, 30} = 7.530$, $p < 0.001$), but not seasons (ANOVA: $F_{3, 36} = 1.796$, $p = 0.165$) (Figure 30), and temperature differed

significantly across seasons (ANOVA: $F_{3, 36} = 42.810$, $p < 0.001$), but not sites (ANOVA: $F_{9, 30} = 0.227$, $p < 0.001$) (Figure 31). Although the interaction could not be investigated, the plots of salinity and temperature across sites for each season can be seen in Figures 30B and 31B, respectively. Water temperature followed expected patterns with the lowest temperatures being observed in the winter, the highest in the summer, and the fall and spring not differing from one another (Figure 31A). Also salinity was not correlated with temperature across all sites ($R^2 = 0.00024$, $F_{1, 38} = 0.009$, $p = 0.9238$, Figure 32). All tests performed for salinity and temperature met normality assumptions, and all but the temperature across seasons test met assumptions of variance.

Isotope Correlation with Salinity and Temperature

Of the 12 isotopes (Mg^{25}, Al^{27}, Mn^{55}, Fe^{57}, Cu^{63}, Zn^{66}, Rb^{85}, Sr^{86}, Sr^{88}, Sn^{118}, Ba^{137}, Pb^{208}) analyzed in otolith edge comparisons only Sr^{86}, Sr^{88}, and Ba^{137} showed any relationship with salinity (Figure 33) or temperature (Figure 34). Strontium 86 (Sr^{86}) was not related to temperature ($R^2 = 0.00846$, $F_{1, 198} = 2.699$, $p = 0.102$), but did demonstrate a positive asymptotic relationship with salinity, which was best described by the following equation.

$$\mathrm{Sr}_{\mathrm{S}}^{86} = \mathrm{Sr}_{\infty} \cdot \left[1 - \mathrm{e}^{-\mathrm{K}(\mathrm{S} - \mathrm{S}_0)}\right]$$

Where Sr_{∞} represents the maximum amount of Sr^{86} that can be incorporated into the otolith, K is the rate at which Sr^{86} concentrations approach the maximum (Sr_{∞}), S equals salinity, S_0 is the theoretical salinity at which the Sr^{86} concentration in the otolith is 0 ppm, and $\mathrm{Sr}_{\mathrm{S}}^{86}$ is equal to the Sr^{86} concentration in the otolith at a given salinity. The parameter estimates for this model were $\mathrm{Sr}_{\infty} = 3450.150$ ($p < 0.001$), K = 0.056 ($p = 0.052$), and $Sr_0 = -16.861$ ($p = 0.013$) (Figure 33).

Strontium 88 (Sr^{88}) exhibited a significant positive linear relationship with temperature (Figure 34) and was affected by salinity. The effects of temperature and salinity on Sr^{88} concentration in the otolith were best described by the following equation.

$$Sr_{ST}^{88} = Sr_0 + xT + z(S \cdot T)$$

Where x is the temperature effect across various temperatures (T), Sr_0 is the concentration of Sr^{88} in the otolith when temperature and salinity are zero, z is the interactive effect of salinity (S) and temperature (T), and Sr_{ST}^{88} is equal to the Sr^{88} concentration in the otolith at a given salinity and temperature. This model predicted Sr_0 = 863.1722 ($p < 0.001$) ppm, T = 83.2593 ($p < 0.001$), and a 1.7779 ($p < 0.001$) ppm increase for the interactive effect (z) of temperature and salinity (Figure 35A, B).

Barium (Ba^{137}) exhibited an exponentially declining relationship with salinity (Figure 33) and an exponentially increasing relationship with temperature (Figure 34). The best model that described these relationships was:

$$Ba_{ST}^{137} = Ba_0 \cdot e^{[-k_s] \cdot S} \cdot (1 + k_t)^T$$

where Ba_0 is the otolith Ba concentration when both salinity and temperature = 0, k_s is the rate at which Ba^{137} concentrations approach zero across varying salinities (S), K_t is proportional to increases in Ba^{137} concentration with temperature (T), and Ba_{ST}^{137} is the concentration of Ba^{137} in the otolith at a given salinity (S) and temperature (T). This model predicted a Ba_0 = 2.782 ($p < 0.001$), a k_s = 0.055 ($p < 0.001$), and k_t = 0.063 ($p < 0.001$) (Figure 36).

Water Chemistry

Variation Among Sites and Seasons

Out of the 13 isotopes that met criteria (> 50% LOD) to be included in otolith analysis, only five elements (Mg, Mn, Fe, Zn, Sr, and Ba) were quantified in water samples or above LOD at least 50% of the time in water samples, and all but Fe were detectable in 100% of samples. All elements were converted into molar ratios with calcium (Ca) prior to analysis and all elements, except for Mg, are reported in element (mmol) per Ca (mol) water. Mg is reported as Mg (mol) per Ca (mol) in water.

Magnesium (Mg:Ca) concentrations in water differed across sites (ANOVA: $F_{9,20} = 2.522$, $p = 0.041$), but not seasons (ANOVA: $F_{2,27} = 1.403$, $p = 0.263$). HT had higher Mg than BB, and all other sites had concentrations that did not differ from these two (Table 12, Figure 37A). Concentrations of manganese (Mn:Ca) in water differed across sites (ANOVA: $F_{9,20} = 4.086$, $p = 0.004$), but not seasons (ANOVA: $F_{2,27} = 0.212$, $p = 0.810$). FR had the highest Mn concentration out of all sites, similar to otolith Mn patterns; although unlike otolith concentrations, FA did not have high Mn water concentrations (Table 12, Figure 37B).

Iron (Fe:Ca) concentrations in water did not differ across sites (ANOVA: $F_{9,20} = 1.519$, $p = 0.208$) or seasons (ANOVA: $F_{2,27} = 1.071$ $p = 0.357$). Zinc (Zn:Ca) differed across sites (ANOVA: $F_{9,20} = 3.628$, $p = 0.008$), but not seasons (ANOVA: $F_{2,27} = 0.709$, $p = 0.501$) with BB having the highest Zn concentrations (Table 12, Figure 37C).

Strontium (Sr:Ca) concentrations in water did not vary across sites (ANOVA: $F_{9,20} = 1.497$, $p = 0.216$), but concentrations were higher in summer than in spring, and concentrations in winter did not differ from either spring or summer (ANOVA: $F_{2,27} = 4.692$, $p = 0.018$) (Table 12, Figure 37D). Barium (Ba:Ca) differed across sites (ANOVA: $F_{9,20} = 10.32$, $p < 0.001$), but not seasons (ANOVA: $F_{2,27} = 0.3663$, $p = 0.697$); concentrations were highest in BB , which did not differ from FA. FA was also similar to BA, FB, and FR (Table 12, Figure 37E).

Correlation with Salinity and Temperature

Water concentrations of Mg, Fe, Sr, and Ba were related to salinity (Figure 38), but no elements were related to temperature (Figure 39). The relationship of magnesium (Mg:Ca) concentrations in water and salinity exhibited a positive asymptotic pattern and was modeled using a simple positive asymptotic concentration equation:

$$\mathrm{Mg} = \mathrm{Mg}_{\infty} \cdot \frac{\mathrm{Salinity}}{\mathrm{K} + \mathrm{Salinity}}$$

where Mg_{∞} is equal to the maximum amount of Mg:Ca that can occur in water and K is the rate at which concentrations approach the maximum. K was 0.670 (p = 0.018) and Mg_{∞} was 4.230 (p < 0.001) (Figure 38).

Iron (Fe:Ca) water concentrations in response to salinity were best described with an exponential decline:

$$\mathrm{Fe} = \mathrm{Fe}_0 \cdot e^{[-k]\cdot S}$$

where Fe_0 is the concentration of Fe:Ca when salinity is zero and k is the rate at which Fe:Ca concentrations approach zero across varying salinities (S). This model predicted a Fe_0 = 3.349 (p< 0.001) and a k = 0.228 (p=0.010) (Figure 38).

The concentration of strontium (Sr:Ca) in water, exhibited a positive asymptotic relationship with salinity and was modeled using the following positive asymptotic equation.

$$\mathrm{Sr} = \mathrm{Sr}_{\infty} \cdot \left[1 - \mathrm{e}^{-\mathrm{K}(\mathrm{Salinity} - \mathrm{S}_0)}\right]$$

Where Sr_{∞} is the highest Sr:Ca concentration that can occur in water no matter how much salinity increases, K is the rate at which it approaches the maximum, and S_0 is the theoretical salinity at which Sr:Ca would equal zero. This model predicted a Sr_{∞} = 7.394 (p < 0.001), k = 0.254 (p = 0.178), and S_0 = -3.479 (p = 0.312) (Figure 38).

Barium (Ba:Ca) in water exhibited an exponential decline with salinity similar to Fe:Ca and was modeled using the following equation:

$$\mathrm{Ba} = \mathrm{Ba}_0 \cdot e^{[-k]\cdot S}$$

where all the parameters are the same as the Fe model. This model predicted Ba_0 = 0.399 (p < 0.001) and k = 0.128 (p < 0.001) (Figure 38).

Otolith and Water Correlation

Investigation of plots of otolith isotope concentration versus water elemental concentrations demonstrated that only Sr^{86} and Sr^{88} exhibited a pattern with water

concentrations of Sr (Figure 40). Sr^{86} had a positive linear relationship with water Sr and was modeled using a simple linear regression.

$$Sr^{86}: Ca_{otolith} = Sr_0 + Sr: Ca_{water} * Z$$

The predicted parameters for the model were 2031.81 (Sr_0, $p < 0.001$) for the amount of Sr:Ca in the otolith when water Sr:Ca equals zero and a 137.51 µmol mol^{-1} increase (Z, $p < 0.001$) in Sr:Ca otolith for every mmol mol^{-1} increase of Sr:Ca in water (Figure 40); this relationship had an R^2 of 0.176, but an overall $p < 0.001$.

The Sr^{88}:Ca otolith and Sr:Ca water relationship was best described using a regression similar to the one used to describe the relationship of otolith Sr^{88} with temperature, given that otolith Sr^{88}:Ca concentrations were more correlated with temperature than water Sr:Ca concentrations. However, increased $Sr:Ca_{water}$ is predicted to result in higher otolith Sr^{88}:Ca as temperatures increase, demonstrated by the following equation.

$$Sr^{88}: Ca_{otolith} = Sr_0 + xT + z(Sr: Ca_{water} * T)$$

Where Sr_0 is equal to the theoretical concentration of otolith Sr^{88}:Ca when temperature and water Sr:Ca concentrations equal zero, x equals the temperature effect across various temperatures (T), and z is the interactive effect of $Sr:Ca_{water}$ and temperature. This regression produced estimates of Sr_0 = 687.844 ($p = 0.005$), x = 98.866 ($p < 0.001$), and z = 4.788 ($p = 0.003$) (Figure 41).

Relative Condition

Gulf Killifish relative condition differed across sites (ANOVA: $F_{9, 729} = 9.108$, $p < 0.001$, Figure 50A) and seasons (ANOVA: $F_{3, 729} = 10.304$, $p < 0.001$, Figure 50B). The interactions of site and season (ANOVA: $F_{27, 729} = 6.377$, $p < 0.001$, Figure 50B) and season and length (ANOVA: $F_{3, 729} = 2.796$, $p = 0.040$, Figure 50A) were significant as well, but length alone did not have a significant effect on relative condition (ANOVA: $F_{1, 729} = 0.331$, $p = 0.565$). Relative condition was

highest at BB and BA, and RF did not differ from these sites (Figure 42A). Also relative condition was highest in summer (Figure 42B).

Discussion

Oil Indicators

A number of elements have been identified in crude and weathered DHOS oil (Mg, Al, V, Cr, Co, Ni, Cu, Zn, As, Se, Sn, and Pb) (Grosser et al. 2012, Liu et al. 2012), refinery effluents (Se) (Miekeley et al. 2005, De Almeida et al. 2009), and other crude oils (Ni and V)(Ellis et al. 2011). In addition, several elements (Na, Mg, and Cr) are incorporated into fish otoliths when exposed to oil (Morales-Nin et al. 2007). Here isotopes of these elements were either below detection limits (V^{51}, Cr^{53}, Ni^{60}, Ni^{62}, Se^{77}, and Se^{78}) or did not vary among sites (Mg^{25}, Al^{27}, Cu^{63}, Zn^{66}, Sn^{118}, Pb^{208}). Given this, no indication of oil exposure from the DHOS oil or refinery processes was found in the otoliths of *F. grandis* when compared between paired oiled and unoiled sites.

I expected that *F. grandis* collected at the oiled site in Barataria Bay (BA) Louisiana would have a trace metal signature in the otolith that reflected oil exposure, given that this site received heavy amounts of oiling that persisted in marshes well into 2011 (gomex.erma.noaa.gov/erma.html). Also weathered DHOS oil in marshes has a higher concentration of metals than does crude DHOS oil (Liu et al. 2012). My fish collections did not start until 2012, but given that *F. grandis* do not exhibit large scale movements (Nelson et al. 2014) and assuming they exhibit similar age and growth patterns (50 – 90 mm = 1 - 4 year old fish) to *F. hetroclitus* (Fritz and Garside 1975, Dibble and Meyerson 2012), then fish collected at these sites should have been exposed to oil throughout their lives.

I expected to find oil and refinery related elements and isotopes in otoliths from Mississippi because the refinery site (RF) is located in a borrow ditch beside an oil refinery,

where exposure is likely to be occurring continuously. Not finding elements in otoliths that were associated with oil exposure in AL sites (FA, PD) was expected, given that the amount of oiling in these marshes was light and patchy. Also, a similar study conducted in close proximity to our killifish collection sites in Alabama, did not find an effect of DHOS oil on trace element or stable isotope uptake into oyster shells (Carmichael et al. 2012).

One plausible reason that Morales-Nin et al. (2007) was able to find an oil signature in Turbot (*Scophthalmus maximus*) otoliths, while my results differ, is because in their experiment oil was added directly to food sources. Therefore, the level of contamination in the lab experiment was likely much higher than in levels experienced in the field. Also a flat-fish species (Pleuronectiformes) was used in Morales-Nin et al. (2007), while *F. grandis* is in a completely different order (Cyprinodontiformes), and even fish that are in the same family have been shown to incorporate elements into the otolith differently (Rooker et al. 2004).

Differences Among Sites

Although differences among sites in whole otolith elemental and isotopic composition that could be attributed to oil exposure were not seen, Mn^{55}, Fe^{57}, Rb^{85}, Sr^{86}, Sr^{88}, Ba^{137}, and U^{238} concentrations differed significantly among sites. Mn^{55}, Sr^{86}, Sr^{88}, and Ba^{137} contributed most of the distinction among both sites and regions in the linear discriminant function analyses and paired sites within estuaries expressed similar concentrations of these elements. This led to failure of the site LDFA analysis to correctly classify fish to collection site. Differences in strontium, barium, and manganese have also been used in many other studies (Thorrold et al. 1998, Campana et al. 2000, Gillanders and Kingsford 2003, Vasconcelos et al. 2007, Tanner et al. 2011) to classify fish to collection areas.

Given the misclassification of fish within pairs of sites and the 2 regional clusters identified in the hierarchical cluster analysis, it is not surprising that the regional LDFA was more

successful (46% - MS, 58% - AL E. – FL, 67% - Al W., 97% - LA correct classified) than for individual sites. The regional LDFA also had classification accuracies similar to other studies (Thorrold et al. 1998, Vasconcelos et al. 2007, Tanner et al. 2011), but the reason for the low percentage of classification accuracy in both the MS and AL east + FL grouping is that these regional groups still experienced similar otolith Sr, Ba, and Mn. Perhaps the addition of $\delta^{13}C$ and $\delta^{18}O$ stable isotope analysis to our study could have improved the correct classification to these regions, given that the addition of these stable isotopes was able to improve classification percentages of Thorrold et al. (1998) and Tanner et al. (2011). Also these isotopes have been shown to be useful for other otolith analyses, such as stock discrimination (Ashford and Jones 2007, Niklitschek et al. 2010) and habitat connectivity (Thorrold et al. 2001, Tanner et al. 2013).

As mentioned above Mn^{55} was a good discriminator for the LDFA when all sites were considered separately and it was even more important as a discriminator in the regional LDFA. This is because Mn whole otolith concentrations were highest in Fowl River (FR) followed by Fowl Bay A (FA) and Fowl Bay B (FB) and although there were significant interactions between site, season, and length the overall patterns across sites were consistent. The high Mn^{55} concentration at these sites also explains why the Alabama west regional grouping (FR, FB, and FA) had a 67% accurate classification in the regional LDFA and was grouped together in the hierarchical cluster analysis. High levels of Mn^{55} in the otoliths of fish from the Fowl River site is also not surprising because water Mn:Ca was highest at this site as well. Although determining the source of manganese into FR was beyond the scope of this study, the high levels of Mn^{55} at FR and the whole Alabama west regional group suggests that this element may serve as a possible natural tag for Alabama waters on the west side of Mobile Bay.

Manganese concentrations in otolith cores also exhibited similar site patterns to whole otolith signatures and were higher than otolith edges at all sites in every season. This

demonstrates that the core concentration difference among sites was the main driving factor for whole otolith differences. Higher Mn^{55} in the core also explains why a negative relationship between fish length and Mn^{55} whole otolith concentration was observed. This relationship exists because core contributions to whole otolith element concentrations would decrease as fish length and resulting otolith diameter increased. Higher core concentrations of manganese, as well as other elements, have been documented previously (Morales-Nin et al. 2005, Ruttenberg et al. 2005, Melancon et al. 2008) and it has been suggested that this phenomenon is driven by lower Ca concentrations in the core (Dove et al. 1996) or maternal element contributions during the embryonic stage (Chittaro et al. 2006).

In our site specific LDFA, Fe^{57} was also a major discriminator, because FB had significantly higher concentrations than other sites. Although not commonly found as a major discriminator in estuarine systems it has been found to be a major component in separating fish from upstream and downstream portions of an estuary and has been attributed to upstream industrial inputs into the estuary (Ranaldi and Gagnon 2008). Even though there was a significant interaction with season, high levels were always present at FB. The highest peak was in the spring and it was higher than most sites in the fall as well, with the same pattern seen in edge and core signatures.

Sr^{86} was the second best discriminator among sites; the pattern among sites was similar to the pattern of mean salinity recorded during each fish collection. This was expected, given that a positive correlation has been found between salinity and otolith Sr concentration in other studies (Lowe et al. 2009, Albuquerque et al. 2012); I also found a positive correlation between salinity and otolith edge concentrations of Sr^{86}. One notable exception to this pattern was that while salinity was higher at the Perdido site than other sites otolith Sr^{86} concentrations did not differ between CK and PD.

Fall had the highest Sr^{86} concentration of any season and all seasons differed. Although there was an interaction between site and season, patterns across sites within each season remained the same. The highest Sr^{86} concentration in fall was to be expected because many sites (CK, FB, FA, FR, and WF) experienced the highest salinities during the fall collection. The length by site interaction was also present, but patterns across sites were similar for all fish lengths. Core and edge patterns of Sr^{86} among sites were similar to whole otolith patterns, but edge signatures from PD were significantly lower than CK, because of higher Sr^{86} in the fall and summer collections from CK. This was the reason for the significant site by season interaction in the edge comparison.

Strontium 88 (Sr^{88}) was the third best site discriminator and patterns among sites and patterns of whole otolith Sr^{88} concentrations were similar to those seen for Sr^{86}, although seasonal differences in Sr^{88} differed from those of Sr^{86}. Average Sr^{88} concentrations in winter were much lower than in other seasons. These low concentrations in winter drove the site by season and the season by length interactions, but patterns across sites remained the same, so these interactions were not important to site discrimination. The season by length interaction was also driven by small fish being overrepresented at PD in the summer, which was the site with the highest Sr^{88} concentration during the summer.

Tin (Sn^{118}) did not differ across sites, but concentrations in otolith edges were significantly higher than in otolith cores in the fall. This is most likely a contamination effect of the double sided tape that adhered otoliths to slides from this collection season as shown in Ludsin et al. (2006). Although this should not be detected until the laser moves off the otolith, it is possible that at the very edge (the thinnest part) of the otolith, the laser ablateded through the otolith to the tape, causing elevated Sn^{118} levels.

Barium was the best discriminator among sites and regions in the LDFAs. This is because Ba^{137} concentrations at Louisiana sites (BB, BA) were much higher than all other sites and concentration at FR was consistently lower than these two sites, but higher than all other sites. All seasons had different concentrations of average whole otolith Ba^{137}, but patterns among sites were similar across all seasons. The length covariate exhibited a significant negative effect on whole otolith Ba^{137} concentrations and this was observed in all seasons except for the fall. This was expected, because the 70-79 mm size class was overrepresented at BA during this collection, leading to increased Ba^{137} concentrations for this size class during the fall.

Patterns of otolith core concentrations were similar to whole otolith patterns among sites, except that PD and CK did not differ from FR. Otolith edge concentration patterns were similar to whole otolith and core patterns. Also otolith edge Ba^{137} concentrations at PD and CK were similar to whole otolith concentrations at these sites. This observation was expected, because higher concentrations of Ba were found in the core of otoliths verses edges. Although in the spring this was not the case. Higher levels of Ba in otolith cores have been documented before (Morales-Nin et al. 2005, Ruttenberg et al. 2005) and have also been attributed to the possibility of lower Ca concentrations in the core (Dove et al. 1996). Although given that estuaries in this study had consistently lower salinity during the spring and Ba has been shown to be correlated with riverine inputs (Coffey et al. 1997), elevated levels in the core are also most likely driven by this.

Given that Ba is a major component of freshwater inputs (Coffey et al. 1997), it would be logical to assume that sites that experienced the lowest salinities should have the highest Ba concentrations. Sites with low salinities tended to have higher Ba otolith concentrations (e.g., FR, BB, BA); however, the concentrations are not always correlated with salinities. For instance, salinities at FR did not differ from BB, but Ba^{137} concentrations were much higher at BB. Also BA

had salinities similar to FB and FA, but had Ba^{137} concentrations very close to BB. This demonstrates that Ba^{137} is not a purely a function of salinity.

The primary source of Ba in estuaries has been shown to be riverine suspended particulate matter (SPM) (Hanor and Chan 1977, Coffey et al. 1997) and the Mississippi River is a very large drainage containing high SPM loads, resulting in high concentrations of Ba (Hanor and Chan 1977, Coffey et al. 1997). Given this, the LA sites located near the mouth of the Mississippi had much higher Ba^{137} concentrations in the otolith, as expected. This occurred even when salinities around 15 ppt were experienced in the fall at the BA site. Given that fish collected in Louisiana had much higher otolith concentrations of Ba^{137} than at other sites, this could prove to be a reliable tag for nursery area discrimination or stock discrimination for members of a species that use estuarine waters close to the Mississippi river.

Salinity and Temperature Effects on Otoliths

The effects of salinity and temperature on element and isotope incorporation into the otoliths of *F. grandis* and the resulting models of these relationships can help to explain some of the seasonal and site variation observed for Sr^{86}, Sr^{88}, and Ba^{137}. Also these models explain the similarity in Sr^{86} concentrations between Perdido (PD) and Crooked Creek (CK), although PD had consistent higher salinities. The modeled relationship between otolith Sr^{86} and salinity started to level out around 20 ppt, with a maximum level of 3450 ppm. The maximum whole otolith mean Sr^{86} concentration observed at any site (CK, PD) was approximately 3200 ppm, indicating why Sr^{86} concentrations were not higher at PD than CK, even though salinity was higher. This relationship with salinity also helps to explain why Sr^{86} was highest in the fall, given that many sites experienced the highest salinity in the fall as well.

The positive asymptotic response of Sr^{86} in the otolith versus salinity is no surprise, given that this response of Sr has been identified previously (Lowe et al. 2009, Albuquerque et

al. 2012). This is a result of water Sr:Ca concentrations exhibiting a similar relationship to salinity (Kraus and Secor 2004, Lowe et al. 2011, Albuquerque et al. 2012) and the linear relationship of otolith Sr and water Sr:Ca concentrations found in this study and elsewhere (Bath et al. 2000, Reis-Santos et al. 2013). Generally as salinity increases, water Sr:Ca also increases because Sr is the 8th most abundant element in ocean water (Hem 1970) with Sr:Ca ratios of approximately 8.5 µmol mol^{-1} for the world's oceans (de Villiers 1999). Also, as salinity increases in estuaries, this usually means an increasing proportion of the water is from oceanic sources. While Sr^{86} did exhibit a positive relationship with salinity it did not have any relationship with temperature, unlike in Martin et al. (2004), where a strong correlation was found between temperature and otolith Sr^{86}.

The low concentration of Sr^{88} in otoliths during the winter can be explained by the positive relationship of Sr^{88} that was found with temperature. Although this relationship was complicated by the fact that the interaction of salinity and temperature also had a positive effect on Sr^{88} concentration in the otolith, the temperature effect was more important, given that the best fitting linear model did not include the main effect of salinity. The model predicted that increasing salinity contributed to slightly higher Sr^{88} concentrations in the otolith across increasing temperatures. Another important result affecting this relationship is that water Sr:Ca had no correlation with temperature, but Sr^{88} still showed a positive correlation with water Sr:Ca. This positive correlation between temperature and Sr has been demonstrated in fish otoliths (Bath et al. 2000, Martin et al. 2004, Webb et al. 2012, Barnes and Gillanders 2013) and coral aragonite skeletons (Smith et al. 1979, Swart 1979). It has also been shown this positive relationship is not always the case (Secor et al. 1995, Chesney et al. 1998, Campana 1999) and may be due to the presence of confounding variables such as salinity.

This study was able to address several factors in free-ranging field populations not previously studied. I was able to use field collected fish to look at the effects of both temperature and salinity on Sr incorporation across a wide range of temperatures and salinities without the interactive and confounding fact that salinity and temperature are usually correlated in estuarine waters. Also the monitoring and subsequent analysis of two separate isotopes of Sr was a unique approach, given that previous studies monitored only Sr^{88} (Thorrold and Shuttleworth 2000, Ranaldi and Gagnon 2008, Tanner et al. 2011, Reis-Santos et al. 2013, Tanner et al. 2013), Sr^{86} (Martin et al. 2004), or did not report which isotope of Sr was used in otolith analysis (Kraus and Secor 2004, Rooker et al. 2004, Lowe et al. 2011). In addition we were able to use fish from the field that did not have to be caged as in other studies (Kraus and Secor 2004, Rooker et al. 2004) given that *F. grandis* have limited movements throughout the course of their life (Nelson et al. 2014). Therefore otolith signatures should reflect fluctuating environmental conditions, such as salinity, experienced in a localized area of tidal marsh.

Using both Sr^{86} and Sr^{88} improved discrimination among sites and allowed for identification of important differences in how otolith concentrations of these two elements change with temperature and salinity. Given that this study showed a minimal effect of salinity on Sr^{88} incorporation into the otolith, but a large effect of temperature, it would be unwise to try to reconstruct past salinities, or monitor fish movements across salinity gradients using this isotope, unless temperature did not change across the gradient being investigated. A better use of Sr^{88} would be to reconstruct past temperature exposure and could prove valuable in monitoring long term oceanic temperature changes. A long lived pelagic marine species would be ideal for this use, given that it should experience relatively constant salinity throughout its life, thus eliminating any salinity influence on Sr^{88}. A better choice for assessing salinity changes in the otolith would be to use the Sr^{86} isotope, given that it did not show any correlation with

temperature in this study (but see Martin et al. 2004). These differing relationships of salinity and temperature on Sr^{88} and Sr^{86} incorporation are somewhat supported by Webb et al. (2012), who found that at their high temperature treatment Sr^{88}/Sr^{86} ratios decreased with increasing salinities, meaning that as salinity increased Sr^{86} had to increase at a rate higher then Sr^{88}, thus driving the ratio value down. This result provides evidence that Sr^{86} was more correlated with salinity then Sr^{88}. Differences between these two isotopes may also be able to help elucidate interactive effects of salinity and temperature seen elsewhere (Elsdon and Gillanders 2002).

The positive relationship between Sr^{88} and temperature must be driven by increased availability of Sr^{88} in the fish or an increased incorporation rate into the otolith, given that this study and others (Bath et al. 2000, Martin et al. 2004) have demonstrated that concentrations of Sr:Ca in water do not increase with increasing temperature. One increased bioavailability possibility would be that concentrations of Sr^{88} in the fish change as a result of changes in physiological processes such as gonad development (Kalish 1991) across temperatures. An explanation of increased incorporation relies on the fact that fish growth are positively related to temperature and otoliths lay down new material at a rate proportional to that of fish growth (Campana and Neilson 1985). Therefore as temperature increases, fish growth rate increases, as well as otolith growth rate and the resulting rate of new material ($CaCO_3$) deposition to the otolith. Given that Sr is randomly substituted into the otolith aragonite matrix in place of calcium (Ca) (Doubleday et al. 2014) increased rates of calcium deposition at higher temperatures should lead to increased Sr deposition, given that substitution rates remain consistent, although Bath et al. (2000) suggested that this was not the case. One probable explanation to why Sr^{88} was correlated with temperature while Sr^{86} was not, is the possibility that Sr^{88} is more readily available for substitution, because it contributes around 80% of naturally occurring strontium (Capo et al. 1998).

Barium concentrations in the otolith exhibited an exponentially declining relationship with increasing salinity similar to the relationship of Ba:Ca in water and salinity. Barium concentration in the otolith was also positively correlated with temperature and was best modeled using an increasing exponential relationship. The best fitting model for Ba^{137} concentration in the otolith was achieved when these two relationships were combined, given that the variability at low salinities was accounted for by variation in temperature, further complicating the relationship of Ba concentrations in the otolith and salinity.

This interactive effect of a positive relationship with temperature and a negative salinity effect on Ba concentrations in the otolith has been found before in both Sparidae (Webb et al. 2012) and Sciaenidae (Barnes and Gillanders 2013). However, no significant relationship of otolith Ba with temperature, salinity, or an interaction of the two was found for Spot (*Leiostimous xanthurus*) (Martin and Thorrold 2005), another sciaenid. Similar to the relationships found with Sr this is the first study to quantify these relationships with Ba in the field without the confounding effect of temperature and salinity correlation. The effects of temperature on otolith Ba^{137} incorporation appears to be a temperature driven physiological effect in the fish, or a result of increased fish growth and subsequent otolith growth rates, given that water Ba:Ca was not correlated with temperature. The same mechanism proposed above for Sr incorporation could be driving increased Ba^{137} incorporation into the otolith with increasing temperature, assuming that Ba substitutes into the otolith similarly to Sr.

These effects of temperature and salinity on otolith Ba concentrations have implications for use of Ba as a natural tag of environmental conditions experienced by a fish. When salinities increase above 15 ppt the discriminatory power for Ba is greatly reduced, given that Ba^{137} otolith concentrations started to level out at this salinity. Also increased temperature may cause higher Ba concentrations than expected at a given salinity, especially low salinity levels.

Conclusions

No element or isotope indicated oil exposure in the otoliths of *F. grandis*, either due to the DHOS or other oil exposure. Perhaps otolith microchemistry analysis may not be a good metric for oil exposure studies, although indicators were found in Turbot (*Scophthalmus maximus*) otoliths (Morales-Nin et al. 2007). Mn^{55}, Sr^{86}, Sr^{88}, and Ba^{137} were the best discriminators among sites and seasons and use of these elements led to a reasonably successful regional classification, particularly for the Louisiana sites. Mn^{55} may be able to be used as a tag to separate the eastern and western sides of Mobile Bay given that it was not detected in otoliths or water samples in high concentrations from sites east of Mobile Bay.

The isotopes of Sr have differing relationships with salinity and temperature, with Sr^{86} being correlated with salinity and not temperature, while Sr^{88} is highly positively correlated with temperature and has a weak positive correlation with salinity, and an interactive relationship with salinity and temperature. Although more research into these relationships needs to be conducted, they provide interesting insights into the complex relationships between salinity and temperature and elemental incorporation into the otolith. These relationships also have implications for reconstructing past salinities and temperatures experienced by a fish based on Sr concentrations in the otolith. Barium incorporation into otoliths is also affected by temperature and salinity, and the interaction of the two, as well as by riverine inputs of barium, demonstrating that Barium is not purely an indicator of fresh water. Given the high concentrations of barium at the Louisiana sites this could be a good otolith marker for identifying fish that use estuarine waters around the Mississippi River.

Relative condition of *F. grandis* did not differ between paired oiled and non-oiled sites and neither did otolith microchemical compositions. This demonstrates no apparent evidence

for impacts of the DHOS spill on *F. grandis*, a trend that has also been observed for other nearshore nekton (Fodrie and Heck 2011, Moody et al. 2013) in the northern Gulf of Mexico.

Literature Cited

Abbriano, R. M., M. M. Carranza, S. L. Hogle, R. A. Levin, A. N. Netburn, K. L. Seto, S. M. Snyder, and P. J. S. Franks. 2011. Deepwater Horizon oil spill a review of the planktonic response. Oceanography 24:294-301.

Able, K. W., S. M. Hagan, and S. A. Brown. 2006. Habitat use, movement, and growth of young-of-the-year *Fundulus spp*. in southern New Jersey salt marshes: Comparisons based on tag/recapture. Journal of Experimental Marine Biology and Ecology 335:177-187.

Able, K. W., D. N. Vivian, G. Petruzzelli, and S. M. Hagan. 2012. Connectivity among salt marsh subhabitats: Residency and movements of the Mummichog (*Fundulus heteroclitus*). Estuaries and Coasts 35:743-753.

Albuquerque, C. Q., N. Miekeley, J. H. Muelbert, B. D. Walther, and A. J. Jaureguizar. 2012. Estuarine dependency in a marine fish evaluated with otolith chemistry. Marine Biology 159:2229-2239.

Ashford, J. and C. Jones. 2007. Oxygen and carbon stable isotopes in otoliths record spatial isolation of Patagonian Toothfish (*Dissostichus eleginoides*). Geochimica Et Cosmochimica Acta 71:87-94.

Barnes, T. C. and B. M. Gillanders. 2013. Combined effects of extrinsic and intrinsic factors on otolith chemistry: implications for environmental reconstructions. Canadian Journal of Fisheries and Aquatic Sciences 70:1159-1166.

Bath, G. E., S. R. Thorrold, C. M. Jones, S. E. Campana, J. W. McLaren, and J. W. H. Lam. 2000. Strontium and barium uptake in aragonitic otoliths of marine fish. Geochimica Et Cosmochimica Acta 64:1705-1714.

Bradbury, I. R., S. E. Campana, and P. Bentzen. 2008. Estimating contemporary early life-history dispersal in an estuarine fish: integrating molecular and otolith elemental approaches. Molecular Ecology 17:1438-1450.

Brazner, J. C., S. E. Campana, and D. K. Tanner. 2004. Habitat fingerprints for Lake Superior coastal wetlands derived from elemental analysis of yellow perch otoliths. Transactions of the American Fisheries Society 133:692-704.

Brownie, C. and D. D. Boos. 1994. Type I error robustness of ANOVA and ANOVA on ranks when the number of treatments is large. Biometrics 50:542-549.

Buckel, J. A., B. L. Sharack, and V. S. Zdanowicz. 2004. Effect of diet on otolith composition in Pomatomus saltatrix, an estuarine piscivore. Journal of Fish Biology 64:1469-1484.

Camilli, R., C. M. Reddy, D. R. Yoerger, B. A. S. Van Mooy, M. V. Jakuba, J. C. Kinsey, C. P. McIntyre, S. P. Sylva, and J. V. Maloney. 2010. Tracking hydrocarbon plume transport and biodegradation at Deepwater Horizon. Science 330:201-204.

Campana, S. E. 1999. Chemistry and composition of fish otoliths: pathways, mechanisms and applications. Marine Ecology Progress Series 188:263-297.

Campana, S. E., G. A. Chouinard, J. M. Hanson, A. Frechet, and J. Brattey. 2000. Otolith elemental fingerprints as biological tracers of fish stocks. Fisheries Research 46:343-357.

Campana, S. E. and J. D. Neilson. 1985. Microstructure of fish otoliths. Canadian Journal of Fisheries and Aquatic Sciences 42:1014-1032.

Campana, S. E. and S. R. Thorrold. 2001. Otoliths, increments, and elements: keys to a comprehensive understanding of fish populations? Canadian Journal of Fisheries and Aquatic Sciences 58:30-38.

Capo, R. C., B. W. Stewart, and O. A. Chadwick. 1998. Strontium isotopes as tracers of ecosystem processes: theory and methods. Geoderma 82:197-225.

Carmichael, R. H., A. L. Jones, H. K. Patterson, W. C. Walton, A. Perez-Huerta, E. B. Overton, M. Dailey, and K. L. Willett. 2012. Assimilation of oil-derived elements by oysters due to the Deepwater Horizon Oil Spill. Environmental Science & Technology 46:12787-12795.

Chesney, E. J., B. M. McKee, T. Blanchard, and L. H. Chan. 1998. Chemistry of otoliths from juvenile Menhaden *Brevoortia patronus*: evaluating strontium, strontium : calcium and strontium isotope ratios as environmental indicators. Marine Ecology Progress Series 171:261-273.

Chittaro, P. M., J. D. Hogan, J. Gagnon, B. J. Fryer, and P. F. Sale. 2006. In situ experiment of ontogenetic variability in the otolith chemistry of *Stegastes partitus*. Marine Biology 149:1227-1235.

Coffey, M., F. Dehairs, O. Collette, G. Luther, T. Church, and T. Jickells. 1997. The behaviour of dissolved barium in estuaries. Estuarine Coastal and Shelf Science 45:113-121.

Courtenay, S. C., K. R. Munkittrick, H. M. C. Dupuis, R. Parker, and J. Boyd. 2002. Quantifying impacts of pulp mill effluent on fish in Canadian marine and estuarine environments: problems and progress. Water Quality Research Journal of Canada 37:79-99.

De Almeida, C. M. S., A. S. Ribeiro, T. D. Saint'Pierre, and N. Miekeley. 2009. Studies on the origin and transformation of selenium and its chemical species along the process of petroleum refining. Spectrochimica Acta Part B-Atomic Spectroscopy 64:491-499.

de Villiers, S. 1999. Seawater strontium and Sr/Ca variability in the Atlantic and Pacific oceans. Earth and Planetary Science Letters 171:623-634.

Dibble, K. L. and L. A. Meyerson. 2012. Tidal flushing restores the physiological condition of fish residing in degraded salt marshes. Plos One 7:e46161. doi:46110.41371/journal.pone.0046161.

Doubleday, Z. A., H. H. Harris, C. Izzo, and B. M. Gillanders. 2014. Strontium randomly substituting for calcium in fish otolith aragonite. Analytical Chemistry 86:865-869.

Doubleday, Z. A., C. Izzo, S. H. Woodcock, and B. M. Gillanders. 2013. Relative contribution of water and diet to otolith chemistry in freshwater fish. Aquatic Biology 18:271-280.

Dove, S. G., B. M. Gillanders, and M. J. Kingsford. 1996. An investigation of chronological differences in the deposition of trace metals in the otoliths of two temperate reef fishes. Journal of Experimental Marine Biology and Ecology 205:15-33.

Ellis, J., C. Rechsteiner, M. Moir, and S. Wilbur. 2011. Determination of volatile nickel and vanadinum species in crude oil and crude oil fractions by gas chromatography coupled to inductively coupled plasma mass spectrometry. Journal of Analytical Atomic Spectrometry 26:1674-1678.

Elsdon, T. S. and B. M. Gillanders. 2002. Interactive effects of temperature and salinity on otolith chemistry: challenges for determining environmental histories of fish. Canadian Journal of Fisheries and Aquatic Sciences 59:1796-1808.

Farmer, T. M., D. R. DeVries, R. A. Wright, and J. E. Gagnon. 2013. Using Seasonal Variation in Otolith Microchemical Composition to Indicate Largemouth Bass and Southern Flounder Residency Patterns across an Estuarine Salinity Gradient. Transactions of the American Fisheries Society 142:1415-1429.

Farrell, J. and S. E. Campana. 1996. Regulation of calcium and strontium deposition on the otoliths of juvenile tilapia, *Oreochromis niloticus*. Comparative Biochemistry and Physiology a-Physiology 115:103-109.

Ferguson, G. J., T. M. Ward, and B. M. Gillanders. 2011. Otolith shape and elemental composition: Complementary tools for stock discrimination of mulloway (*Argyrosomus japonicus*) in southern Australia. Fisheries Research 110:75-83.

Finley, M. A., S. C. Courtenay, K. L. Teather, and M. R. van den Heuvel. 2009. Assessment of northern Mummichog (*Fundulus heteroclitus macrolepidotus*) as an estuarine pollution monitoring species. Water Quality Research Journal of Canada 44:323-332.

Fodrie, F. J. and K. L. Heck. 2011. Response of coastal fishes to the Gulf of Mexico oil disaster. Plos One 6:e21609. doi:21610.21371/journal.pone.0021609.

Fritz, E. S. and E. T. Garside. 1975. Comparison of age composition, growth, and fecundity between 2 populations each of *Fundulus heteroclitus* and *Fundulus diaphanus* (Pisces-Cyprinodontidae). Canadian Journal of Zoology-Revue Canadienne De Zoologie 53:361-369.

Geffen, A. J., K. Jarvis, J. P. Thorpe, R. T. Leah, and R. D. M. Nash. 2003. Spatial differences in the trace element concentrations of Irish Sea Plaice *Pleuronectes platessa* and Whiting *Merlangius merlangus* otoliths. Journal of Sea Research 50:245-254.

Gillanders, B. M. and M. J. Kingsford. 2003. Spatial variation in elemental composition of otoliths of three species of fish (family Sparidae). Estuarine Coastal and Shelf Science 57:1049-1064.

Gonzalez, I., M. Levin, S. Jermanus, B. Watson, and M. R. Gilg. 2009. Genetic assessment of species ranges in *Fundulus heteroclitus* and *F-grandis* in northeastern Florida salt marshes. Southeastern Naturalist 8:227-244.

Grosser, Z. A., D. Bass, L. Foglio, and L. Davidowski. 2012. Determination of metals as markers oil Contamination in seafood by ICP-MS. Agro Food Industry Hi-Tech 23:24-26.

Hanor, J. S. and L. H. Chan. 1977. Non-Conservative Behavior of barium during mixing of Mississippi River and Gulf of Mexico waters. Earth and Planetary Science Letters 37:242-250.

Hem, J. D. 1970. Study and interpretation of the chemical charactoristics of natural water. USGS, Washington, D.C.

Kahn, A. and G. D. Rayner. 2003. Robustness to non-normality of common tests for the many-sample location problem. Journal of Applied Mathematics and decesion sciences 7:187-206.

Kalish, J. M. 1991. Determinants of otolith chemistry: seasonal variation in the composition of blood plasma, endolymph and otoliths of Bearded Rock Cod *Pseudophycis barbatus*. Marine Ecology-Progress Series 74:137-159.

Kennedy, B. P., J. D. Blum, C. L. Folt, and K. H. Nislow. 2000. Using natural strontium isotopic signatures as fish markers: methodology and application. Canadian Journal of Fisheries and Aquatic Sciences 57:2280-2292.

Kneib, R. T. 1986. The role of *Fundulus heteroclitus* in salt marsh trophic dynamics. American Zoologist 26:259-269.

Kneib, R. T. and A. E. Stiven. 1978. Growth, reproduction, and feeding of *Fundulus heteroclitus* (L) on a North Carolina salt marsh. Journal of Experimental Marine Biology and Ecology 31:121-140.

Kneib, R. T. and S. L. Wagner. 1994. Nekton use of vegetated marsh habitats at different stages of tidal inundation. Marine Ecology-Progress Series 106:227-238.

Kraus, R. T. and D. H. Secor. 2004. Incorporation of strontium into otoliths of an estuarine fish. Journal of Experimental Marine Biology and Ecology 302:85-106.

Liu, Z. F., J. Q. Liu, Q. Z. Zhu, and W. Wu. 2012. The weathering of oil after the Deepwater Horizon oil spill: insights from the chemical composition of the oil from the sea surface, salt marshes and sediments. Environmental Research Letters 7:035302. doi:035310.031088/031748-039326/035307/035303/035302.

Longerich, H. P., S. E. Jackson, and D. Gunther. 1996. Laser ablation inductively coupled plasma mass spectrometric transient signal data acquisition and analyte concentration calculation. Journal of Analytical Atomic Spectrometry 11:899-904.

Longmore, C., K. Fogarty, F. Neat, D. Brophy, C. Trueman, A. Milton, and S. Mariani. 2010. A comparison of otolith microchemistry and otolith shape analysis for the study of spatial variation in a deep-sea teleost, *Coryphaenoides rupestris*. Environmental Biology of Fishes 89:591-605.

Lotrich, V. A. 1975. Summer home range and movements of *Fundulus heteroclitus* (Pisces Cyprinodontidae) in a tidal creek. Ecology 56:191-198.

Lowe, M. R., D. R. DeVries, R. A. Wright, S. A. Ludsin, and B. J. Fryer. 2009. Coastal Largemouth Bass (*Micropterus salmoides*) movement in response to changing salinity. Canadian Journal of Fisheries and Aquatic Sciences 66:2174-2188.

Lowe, M. R., D. R. DeVries, R. A. Wright, S. A. Ludsin, and B. J. Fryer. 2011. Otolith microchemistry reveals substantial use of freshwater by Southern Flounder in the northern Gulf of Mexico. Estuaries and Coasts 34:630-639.

Ludden, J. N., R. Feng, G. Gauthier, J. Stix, L. Shi, D. Francis, N. Machado, and G. P. Wu. 1995. Applications of LAM-ICP-MS analysis to minerals. Canadian Mineralogist 33:419-434.

Ludsin, S. A., B. J. Fryer, and J. E. Gagnon. 2006. Comparison of solution-based versus laser ablation inductively coupled plasma mass spectrometry for analysis of larval fish otolith microelemental composition. Transactions of the American Fisheries Society 135:218-231.

Martin, G. B. and S. R. Thorrold. 2005. Temperature and salinity effects on magnesium, manganese, and barium incorporation in otoliths of larval and early juvenile spot Leiostomus xanthurus. Marine Ecology Progress Series 293:223-232.

Martin, G. B., S. R. Thorrold, and C. M. Jones. 2004. Temperature and salinity effects on strontium incorporation in otoliths of larval Spot (*Leiostomus xanthurus*). Canadian Journal of Fisheries and Aquatic Sciences 61:34-42.

Melancon, S., B. J. Fryer, J. E. Gagnon, and S. A. Ludsin. 2008. Mineralogical approaches to the study of biomineralization in fish otoliths. Mineralogical Magazine 72:627-637.

Miekeley, N., R. C. Pereira, E. A. Casartelli, A. C. Almeida, and M. D. Carvalho. 2005. Inorganic speciation analysis of selenium by ion chromatography-inductively coupled plasma-mass spectrometry and its application to effluents from a petroleum refinery. Spectrochimica Acta Part B-Atomic Spectroscopy 60:633-641.

Moody, R. M., J. Cebrian, and K. L. Heck, Jr. 2013. Interannual recruitment dynamics for resident and transient marsh species: evidence for a lack of impact by the Macondo oil spill. Plos One 8:e58376. doi:58310.51371/journal.pone.0058376.

Morales-Nin, B., A. J. Geffen, F. Cardona, C. Kruber, and F. Saborido-Rey. 2007. The effect of Prestige oil ingestion on the growth and chemical composition of Turbot otoliths. Marine Pollution Bulletin 54:1732-1741.

Morales-Nin, B., S. C. Swan, J. D. M. Gordon, M. Palmer, A. J. Geffen, T. Shimmield, and T. Sawyer. 2005. Age-related trends in otolith chemistry of *Merluccius merluccius* from the north-eastern Atlantic Ocean and the western Mediterranean Sea. Marine and Freshwater Research 56:599-607.

Muhlfeld, C. C., S. R. Thorrold, T. E. McMahon, and B. Marotz. 2012. Estimating westslope Cutthroat Trout (*Oncorhynchus clarkii lewisi*) movements in a river network using strontium isoscapes. Canadian Journal of Fisheries and Aquatic Sciences 69:906-915.

Nelson, T. R., D. Sutton, and D. DeVries. 2014. Summer movements of the Gulf Killifish (*Fundulus grandis*) in a northern Gulf of Mexico salt marsh. Estuaries and Coasts Epub:doi:10.1007/s12237-12013-19762-12235.

Neumann, R. M., C. S. Guy, and D. W. Willis. 2012. Length, weight, and associated indices. Pages 637-676 *in* A. V. Zale, D. L. Parrish, and T. M. Sutton, editors. Fisheries techniques, 3rd edition. American Fisheries Society, Bethesda, Maryland.

Niklitschek, E. J., D. H. Secor, P. Toledo, A. Lafon, and M. George-Nascimento. 2010. Segregation of SE Pacific and SW Atlantic Southern Blue Whiting stocks: integrating evidence from complementary otolith microchemistry and parasite assemblage approaches. Environmental Biology of Fishes 89:399-413.

Oros, D. R., J. R. M. Ross, R. B. Spies, and T. Mumley. 2007. Polycyclic aromatic hydrocarbon (PAH) contamination in San Francisco Bay: A 10-year retrospective of monitoring in an urbanized estuary. Environmental Research 105:101-118.

Petersen, C. W., S. Salinas, R. L. Preston, and G. W. Kidder. 2010. Spawning periodicity and reproductive behavior of *Fundulus heteroclitus* in a New England salt marsh. Copeia 2:203-210.

Ranaldi, M. M. and M. M. Gagnon. 2008. Trace metal incorporation in otoliths of Black Bream (*Acanthopagrus butcheri munro*), an indicator of exposure to metal contamination. Water Air and Soil Pollution 194:31-43.

Reay, W. G. 2009. Water quality within the York River estuary. Journal of Coastal Research 57:23-39.

Reis-Santos, P., S. E. Tanner, T. S. Elsdon, H. N. Cabral, and B. M. Gillanders. 2013. Effects of temperature, salinity and water composition on otolith elemental incorporation of *Dicentrarchus labrax*. Journal of Experimental Marine Biology and Ecology 446:245-252.

Rooker, J. R., L. L. Kitchens, M. A. Dance, R. J. D. Wells, B. Falterman, and M. Cornic. 2013. Spatial, temporal, and habitat-related variation in abundance of pelagic fishes in the Gulf of Mexico: Potential implications of the Deepwater Horizon Oil Spill. Plos One 8:e76080. doi:76010.71371/journal.pone.0076080.

Rooker, J. R., R. T. Kraus, and D. H. Secor. 2004. Dispersive behaviors of Black Drum and Red Drum: Is otolith Sr : Ca a reliable indicator of salinity history? Estuaries 27:334-341.

Rozas, L. P. and M. W. LaSalle. 1990. A comparison of the diets of Gulf Killifish, *Fundulus grandis* Baird and Girard, entering and leaving a Mississippi brackish marsh. Estuaries 13:332-336.

Rozas, L. P. and D. J. Reed. 1993. Nekton use of marsh-surface habitats in Louisiana (USA) deltaic salt marshes undergoing submergence. Marine Ecology-Progress Series 96:147-157.

Rozas, L. P. and R. J. Zimmerman. 2000. Small-scale patterns of nekton use among marsh and adjacent shallow nonvegetated areas of the Galveston Bay Estuary, Texas (USA). Marine Ecology-Progress Series 193:217-239.

Ruttenberg, B. I., S. L. Hamilton, M. J. H. Hickford, G. L. Paradis, M. S. Sheehy, J. D. Standish, O. Ben-Tzvi, and R. R. Warner. 2005. Elevated levels of trace elements in cores of otoliths and their potential for use as natural tags. Marine Ecology Progress Series 297:273-281.

Secor, D. H., A. Hendersonarzapalo, and P. M. Piccoli. 1995. Can otolith microchemistry chart patterns of migration and habitat utilization in anadromous fishes. Journal of Experimental Marine Biology and Ecology 192:15-33.

Shaw, R. G. and T. Mitchellolds. 1993. ANOVA for unbalanced data - an overview. Ecology 74:1638-1645.

Skinner, M. A., S. C. Courtenay, W. R. Parker, and R. A. Curry. 2005. Site fidelity of Mummichogs (*Fundulus heteroclitus*) in an Atlantic Canadian estuary. Water Quality Research Journal of Canada 40:288-298.

Smith, G. M., A. T. Khan, J. S. Weis, and P. Weis. 1995. Behavior and brain chemistry correlates in Mummichogs (*Fundulus heteroclitus*) from polluted and unpolluted environments. Marine Environmental Research 39:329-333.

Smith, G. M. and J. S. Weis. 1997. Predator-prey relationships in Mummichogs (*Fundulus heteroclitus* (L)): Effects of living in a polluted environment. Journal of Experimental Marine Biology and Ecology 209:75-87.

Smith, S. V., R. W. Buddemeier, R. C. Redalje, and J. E. Houck. 1979. Strontium-calcium thermometry in coral skeletons. Science 204:404-407.

Sohn, D., S. Kang, and S. Kim. 2005. Stock identification of Chum Salmon (*Oncorhynchus keta*) using trace elements in otoliths. Journal of Oceanography 61:305-312.

Speed, F. M., R. R. Hocking, and O. P. Hackney. 1978. Methods of analysis of linear-models with unbalanced data. Journal of the American Statistical Association 73:105-112.

Statham, P. J. 2012. Nutrients in estuaries - An overview and the potential impacts of climate change. Science of the Total Environment 434:213-227.

Sturrock, A. M., C. N. Trueman, A. M. Darnaude, and E. Hunter. 2012. Can otolith elemental chemistry retrospectively track migrations in fully marine fishes? Journal of Fish Biology 81:766-795.

Swart, P. K. 1979. Effect of seawater calcium concentrations on the growth ans skeletal compositions of a Scleractinian coral *Acropora squamosa*. Journal of Sedimentary Petrology 49:951-954.

Szedlmayer, S. T. and P. A. Mudrak. 2014. Influence of age-1 conspecifics, sediment type, dissolved oxygen, and the Deepwater Horizion Oil Spill on the recruitment of age-0 Red Snapper in the Northeast Gulf of Mexico during 2010 and 2011. North American Journal of Fisheries Management 34:443-452.

Tanner, S. E., P. Reis-Santos, R. P. Vasconcelos, V. F. Fonseca, S. Franca, H. N. Cabral, and S. R. Thorrold. 2013. Does otolith geochemistry record ambient environmental conditions in a temperate tidal estuary? Journal of Experimental Marine Biology and Ecology 441:7-15.

Tanner, S. E., R. P. Vasconcelos, P. Reis-Santos, H. N. Cabral, and S. R. Thorrold. 2011. Spatial and ontogenetic variability in the chemical composition of juvenile Common Sole (*Solea solea*) otoliths. Estuarine Coastal and Shelf Science 91:150-157.

Teo, S. L. H. and K. W. Able. 2003a. Growth and production of the Mummichog (*Fundulus heteroclitus*) in a restored salt marsh. Estuaries 26:51-63.

Teo, S. L. H. and K. W. Able. 2003b. Habitat use and movement of the Mummichog (*Fundulus heteroclitus*) in a restored salt marsh. Estuaries 26:720-730.

Thorrold, S. R., C. M. Jones, P. K. Swart, and T. E. Targett. 1998. Accurate classification of juvenile Weakfish *Cynoscion regalis* to estuarine nursery areas based on chemical signatures in otoliths. Marine Ecology-Progress Series 173:253-265.

Thorrold, S. R., C. Latkoczy, P. K. Swart, and C. M. Jones. 2001. Natal homing in a marine fish metapopulation. Science 291:297-299.

Thorrold, S. R. and S. Shuttleworth. 2000. In situ analysis of trace elements and isotope ratios in fish otoliths using laser ablation sector field inductively coupled plasma mass spectrometry. Canadian Journal of Fisheries and Aquatic Sciences 57:1232-1242.

Thresher, R. E. 1999. Elemental composition of otoliths as a stock delineator in fishes. Fisheries Research 43:165-204.

Vasconcelos, R. P., P. Reis-Santos, S. Tanner, V. Fonseca, C. Latkoczy, D. Gunther, M. J. Costa, and H. Cabral. 2007. Discriminating estuarine nurseries for five fish species through otolith elemental fingerprints. Marine Ecology-Progress Series 350:117-126.

Walther, B. D., T. Dempster, M. Letnic, and M. T. McCulloch. 2011. Movements of diadromous fish in large unregulated tropical rivers inferred from geochemical tracers. Plos One 6.

Walther, B. D. and S. R. Thorrold. 2006. Water, not food, contributes the majority of strontium and barium deposited in the otoliths of a marine fish. Marine Ecology-Progress Series 311:125-130.

Wang, Y., X. Li, B. H. H. Li, Z. Y. Y. Shen, C. H. H. Feng, and Y. X. X. Chen. 2012. Characterization, sources, and potential risk assessment of PAHs in surface sediments from nearshore and farther shore zones of the Yangtze estuary, China. Environmental Science and Pollution Research 19:4148-4158.

Ward, J. H. 1963. Hierarchical grouping to optimize an objective function. Journal of the American Statistical Association 58:236-244.

Webb, S. D., S. H. Woodcock, and B. M. Gillanders. 2012. Sources of otolith barium and strontium in estuarine fish and the influence of salinity and temperature. Marine Ecology Progress Series 453:189-199.

Weis, J. S. and A. A. Khan. 1990. Effects of mercury on the feeding-behavior of the Mummichog, *Fundulus-heteroclitus* from a polluted habitat. Marine Environmental Research 30:243-249.

Weis, J. S., J. Samson, T. Zhou, J. Skurnick, and P. Weis. 2001. Prey capture ability of Mummichogs (*Fundulus heteroclitus*) as a behavioral biomarker for contaminants in estuarine systems. Canadian Journal of Fisheries and Aquatic Sciences 58:1442-1452.

Whitehead, A. 2010. The evolutionary radiation of diverse osmotolerant physiologies in Killifish (*Fundulus* sp.). Evolution 64:2070-2085.

Whitehead, A., B. Dubansky, C. Bodinier, T. I. Garcia, S. Miles, C. Pilley, V. Raghunathan, J. L. Roach, N. Walker, R. B. Walter, C. D. Rice, and F. Galvez. 2012. Genomic and physiological footprint of the Deepwater Horizon oil spill on resident marsh fishes. Proceedings of the National Academy of Sciences 109:doi: 10.1073/pnas.1109545108

Wishart, D. 1969. An algorithm for hierarchical classifications. Biometrics 25:165-170.

Wolff, B. A., B. M. Johnson, A. R. Breton, P. J. Martinez, and D. L. Winkelman. 2012. Origins of invasive piscivores determined from the strontium isotope ratio (Sr-87/Sr-86) of otoliths. Canadian Journal of Fisheries and Aquatic Sciences 69:724-739.

Zeigler, J. M. and G. W. Whitledge. 2010. Otolith trace element and stable isotopic compositions differentiate fishes from the Middle Mississippi River, its tributaries, and floodplain lakes. Hydrobiologia 661:289-302.

Table 1. Sampling sites in each state, with lat/lon coordinates, and an indication of whether they had any oil exposure during the DHOS. Waters surrounding the Chevron Refinery are assumed to have oil and refinery related effluents.

Site	Oil / No Oil	Coordinates
Louisiana		
Barataria A (BA)	Oil	29.458115°N -89.891896°W
Barataria B (BB)	No Oil	29.466678°N -90.035479°W
Mississippi		
Refinery (RF)	Oil*	30.345690°N -88.471610°W
Crooked Creek (CK)	No Oil	30.362454°N -88.426863°W
Alabama		
Fowl River (FR)	No Oil	30.433143°N -88.135780°W
Fowl A (FA)	Oil	30.341470°N -88.190090°W
Fowl B (FB)	No Oil	30.362537°N -88.198353°W
Perdido (PD)	Oil	30.298364°N -87.525678°W
Wolf (WF)	No Oil	30.304972°N -87.578985°W
Florida		
Hogtown Bayou (HT)	No Oil	30.399154°N -86.231548°W

Table 2. Numbers of *Fundulus grandis* used for otolith microchemistry analysis from each size class (≤59, 60-69, 70-79, 80-89, ≥90 (mm)), for each site and each season.

Fall		**BB**	**BA**	**RF**	**CK**	**FB**	**FA**	**FR**	**WF**	**PD**	**HT**
Size Class (mm)	≤ 59	4	4	4	4	4	4	4	3	3	3
	60-69	7	0	4	3	4	4	4	4	3	2
	70-79	3	9	4	3	9	6	4	4	4	4
	80-89	3	3	6	3	2	5	4	4	4	5
	≥ 90	3	4	2	5	0	1	4	4	4	6
Total Otolith Site		20	20	20	18	19	20	20	19	18	20
Total Otolith Season		194									
Winter											
Size Class (mm)	≤ 59	5	12	18	4	9	4	4	3	4	4
	60-69	5	6	0	4	2	4	3	4	3	4
	70-79	1	2	1	4	2	4	4	4	7	4
	80-89	0	0	0	7	0	7	4	4	5	4
	≥ 90	0	0	0	1	0	1	4	4	0	4
Total Otolith Site		11	20	19	20	13	20	19	19	19	20
Total Otolith Season		180									
Spring											
Size Class (mm)	≤ 59	4	4	4	0	4	4	4	4	0	2
	60-69	5	5	4	8	4	4	6	4	5	6
	70-79	8	10	4	4	4	6	8	4	7	4
	80-89	3	1	8	4	4	3	1	3	4	4
	≥ 90	0	0	0	4	4	3	1	4	4	4
Total Otolith Site		20	20	20	20	20	20	20	19	20	20
Total Otolith Season		199									
Summer											
Size Class (mm)	≤ 59	3	4	4	4	4	4	17	0	18	4
	60-69	7	4	5	4	4	6	0	3	0	0
	70-79	3	4	3	4	4	2	2	6	0	5
	80-89	5	4	4	4	5	5	0	6	2	7
	≥ 90	2	4	4	4	3	3	1	5	0	4
Total Otolith Site		20	20	20	20	20	20	20	20	20	20
Total Otolith Season		200									
Total Otolith Samples		773									

Table 3. Elements whose concentrations were above detection limit in at least 50% of otoliths during otolith microchemistry analysis. The total number of samples that were above detection limit for each element is shown by the # > LOD row, and the percentage of samples this number equals is shown in the % > LOD row.

Element	**Mg^{25}**	**Al^{27}**	**Mn^{55}**	**Fe^{57}**	**Cu^{63}**	**Zn^{66}**	**Rb^{85}**
# > LOD	616	729	731	773	655	764	549
% > LOD	79.7	94.3	94.6	100	84.7	98.8	71.0

Element	**Sr^{86}**	**Sr^{88}**	**Sn^{118}**	**Ba^{137}**	**Pb^{208}**	**U^{238}**
# > LOD	773	773	549	773	711	596
% > LOD	100	100	71.0	100	92.0	77.1

Table 4. Mean (± 1SE) whole otolith concentrations (ppm) for elements that were significantly different across sites (Mn^{55}, Fe^{57}, Rb^{85}, Sr^{86}, Sr^{88}, Ba^{137}, Pb^{208}, and U^{238}), for each site and season.

Sites	**BB**	**BA**	**RF**	**CK**	**FB**
Mn^{55}	1.665 ± 0.095	1.406 ± 0.083	1.006 ± 0.051	1.045 ± 0.060	1.780 ± 0.119
Fe^{57}	349.381 ± 9.60	361.838 ± 7.56	361.552 ± 14.589	357.953 ± 12.698	471.355 ± 17.816
Rb^{85}	0.118 ± 0.012	0.110 ± 0.012	0.098 ± 0.011	0.103 ± 0.013	0.126 ± 0.009
Sr^{86}	2332.074 ± 38.010	2577.348 ± 44.455	2905.258 ± 40.657	3207.657 ± 51.534	2964.243 ± 52.912
Sr^{88}	2917.919 ± 48.746	3225.212 ± 67.693	3647.544 ± 64.757	4110.839 ± 67.126	3743.039 ± 88.085
Ba^{137}	17.244 ± 0.569	15.872 ± 0.578	4.400 ± 0.287	5.357 ± 0.251	4.143 ± 0.121
Pb^{208}	0.298 ± 0.030	0.381 ± 0.045	0.198 ± 0.023	0.263 ± 0.036	0.278 ± 0.051
U^{238}	0.0008 ± 0.0001	0.0013 ± 0.0003	0.0009 ± 0.0002	0.0009 ± 0.0001	0.0009 ± 0.0001
Sites	**FA**	**FR**	**WF**	**PD**	**HT**
Mn^{55}	2.448 ± 0.172	2.806 ± 0.160	1.046 ± 0.092	0.935 ± 0.098	1.107 ± 0.085
Fe^{57}	417.878 ± 10.697	379.817 ± 16.608	387.693 ± 7.787	380.891 ± 9.829	414.025 ± 19.168
Rb^{85}	0.105 ± 0.008	0.135 ± 0.015	0.122 ± 0.009	0.102 ± 0.011	0.079 ± 0.009
Sr^{86}	2904.567 ± 42.556	2692.949 ± 30.388	2845.266 ± 28.382	3230.709 ± 43.205	2989.972 ± 39.772
Sr^{88}	3571.960 ± 76.398	3273.541 ± 75.834	3729.452 ± 59.314	4146.362 ± 75.048	3680.612 ± 87.677
Ba^{137}	4.429 ± 0.115	9.247 ± 0.321	3.571 ± 0.100	4.780 ± 0.306	3.107 ± 0.108
Pb^{208}	0.417 ± 0.142	0.490 ± 0.230	0.618 ± 0.191	0.381 ± 0.107	0.762 ± 0.643
U^{238}	0.0009 ± 0.0001	0.0008 ± 0.0001	0.0009 ± 0.0001	0.0007 ± 0.0001	0.0006 ± 0.00009
Seasons	**Fall**	**Winter**	**Spring**	**Summer**	
Mn^{55}	1.647 ± 0.080	1.546 ± 0.100	1.204 ± 0.041	1.706 ± 0.093	
Fe^{57}	274.030 ± 6.033	381.315 ± 8.307	458.556 ± 6.037	434.305 ± 7.666	
Rb^{85}	0.031 ± 0.004	0.141 ± 0.011	0.124 ± 0.003	0.143 ± 0.005	
Sr^{86}	3276.539 ± 30.031	2863.565 ± 28.231	2631.676 ± 23.291	2711.328 ± 24.799	
Sr^{88}	3847.070 ± 41.757	2770.011 ± 45.514	3774.076 ± 35.693	3963.840 ± 37.767	
Ba^{137}	8.824 ± 0.530	6.321 ± 0.325	6.075 ± 0.323	7.379 ± 0.377	
Pb^{208}	0.529 ± 0.265	0.103 ± 0.012	0.173 ± 0.021	0.812 ± 0.132	
U^{238}	0.0012 ± 0.00009	0.0011 ± 0.0001	0.0005 ± 0.00003	0.0008 ± 0.00007	

Table 5. Results of the Linear Discriminant Function Analysis (LDFA) using each site as a group in the analysis (prior probability of being placed into each group = 10%). Percentage of correct classification of *F. grandis* to site is shown by the bolded diagonal and rows correspond to the actual collection site, while columns are the site assigned by the LDFA.

	BB	**BA**	**RF**	**CK**	**FB**	**FA**	**FR**	**WF**	**PD**	**HT**
BB	**68**	31	0	0	0	0	1	0	0	0
BA	22	**64**	0	0	0	0	14	0	0	0
RF	1	3	**22**	11	14	1	0	38	6	4
CK	0	1	19	**13**	4	3	1	14	36	9
FB	0	0	3	4	**36**	18	1	19	12	6
FA	0	0	8	4	25	**41**	4	10	4	5
FR	0	1	4	0	4	4	**86**	1	0	0
WF	0	0	21	9	1	6	0	**40**	9	13
PD	1	1	0	19	0	3	3	13	**45**	14
HT	0	0	18	4	22	10	0	18	15	**14**

Table 6. Linear dscriminant variables generated by the LDFA (LD-1 - LD-7) with all sites as groups, and the importance of each discriminant variable in classifying fish to sites, the proportion of trace column. The value for each element in a discriminant variable column corresponds to the effect each has on a discriminator. The larger the absolute value of each element, the greater the effect.

Linear Discriminants		LD-1	LD-2	LD-3	LD-4	LD-5	LD-6	LD-7
Proportion of trace (%)		88.42	8.27	1.68	1.06	0.32	0.22	0.03
Significantly different elements across sites used in LDA	**Mn^{55}**	0.028	-1.150	0.179	-0.331	-0.053	0.149	-0.207
	Fe^{57}	0.121	-0.250	0.625	1.004	0.141	-0.143	-0.043
	Rb^{85}	0.030	0.150	0.069	-0.499	0.660	-0.457	0.600
	Sr^{86}	0.830	0.096	1.026	0.152	-0.499	-0.193	0.840
	Sr^{88}	0.196	0.356	0.006	-0.505	0.572	0.179	-1.032
	Ba^{137}	-2.084	0.367	0.696	0.082	-0.046	-0.123	-0.026
	U^{238}	-0.071	0.113	-0.053	0.195	0.292	0.988	0.080

Table 7. Results of the Linear Discriminant Function Analysis (LDFA) using regional site clusters as each group in the analysis (prior probability of being placed into each group = 25%). Percentage of correct classification of *F. grandis* to region is shown by the bolded diagonal and rows correspond to the actual collection region, while columns are the region assigned by the LDFA.

	LA	MS	AL W.	AL E. - FL
LA	**97**	0	3	0
MS	3	**46**	4	47
AL W.	3	15	**67**	15
AL E.- FL	1	31	9	**58**

Table 8. Linear discriminant variables generated by the LDFA (LD-1 - LD-3) with regional sites as groups, and the importance of each discriminant variable in classifying fish to regions, the proportion of trace column. The value for each element in a discriminant variable column corresponds to the effect each has on a discriminator variable. The larger the absolute value of each element the greater the effect.

Linear Discriminants		LD-1	LD-2	LD-3
Proportion of trace (%)		91.06	8.70	0.24
Significantly different elements across sites used in LDA	**Mn^{55}**	-0.176	-1.109	0.367
	Fe^{57}	0.032	-0.420	-0.827
	Rb^{85}	-0.079	0.122	0.254
	Sr^{86}	-0.609	-0.045	0.052
	Sr^{88}	-0.161	0.336	0.299
	Ba^{137}	1.838	0.167	-0.011
	U^{238}	0.128	0.089	0.317

Table 9. Mean (± 1SE) otolith core concentrations (ppm) for elements that were significantly different across sites (Mn^{55}, Fe^{57}, Sr^{86}, Sr^{88}, and Ba^{137}) and seasons (Fe^{57}, Rb^{85}, Sr^{86}, and Ba^{137}), for each site and season.

Sites	**BB**	**BA**	**RF**	**CK**	**FB**
Mn^{55}	2.741 ± 0.396	1.641 ± 0.162	1.305 ± 0.134	1.509 ± 0.256	1.880 ± 0.188
Fe^{57}	416.953 ± 35.585	368.391 ± 21.039	371.424 ± 31.682	361.682 ± 33.017	455.685 ± 30.976
Sr^{86}	2531.176 ± 85.091	2878.238 ± 98.708	3168.058 ± 99.793	3437.262 ± 121.649	3341.432 ± 123.728
Sr^{88}	3146.566 ± 134.516	3686.456 ± 116.628	4046.660 ± 164.351	4431.836 ± 139.272	4145.091 ± 216.105
Ba^{137}	18.221 ± 1.173	17.483 ± 1.182	4.752 ± 0.712	6.564 ± 0.611	4.119 ± 0.288

Sites	**FA**	**FR**	**WF**	**PD**	**HT**
Mn^{55}	3.005 ± 0.480	3.300 ± 0.361	1.479 ± 0.145	1.446 ± 0.392	1.168 ± 0.179
Fe^{57}	453.917 ± 19.065	374.535 ± 36.674	388.399 ± 17.540	387.111 ± 26.547	400.886 ± 48.978
Sr^{86}	3113.449 ± 107.278	2944.644 ± 69.799	3073.839 ± 70.381	3352.637 ± 121.967	3284.897 ± 113.180
Sr^{88}	3832.628 ± 180.945	3619.543 ± 190.196	4078.653 ± 147.973	4225.138 ± 173.205	4196.871 ± 212.131
Ba^{137}	4.777 ± 0.631	9.228 ± 0.734	3.344 ± 0.227	6.604 ± 1.225	3.056 ± 0.268

Seasons	**Fall**	**Winter**	**Spring**	**Summer**
Fe^{57}	277.455 ± 15.185	392.023 ± 21.876	479.900 ± 12.213	442.216 ± 16.911
Rb^{85}	0.069 ± 0.028	0.238 ± 0.058	0.099 ± 0.008	0.123 ± 0.012
Sr^{86}	3536.768 ± 73.392	3147.475 ± 68.637	2895.564 ± 52.279	2870.446 ± 56.945
Ba^{137}	9.413 ± 1.049	7.502 ± 0.857	7.600 ± 0.903	6.744 ± 0.739

Table 10. Mean (± 1SE) otolith edge concentrations (ppm) for elements that were significantly different across sites (Fe^{57}, Sr^{86}, Sr^{88}, and Ba^{137}) and seasons (Fe^{57}, Sr^{86}, Sr^{88}, and Ba^{137}), for each site and season.

Sites	**BB**	**BA**	**RF**	**CK**	**FB**
Fe^{57}	385.757 ± 25.312	354.748 ± 19.528	360.654 ± 34.346	340.089 ± 29.662	452.062 ± 33.544
Sr^{86}	2214.027 ± 75.823	2508.125 ± 85.205	2827.173 ± 64.805	3170.635 ± 115.165	2796.220 ± 127.995
Sr^{88}	2604.115 ± 113.638	3077.932 ± 159.764	3451.961 ± 161.579	3886.739 ± 247.201	3361.128 ± 170.602
Ba^{137}	16.879 ± 1.121	15.477 ± 1.281	3.532 ± 0.293	5.108 ± 0.437	4.351 ± 0.261

Sites	**FA**	**FR**	**WF**	**PD**	**HT**
Fe^{57}	440.235 ± 24.242	381.610 ± 37.335	384.091 ± 19.336	358.827 ± 29.425	406.778 ± 46.852
Sr^{86}	2776.422 ± 86.462	2506.956 ± 73.118	2738.585 ± 70.349	2885.048 ± 84.497	2878.117 ± 73.350
Sr^{88}	3469.056 ± 191.904	3043.929 ± 160.522	3376.255 ± 183.821	3471.871 ± 152.449	3561.162 ± 195.720
Ba^{137}	4.082 ± 0.267	9.114 ± 0.986	3.267 ± 0.151	2.935 ± 0.287	2.635 ± 0.227

Seasons	**Fall**	**Winter**	**Spring**	**Summer**
Fe^{57}	263.557 ± 14.469	357.401 ± 20.673	483.679 ± 12.265	441.303 ± 15.014
Sr^{86}	3116.229 ± 59.105	2610.515 ± 54.170	2472.605 ± 49.299	2721.173 ± 59.080
Sr^{88}	3521.139 ± 87.594	2289.648 ± 50.749	3558.796 ± 85.554	3952.076 ± 89.749
Ba^{137}	8.804 ± 1.109	5.630 ± 0.648	5.249 ± 0.521	7.269 ± 0.824

Table 11. Salinity (ppt) and temperature (°C) at each site and season during each collection event.

Fall	**BB**	**BA**	**RF**	**CK**	**FB**	**FA**	**FR**	**WF**	**PD**	**HT**
Salinity (ppt)	7.1	16.7	17.3	20.3	22.7	21.2	8.1	18.7	20.6	12.2
Temperature (°C)	29.3	31	28.4	28.6	19.4	19.8	21.3	20.2	21.1	26.8
Winter										
Salinity (ppt)	1.5	13.6	19.8	14.9	10.3	6.6	0.8	14.4	25.2	4.2
Temperature (°C)	17	15.9	16.5	15.1	16	13.2	16	19	18.1	15.4
Spring										
Salinity (ppt)	0.4	5.7	13	15.4	7	7.1	2.4	12.5	25.4	13.2
Temperature (°C)	24.9	23.9	25.4	23.8	23.4	21.6	23.8	24.3	23.8	22.5
Summer										
Salinity (ppt)	5.5	9.7	14.1	14.7	9.8	11.1	2.4	13.6	22.1	13.2
Temperature (°C)	30.2	29	28.9	30.3	30.8	30.3	28.2	27.3	26.7	30.2

Table 12. Mean (± 1SE) water concentrations (element mmol, mol^{-1} Ca_{water}, Mg reported in Mg mol, mol^{-1} Ca_{water}) of elements that were significantly different across sites (Mg:Ca, Mn:Ca, Zn:Ca, and Ba:Ca) and seasons (Sr:Ca), for each site and season.

Sites	**BB**	**BA**	**RF**	**CK**	**FB**
Mg:Ca	2.291 ± 0.833	3.577 ± 0.322	4.076 ± 0.220	3.802 ± 0.445	3.854 ± 0.175
Mn:Ca	0.117 ± 0.033	0.093 ± 0.038	0.220 ± 0.070	0.143 ± 0.013	0.087 ± 0.009
Zn:Ca	8.490 ± 4.090	1.607 ± 0.534	0.530 ± 0.300	0.567 ± 0.286	0.320 ± 0.147
Ba:Ca	0.421 ± 0.065	0.192 ± 0.022	0.037 ± 0.004	0.036 ± 0.008	0.105 ± 0.045

Sites	**FA**	**FR**	**WF**	**PD**	**HT**
Mg:Ca	4.164 ± 0.085	3.018 ± 0.748	4.164 ± 0.169	4.318 ± 0.179	4.370 ± 0.016
Mn:Ca	0.083 ± 0.028	1.603 ± 0.675	0.383 ± 0.117	0.033 ± 0.013	0.640 ± 0.295
Zn:Ca	1.047 ± 0.460	0.823 ± 0.226	0.370 ± 0.093	0.087 ± 0.047	0.347 ± 0.252
Ba:Ca	0.259 ± 0.091	0.196 ± 0.042	0.041 ± 0.002	0.017 ± 0.003	0.031 ± 0.007

Seasons	**Winter**	**Spring**	**Summer**
Sr:Ca	6.577 ± 0.268	6.139 ± 0.467	7.788 ± 0.420

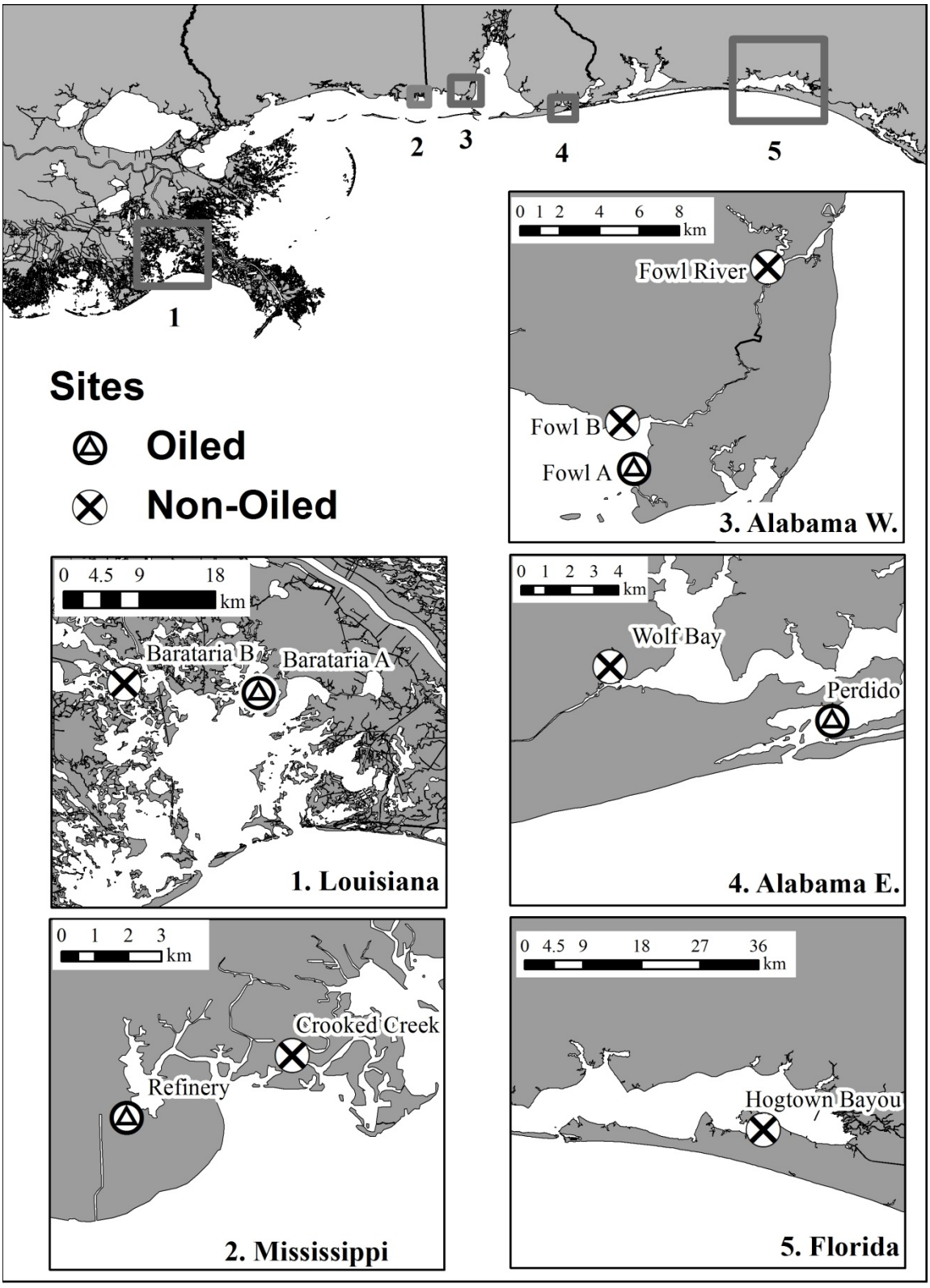
1
2
3
4
5
Sites
Oiled
Non-Oiled
0 1 2 4 6 8
km
Fowl River
Fowl B
Fowl A
3. Alabama W.
0 4.5 9 18
km
Barataria B
Barataria A
1. Louisiana
0 1 2 3 4
km
Wolf Bay
Perdido
4. Alabama E.
0 1 2 3
km
Crooked Creek
Refinery
2. Mississippi
0 4.5 9 18 27 36
km
Hogtown Bayou
5. Florida

Figure 1

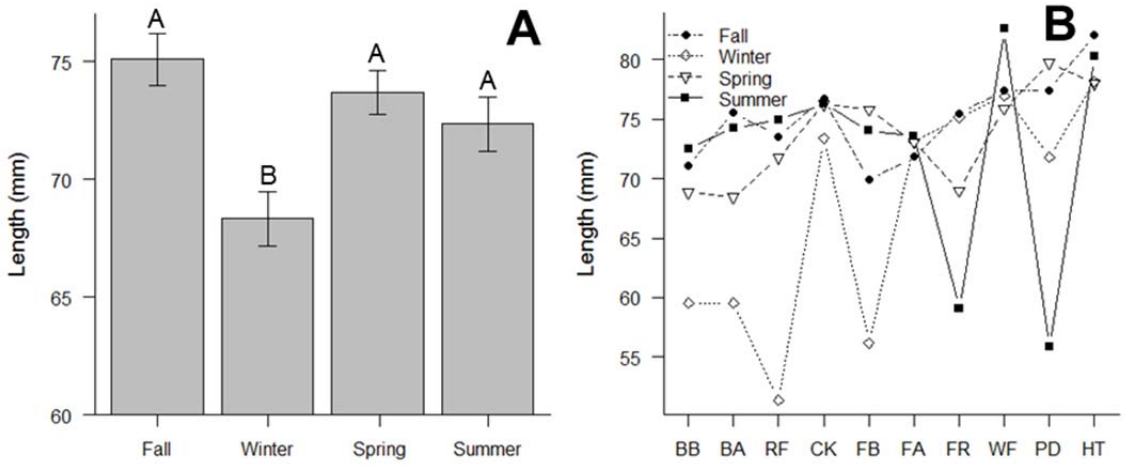
A
Length (mm)
75
70
65
60
A
B
A
A
Fall
Winter
Spring
Summer
B
Fall
Winter
Spring
Summer
Length (mm)
80
75
70
65
60
55
BB
BA
RF
CK
FB
FA
FR
WF
PD
HT

Figure 2

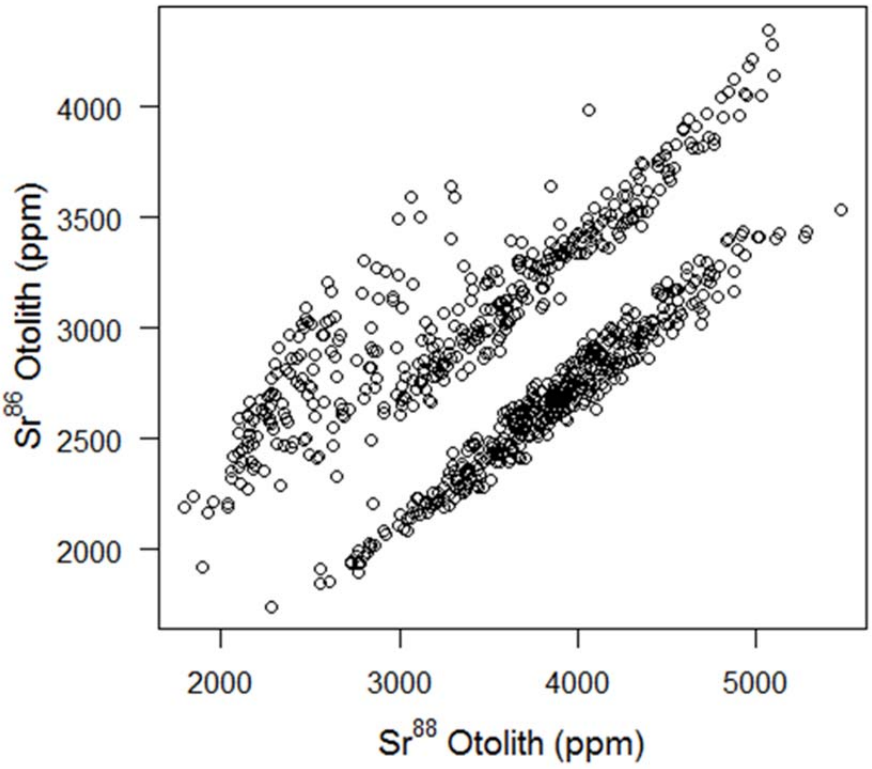
4000
3500
3000
2500
2000
Sr^{86} Otolith (ppm)
2000
3000
4000
5000
Sr^{88} Otolith (ppm)

Figure 3

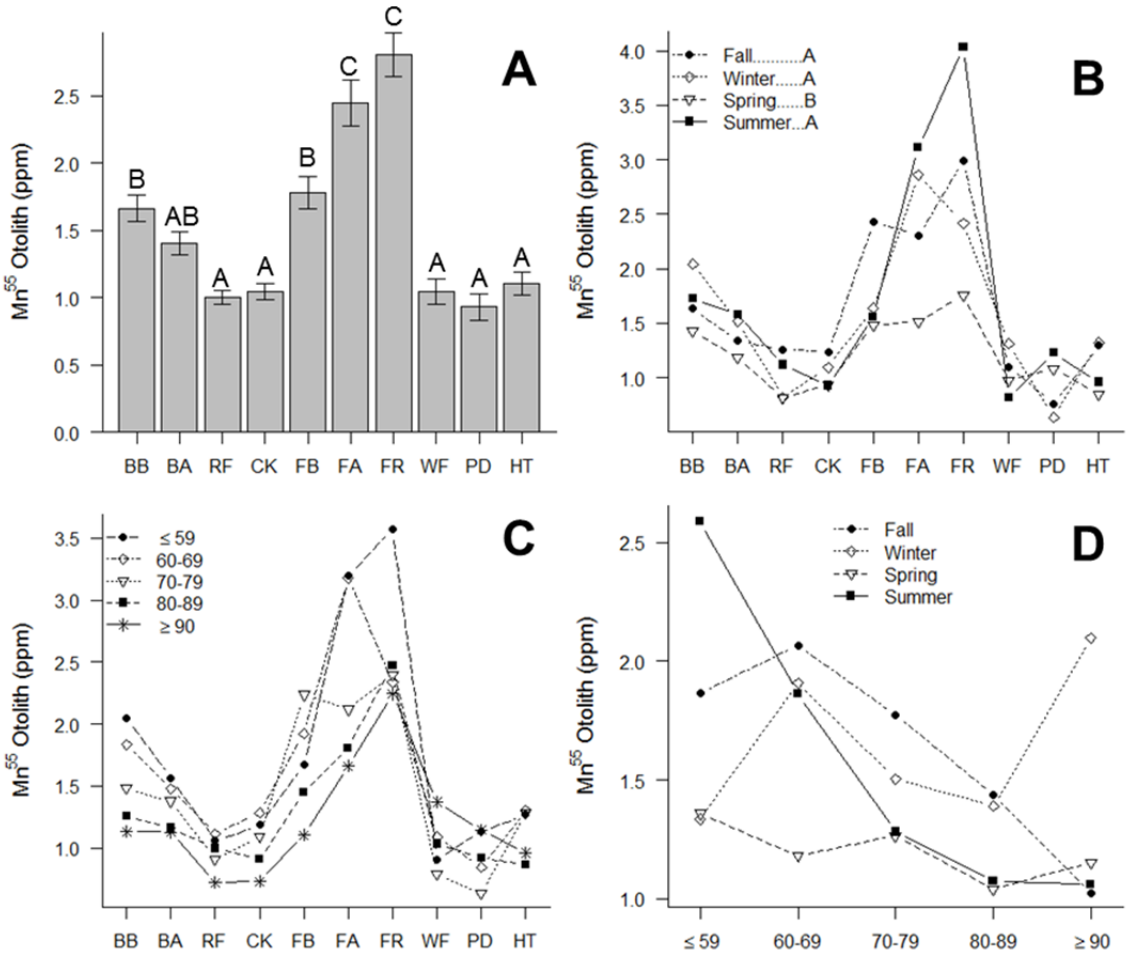
A
B
C
D
Mn55 Otolith (ppm)
BB BA RF CK FB FA FR WF PD HT
B AB A A B C C A A A
Fall.....A
Winter.....A
Spring.....B
Summer...A
≤ 59
60-69
70-79
80-89
≥ 90
Fall
Winter
Spring
Summer

Figure 4

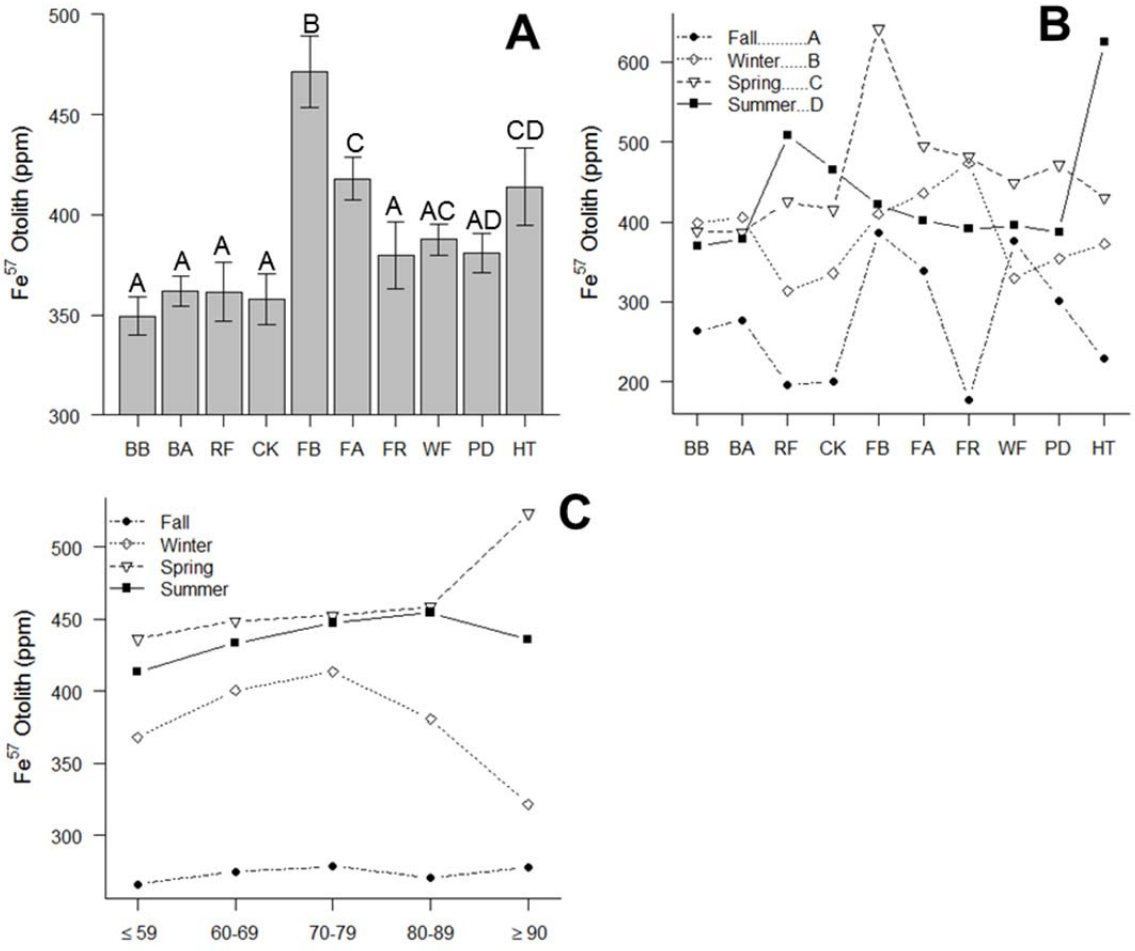
A
B
C
Fe57 Otolith (ppm)
BB BA RF CK FB FA FR WF PD HT
A A A A B C A AC AD CD
Fall.....A
Winter.....B
Spring.....C
Summer...D
Fall
Winter
Spring
Summer
≤ 59
60-69
70-79
80-89
≥ 90

Figure 5

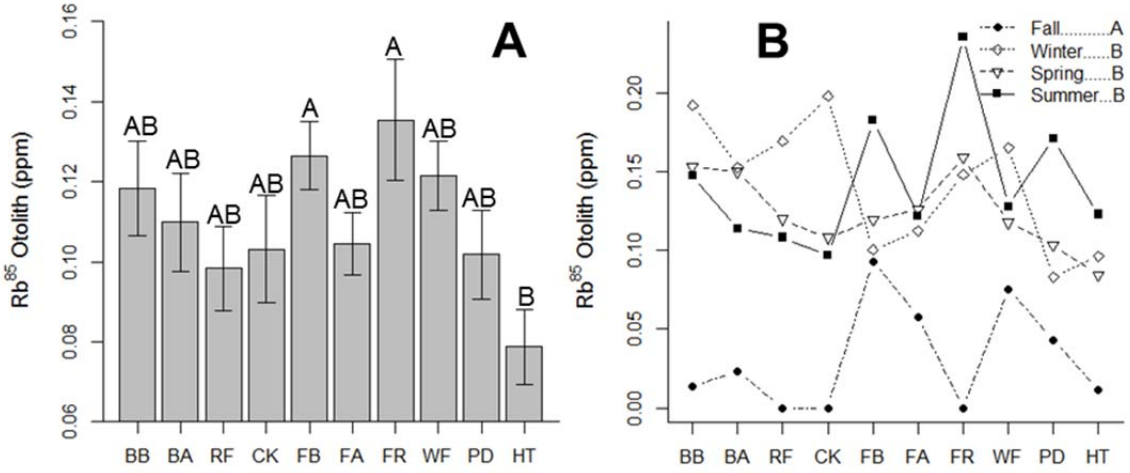
A
B
Rb85 Otolith (ppm)
0.06
0.08
0.10
0.12
0.14
0.16
0.00
0.05
0.10
0.15
0.20
AB
AB
AB
AB
A
AB
A
AB
AB
B
BB
BA
RF
CK
FB
FA
FR
WF
PD
HT
Fall.....A
Winter.....B
Spring.....B
Summer...B

Figure 6

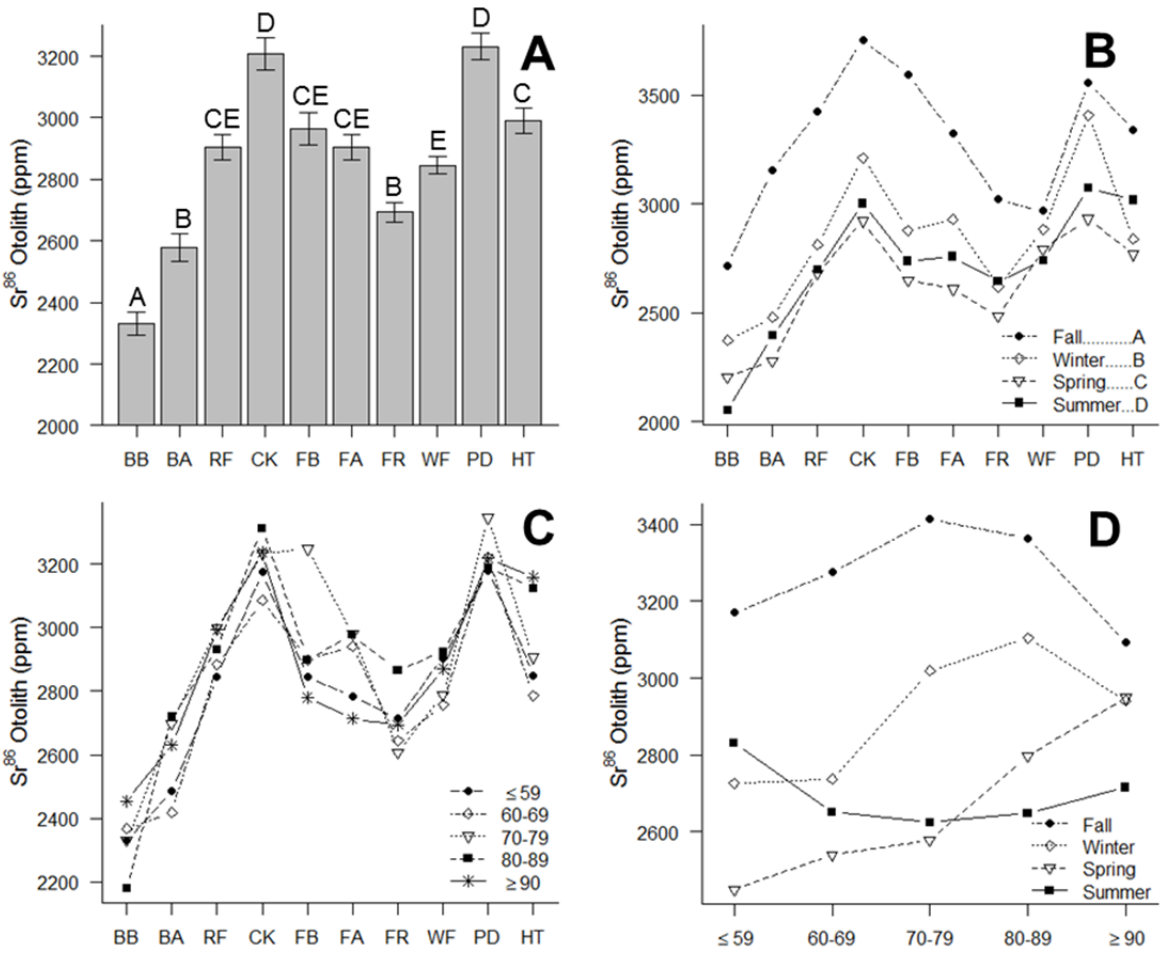
A
B
C
D
Sr^{86} Otolith (ppm)
BB BA RF CK FB FA FR WF PD HT
Fall.....A
Winter.....B
Spring.....C
Summer...D
≤59
60-69
70-79
80-89
≥90
Fall
Winter
Spring
Summer

Figure 7

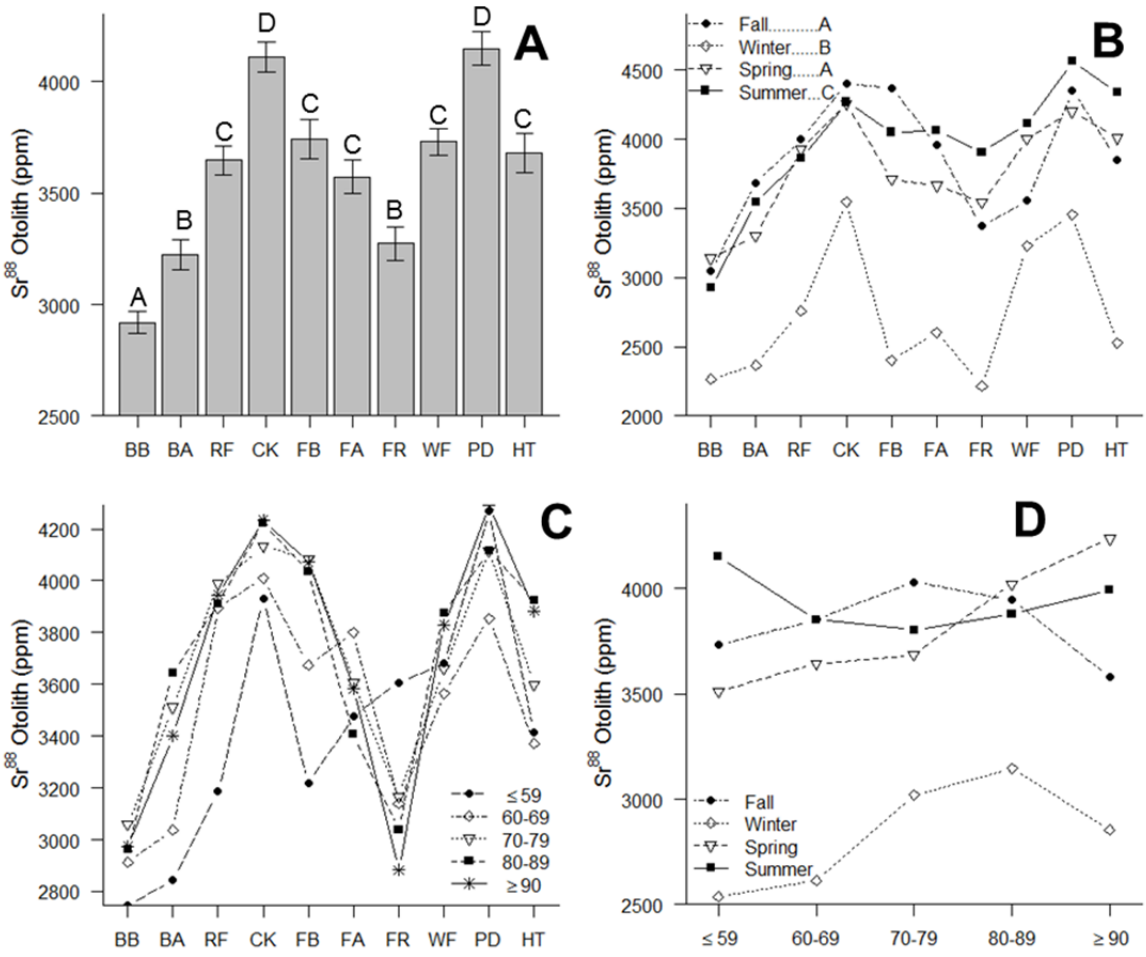
A
B
C
D
Sr88 Otolith (ppm)
BB BA RF CK FB FA FR WF PD HT
Fall.....A
Winter.....B
Spring.....A
Summer....C
≤ 59
60-69
70-79
80-89
≥ 90
Fall
Winter
Spring
Summer

Figure 8

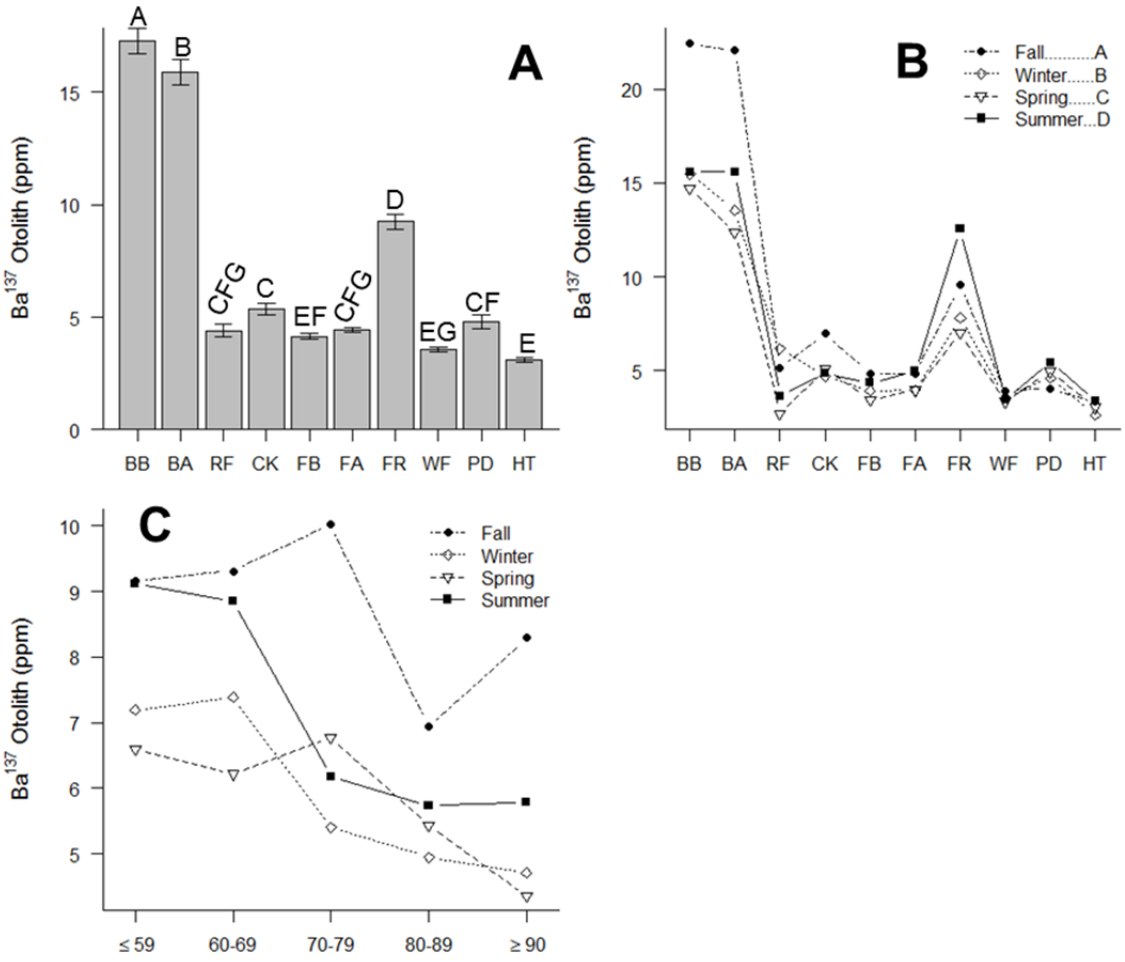
A
B
CFG
C
EF
CFG
D
EG
CF
E
Ba137 Otolith (ppm)
BB BA RF CK FB FA FR WF PD HT
B
Fall.....A
Winter.....B
Spring.....C
Summer...D
C
Fall
Winter
Spring
Summer
≤ 59
60-69
70-79
80-89
≥ 90

Figure 9

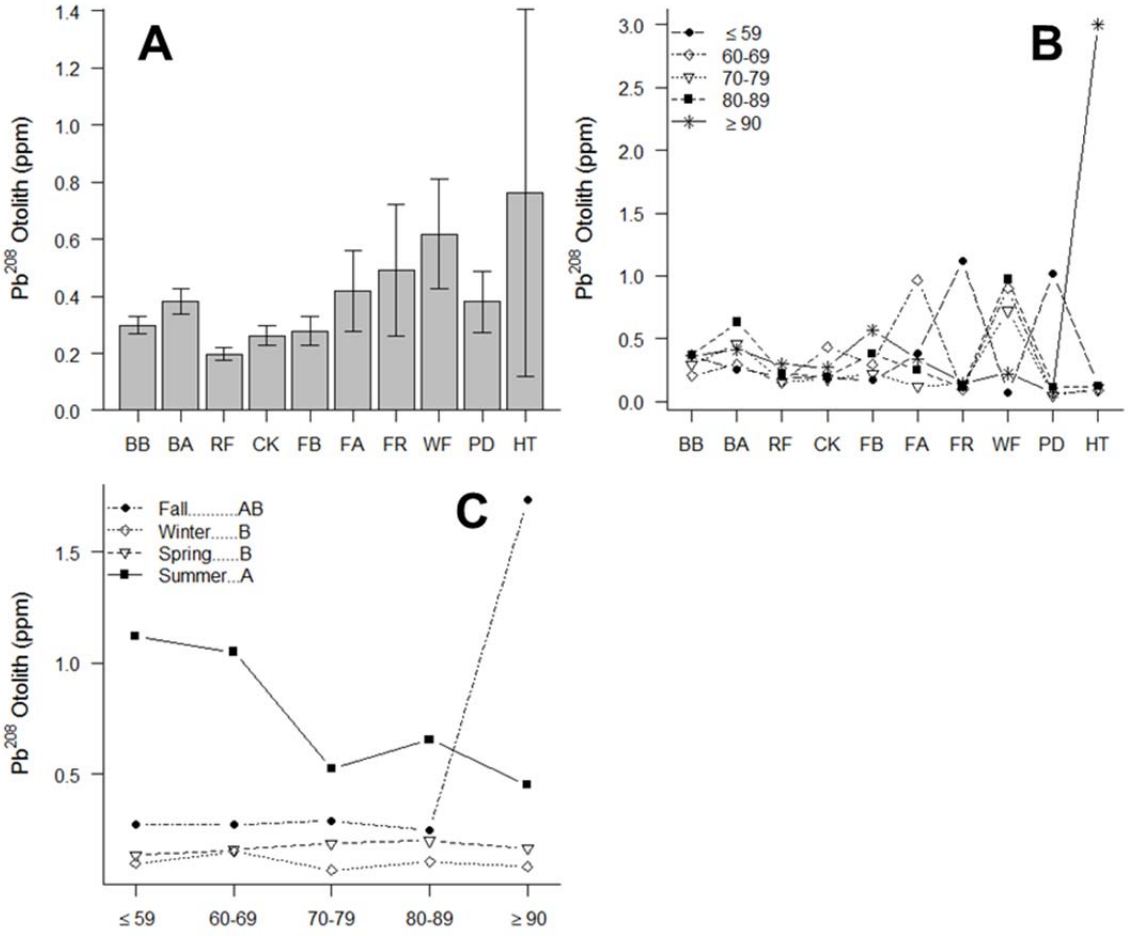
A
B
C
Pb208 Otolith (ppm)
BB BA RF CK FB FA FR WF PD HT
≤ 59
60-69
70-79
80-89
≥ 90
Fall.....AB
Winter.....B
Spring.....B
Summer...A

Figure 10

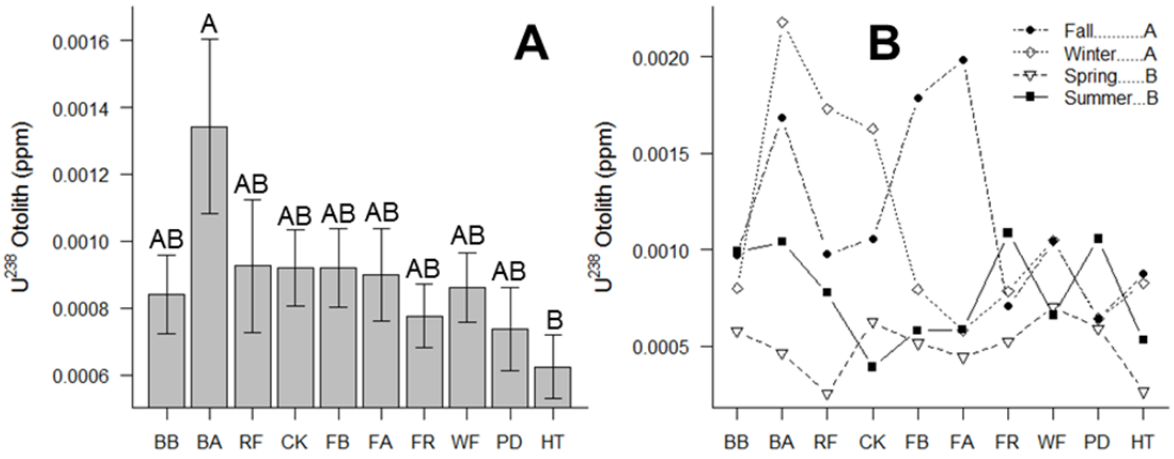
A
B
U^{238} Otolith (ppm)
0.0016
0.0014
0.0012
0.0010
0.0008
0.0006
0.0020
0.0015
0.0010
0.0005
AB
A
AB
AB
AB
AB
AB
AB
AB
B
BB
BA
RF
CK
FB
FA
FR
WF
PD
HT
Fall.....A
Winter.....A
Spring.....B
Summer...B

Figure 11

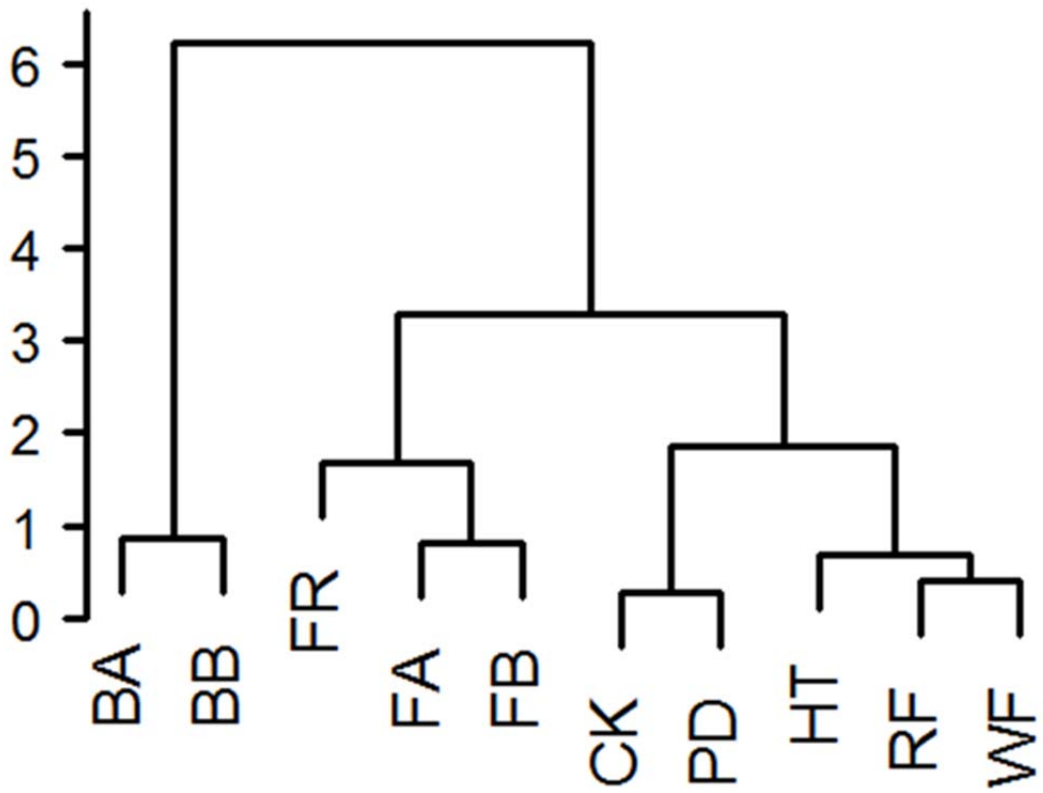

Figure 12

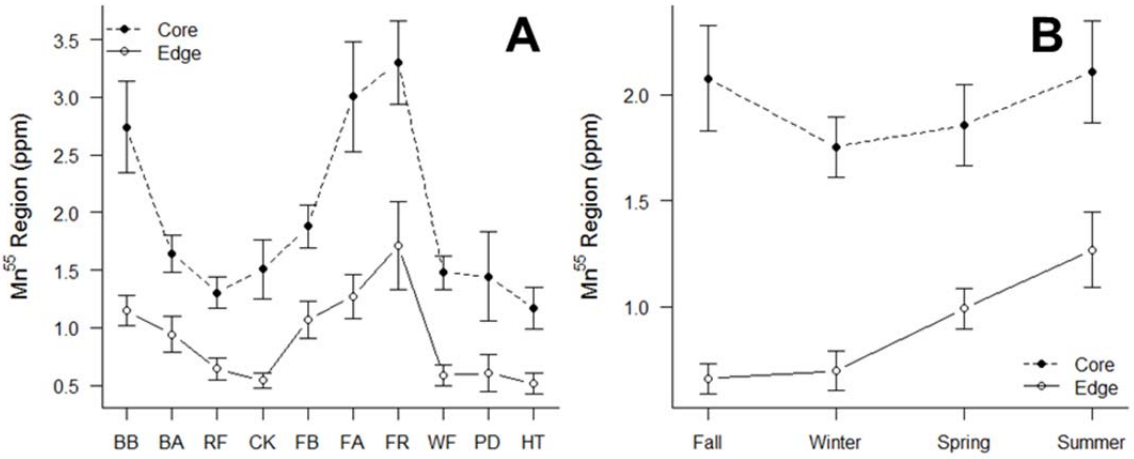
A
Core
Edge
Mn55 Region (ppm)
3.5
3.0
2.5
2.0
1.5
1.0
0.5
BB
BA
RF
CK
FB
FA
FR
WF
PD
HT
B
Mn55 Region (ppm)
2.0
1.5
1.0
Core
Edge
Fall
Winter
Spring
Summer

Figure 13

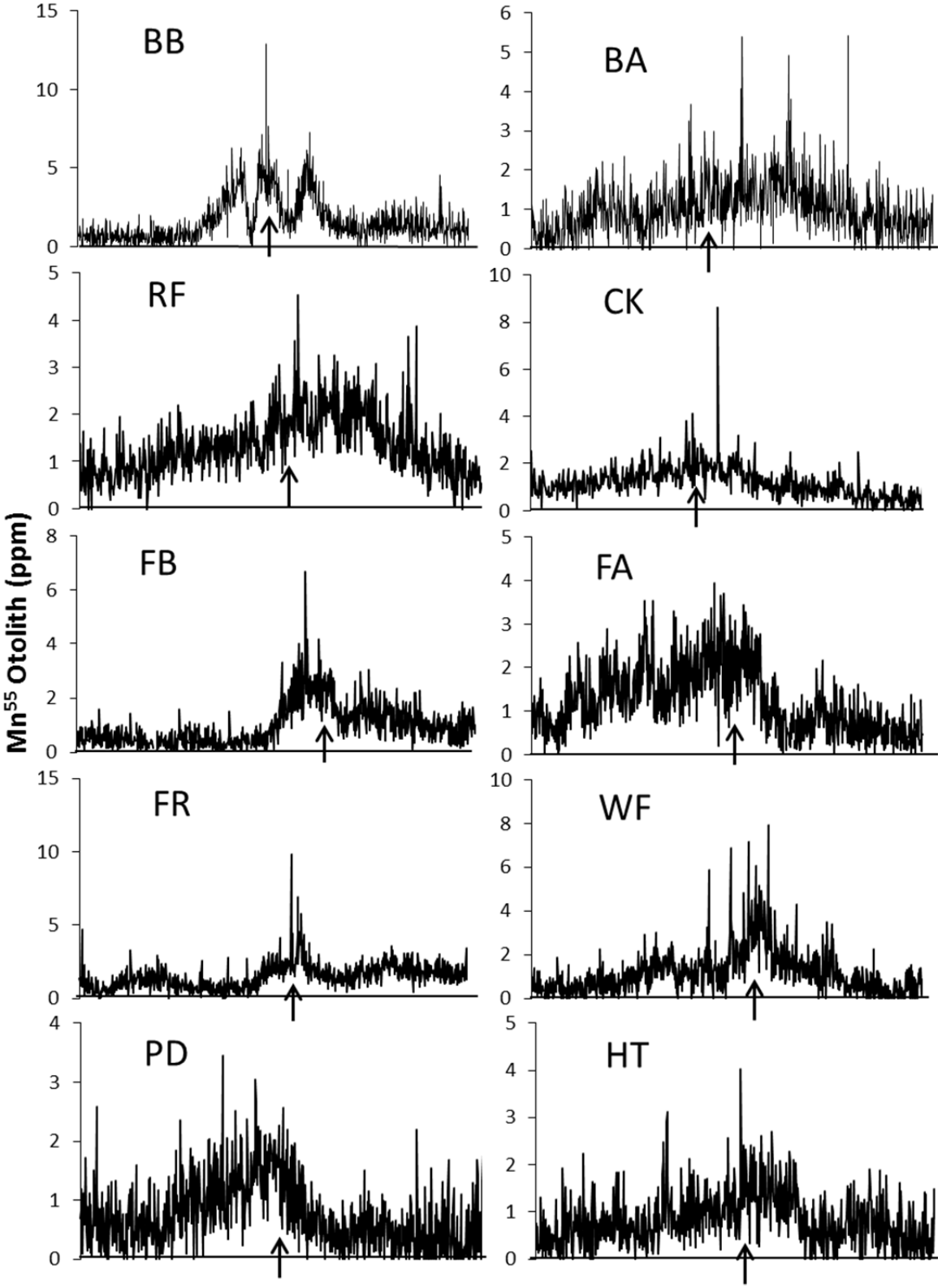

Figure 14

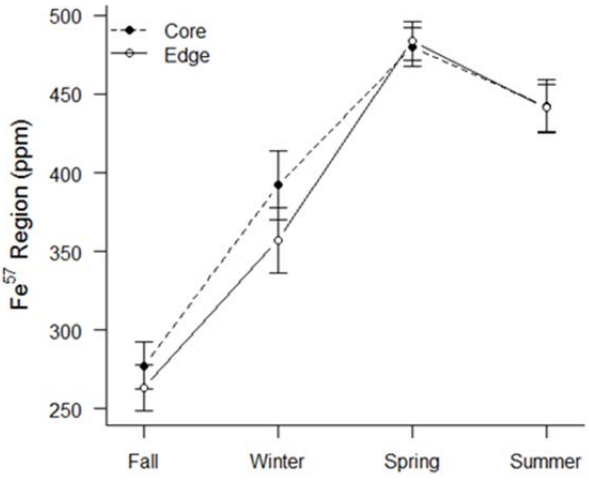
500
450
400
350
300
250
Core
Edge
Fe57 Region (ppm)
Fall
Winter
Spring
Summer

Figure 15

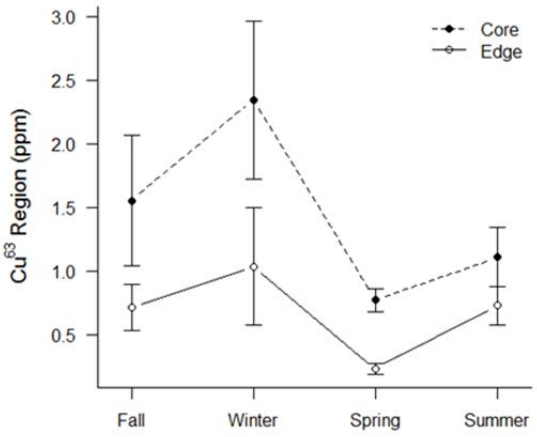
3.0
2.5
2.0
1.5
1.0
0.5
Cu63 Region (ppm)
Core
Edge
Fall
Winter
Spring
Summer

Figure 16

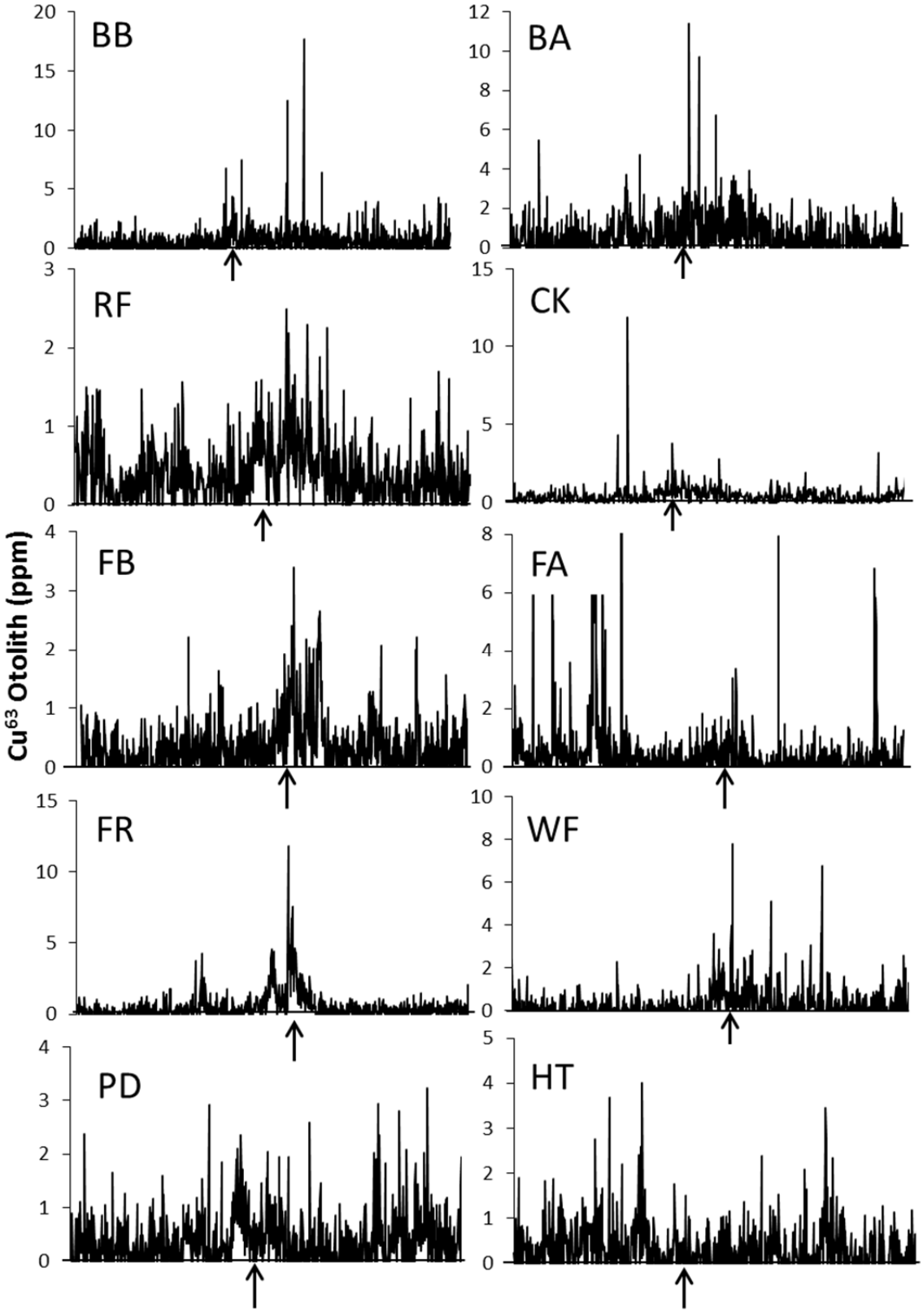

Figure 17

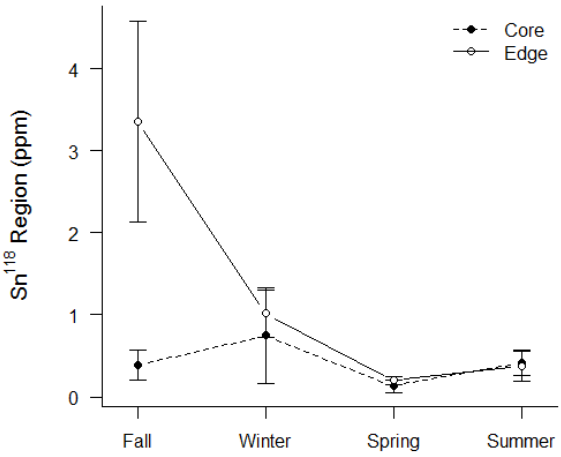

Figure 18

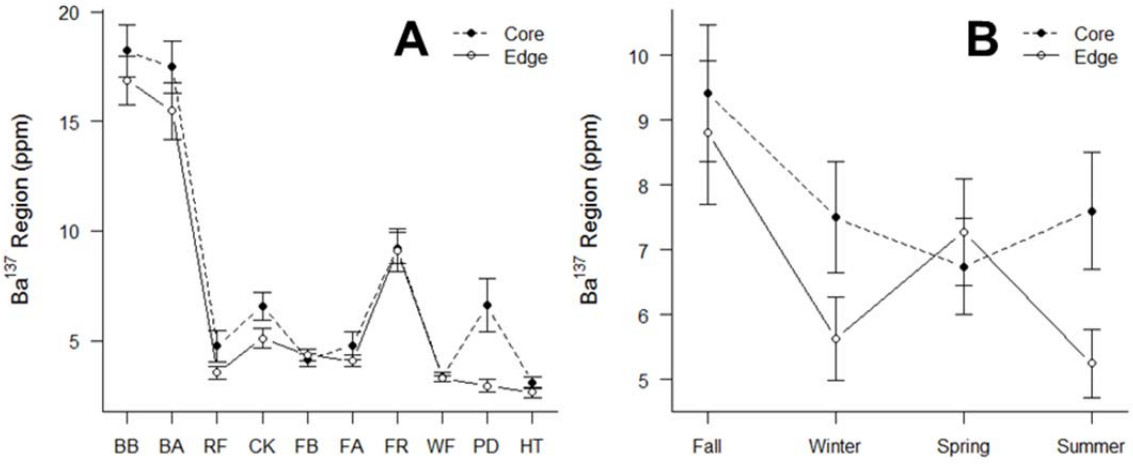
A
Core
Edge
Ba137 Region (ppm)
20
15
10
5
BB
BA
RF
CK
FB
FA
FR
WF
PD
HT
B
Core
Edge
Ba137 Region (ppm)
10
9
8
7
6
5
Fall
Winter
Spring
Summer

Figure 19

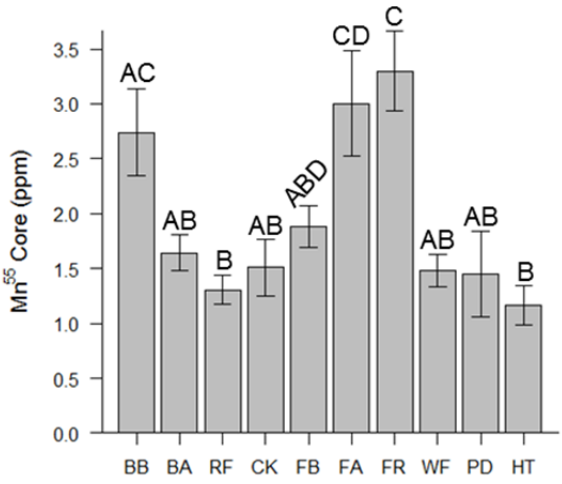
Mn55 Core (ppm)
3.5
3.0
2.5
2.0
1.5
1.0
0.5
0.0
AC
AB
B
AB
ABD
CD
C
AB
AB
B
BB
BA
RF
CK
FB
FA
FR
WF
PD
HT

Figure 20

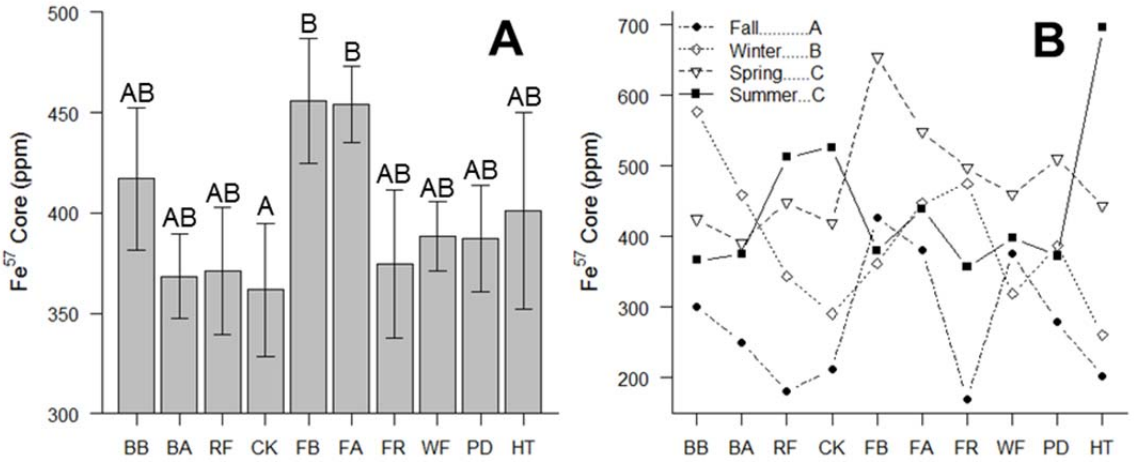
A
B
Fe57 Core (ppm)
500
450
400
350
300
AB
AB
AB
A
B
B
AB
AB
AB
BB
BA
RF
CK
FB
FA
FR
WF
PD
HT
700
600
500
400
300
200
Fall.....A
Winter.....B
Spring.....C
Summer...C

Figure 21

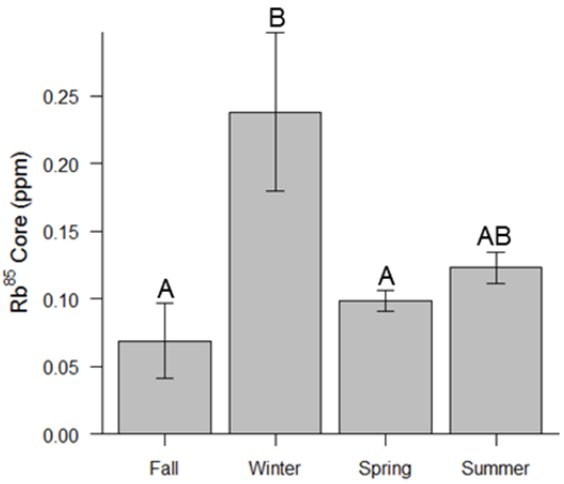
B
A
A
AB
0.25
0.20
0.15
0.10
0.05
0.00
Rb85 Core (ppm)
Fall
Winter
Spring
Summer

Figure 22

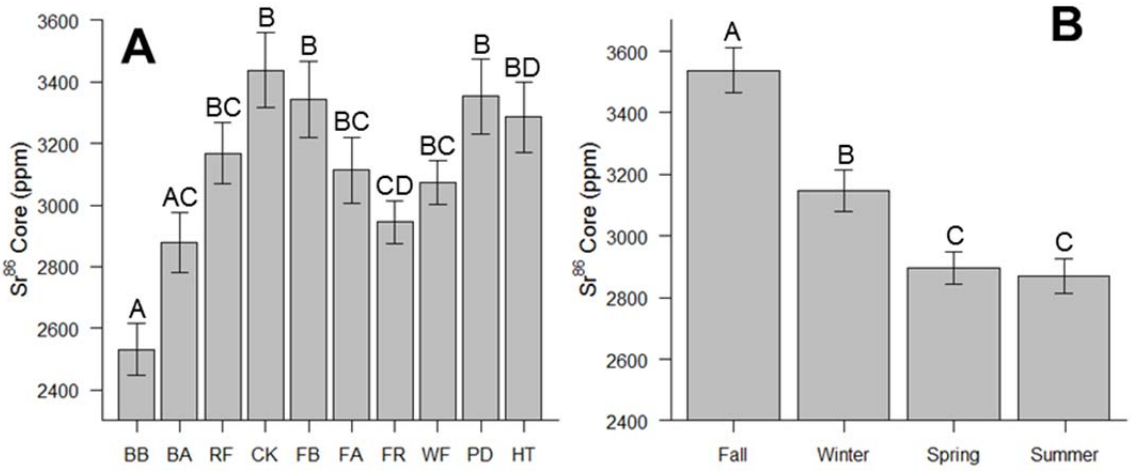
A
B
Sr^{86} Core (ppm)
3600
3400
3200
3000
2800
2600
2400
A
AC
BC
B
B
BC
CD
BC
B
BD
BB
BA
RF
CK
FB
FA
FR
WF
PD
HT
A
B
C
C
Fall
Winter
Spring
Summer

Figure 23

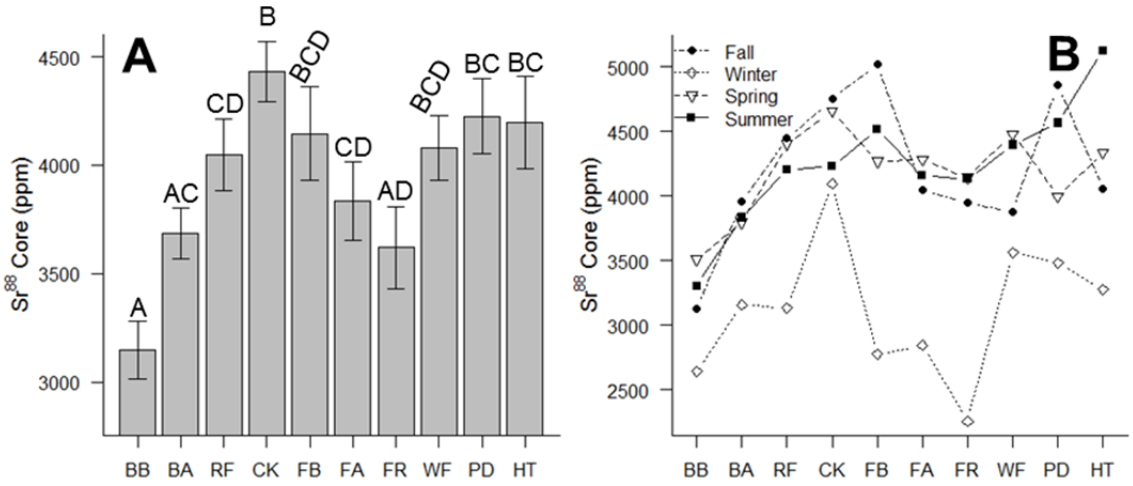
A
B
CD
BCD
CD
AD
BCD
BC
BC
A
AC
Sr^{88} Core (ppm)
4500
4000
3500
3000
BB
BA
RF
CK
FB
FA
FR
WF
PD
HT
B
Fall
Winter
Spring
Summer
5000
4500
4000
3500
3000
2500

Figure 24

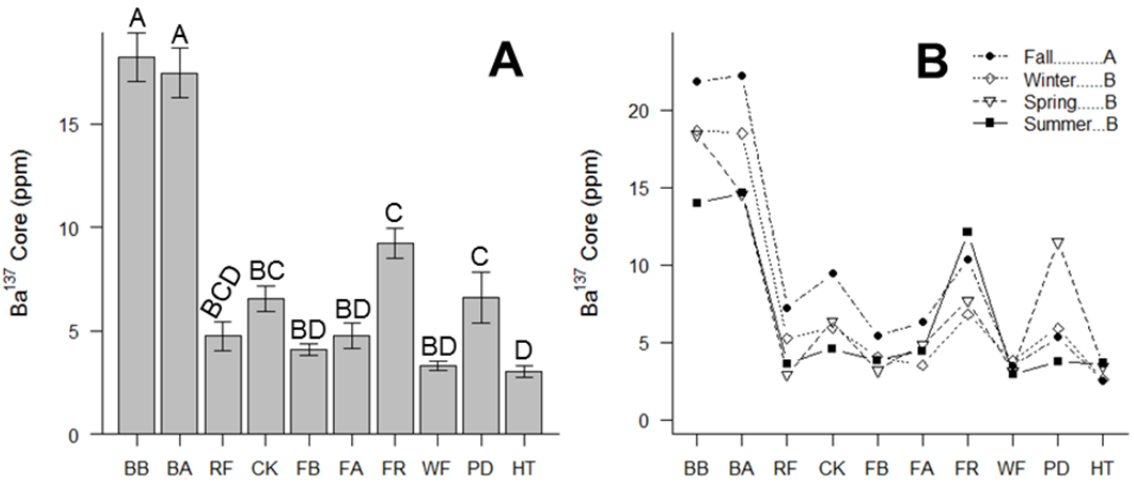
A
B
Ba137 Core (ppm)
A
A
BCD
BC
BD
BD
C
BD
C
D
BB BA RF CK FB FA FR WF PD HT
Fall.....A
Winter.....B
Spring.....B
Summer...B

Figure 25

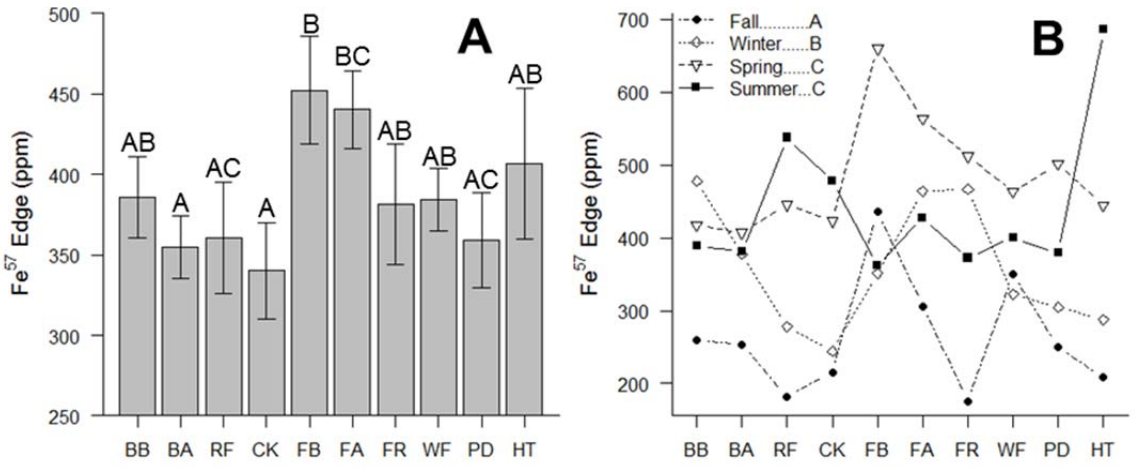
A
B
Fe57 Edge (ppm)
500
450
400
350
300
250
AB
A
AC
A
B
BC
AB
AB
AC
AB
BB
BA
RF
CK
FB
FA
FR
WF
PD
HT
700
600
500
400
300
200
Fall.....A
Winter.....B
Spring.....C
Summer...C

Figure 26

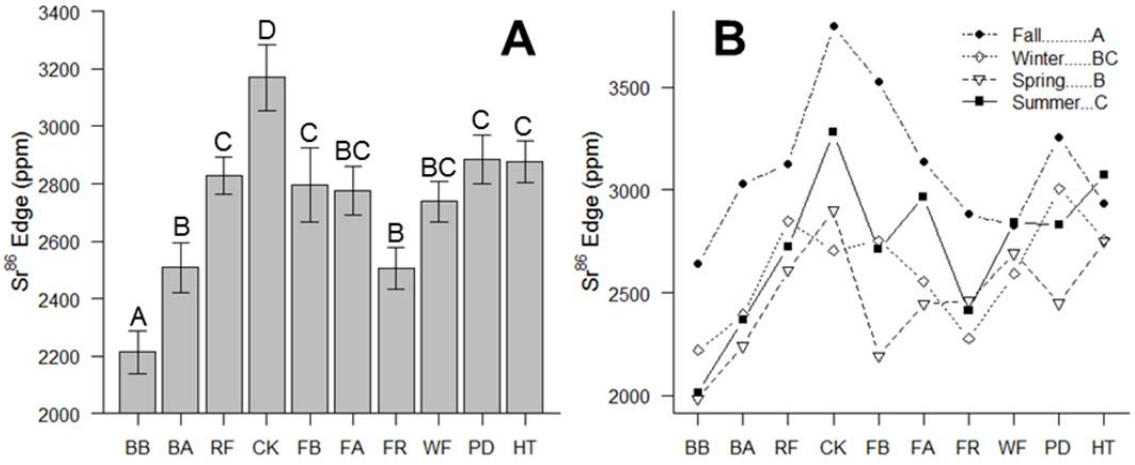
A
B
Sr^{86} Edge (ppm)
3400
3200
3000
2800
2600
2400
2200
2000
3500
2500
A
B
C
D
C
BC
B
BC
C
C
BB
BA
RF
CK
FB
FA
FR
WF
PD
HT
Fall.....A
Winter.....BC
Spring.....B
Summer...C

Figure 27

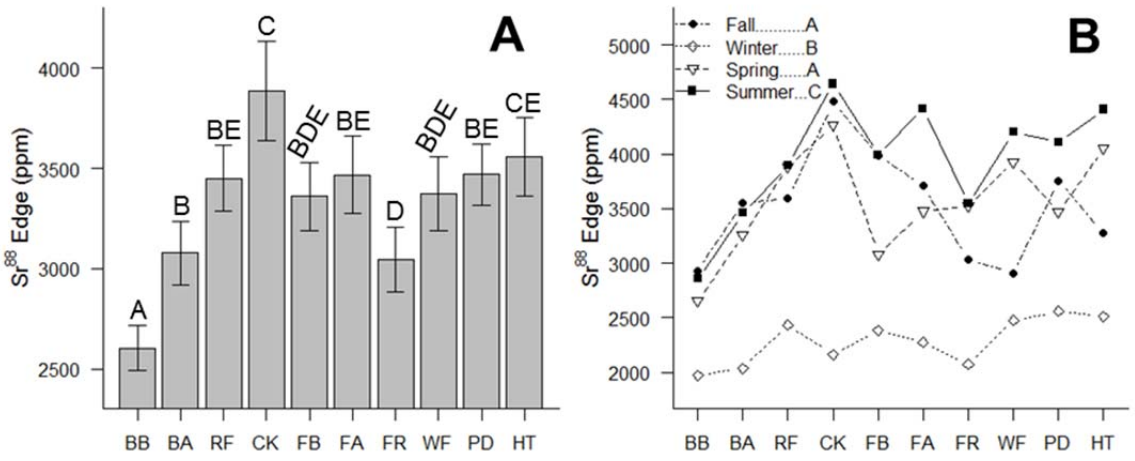
A
B
BE
C
BDE
BE
D
BDE
BE
CE
Sr^{88} Edge (ppm)
2500
3000
3500
4000
BB BA RF CK FB FA FR WF PD HT
B
Fall.....A
Winter.....B
Spring.....A
Summer...C
2000
2500
3000
3500
4000
4500
5000
Sr^{88} Edge (ppm)
BB BA RF CK FB FA FR WF PD HT

Figure 28

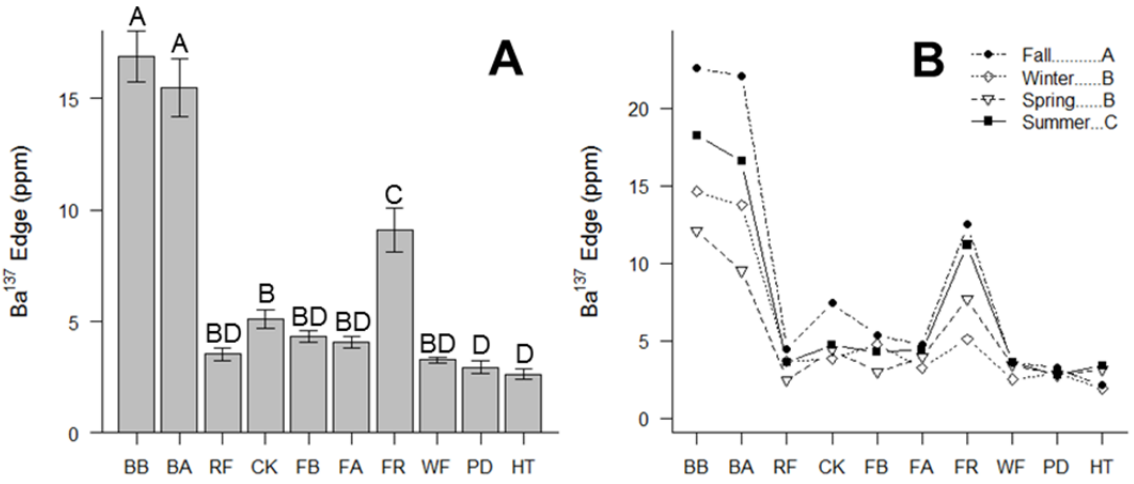
A
A
BD
B
BD
BD
C
BD
D
D
A
Ba137 Edge (ppm)
0
5
10
15
BB
BA
RF
CK
FB
FA
FR
WF
PD
HT
B
Fall.....A
Winter.....B
Spring.....B
Summer...C
Ba137 Edge (ppm)
0
5
10
15
20
BB
BA
RF
CK
FB
FA
FR
WF
PD
HT

Figure 29

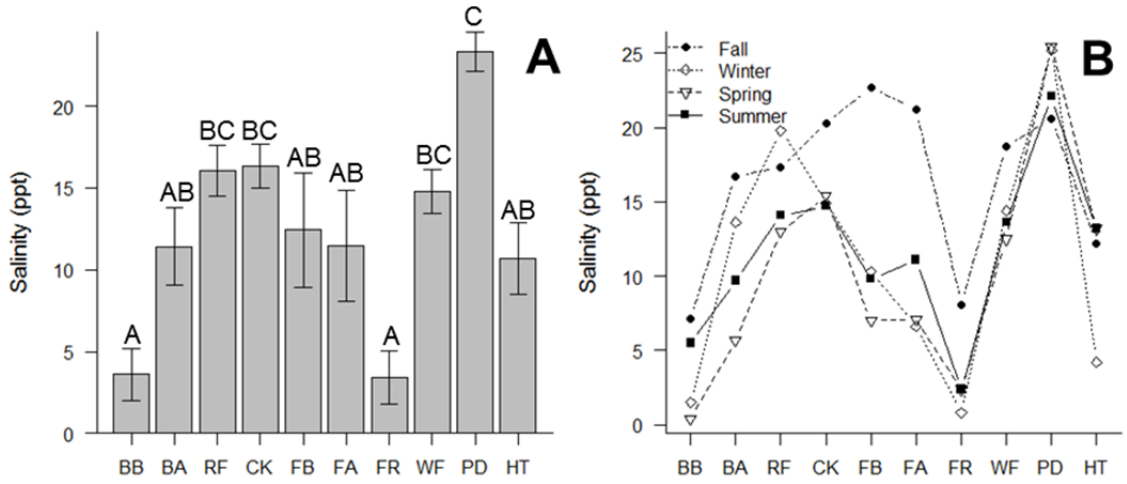
A
Salinity (ppt)
0
5
10
15
20
A
AB
BC BC
AB
AB
A
BC
C
AB
BB BA RF CK FB FA FR WF PD HT
B
Salinity (ppt)
0
5
10
15
20
25
Fall
Winter
Spring
Summer
BB BA RF CK FB FA FR WF PD HT

Figure 30

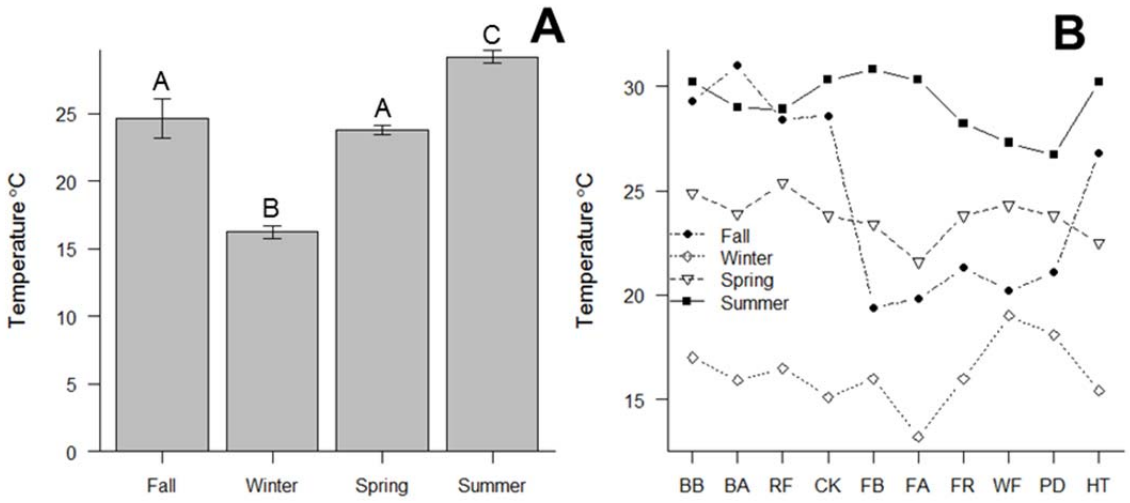
A
C
A
B
Temperature °C
0
5
10
15
20
25
Fall
Winter
Spring
Summer
B
Temperature °C
15
20
25
30
Fall
Winter
Spring
Summer
BB
BA
RF
CK
FB
FA
FR
WF
PD
HT

Figure 31

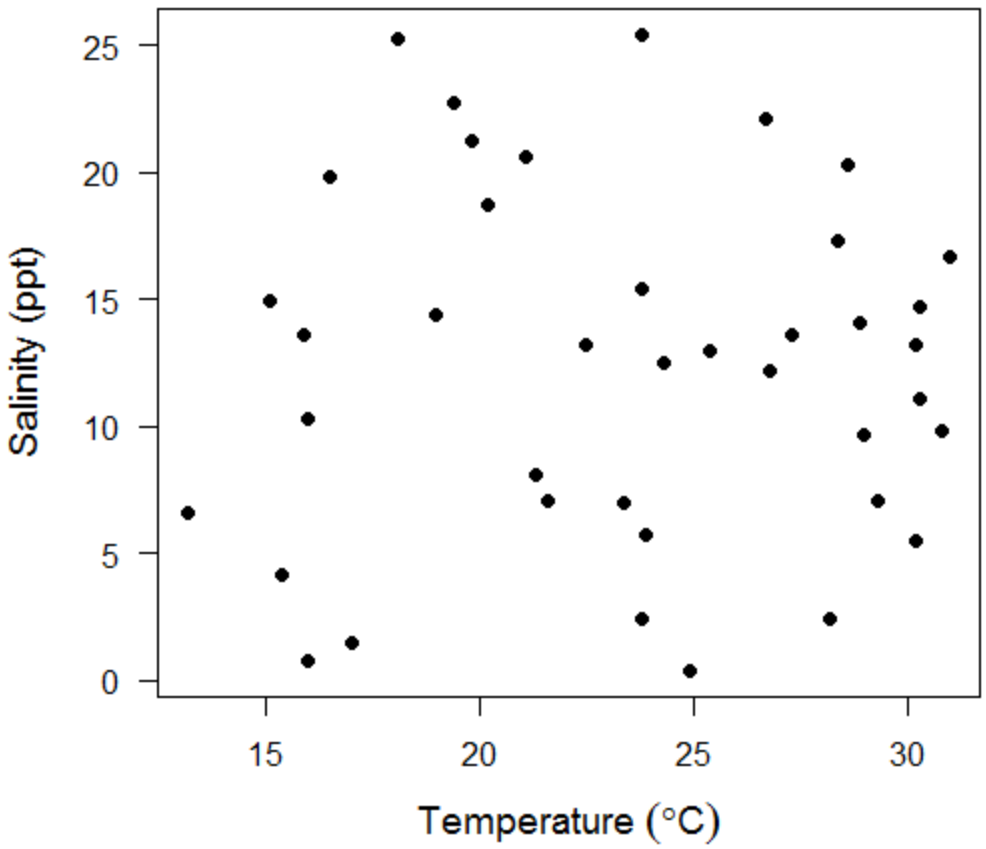

Figure 32

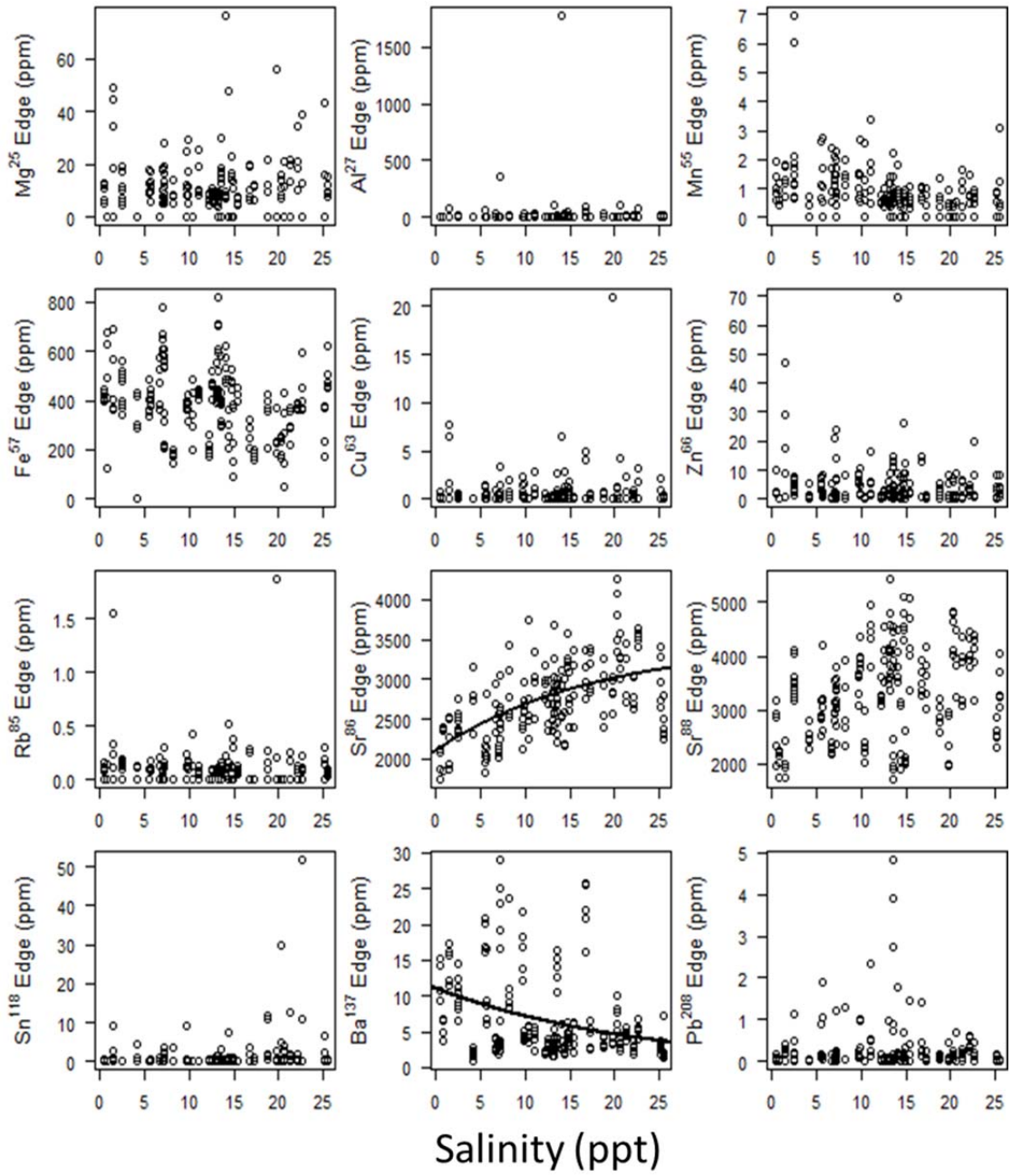
Mg25 Edge (ppm)
Al27 Edge (ppm)
Mn55 Edge (ppm)
Fe57 Edge (ppm)
Cu63 Edge (ppm)
Zn66 Edge (ppm)
Rb85 Edge (ppm)
Sr86 Edge (ppm)
Sr88 Edge (ppm)
Sn118 Edge (ppm)
Ba137 Edge (ppm)
Pb208 Edge (ppm)
Salinity (ppt)

Figure 33

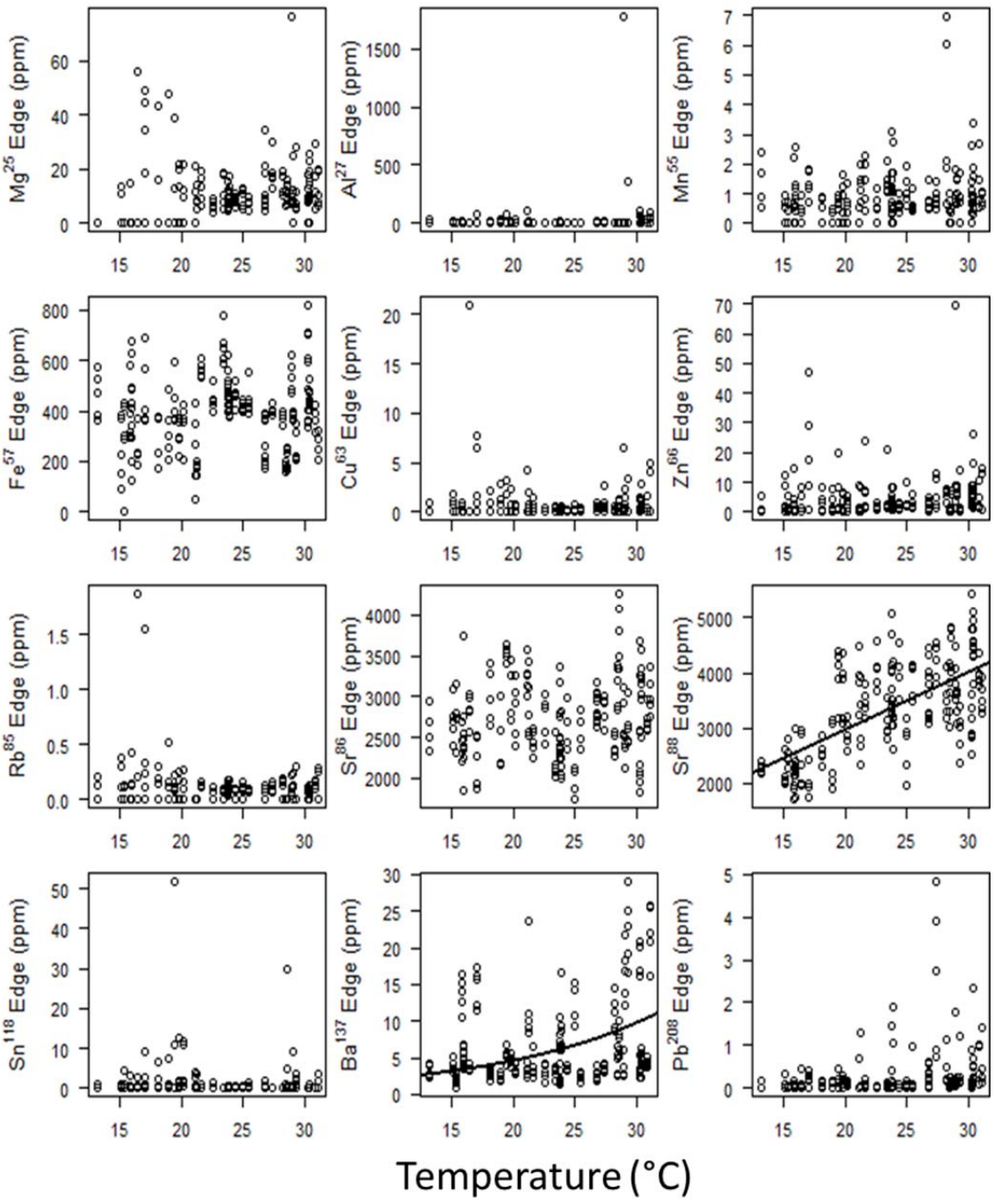
Mg25 Edge (ppm)
Al27 Edge (ppm)
Mn55 Edge (ppm)
Fe57 Edge (ppm)
Cu63 Edge (ppm)
Zn66 Edge (ppm)
Rb85 Edge (ppm)
Sr86 Edge (ppm)
Sr88 Edge (ppm)
Sn118 Edge (ppm)
Ba137 Edge (ppm)
Pb208 Edge (ppm)
Temperature (°C)

Figure 34

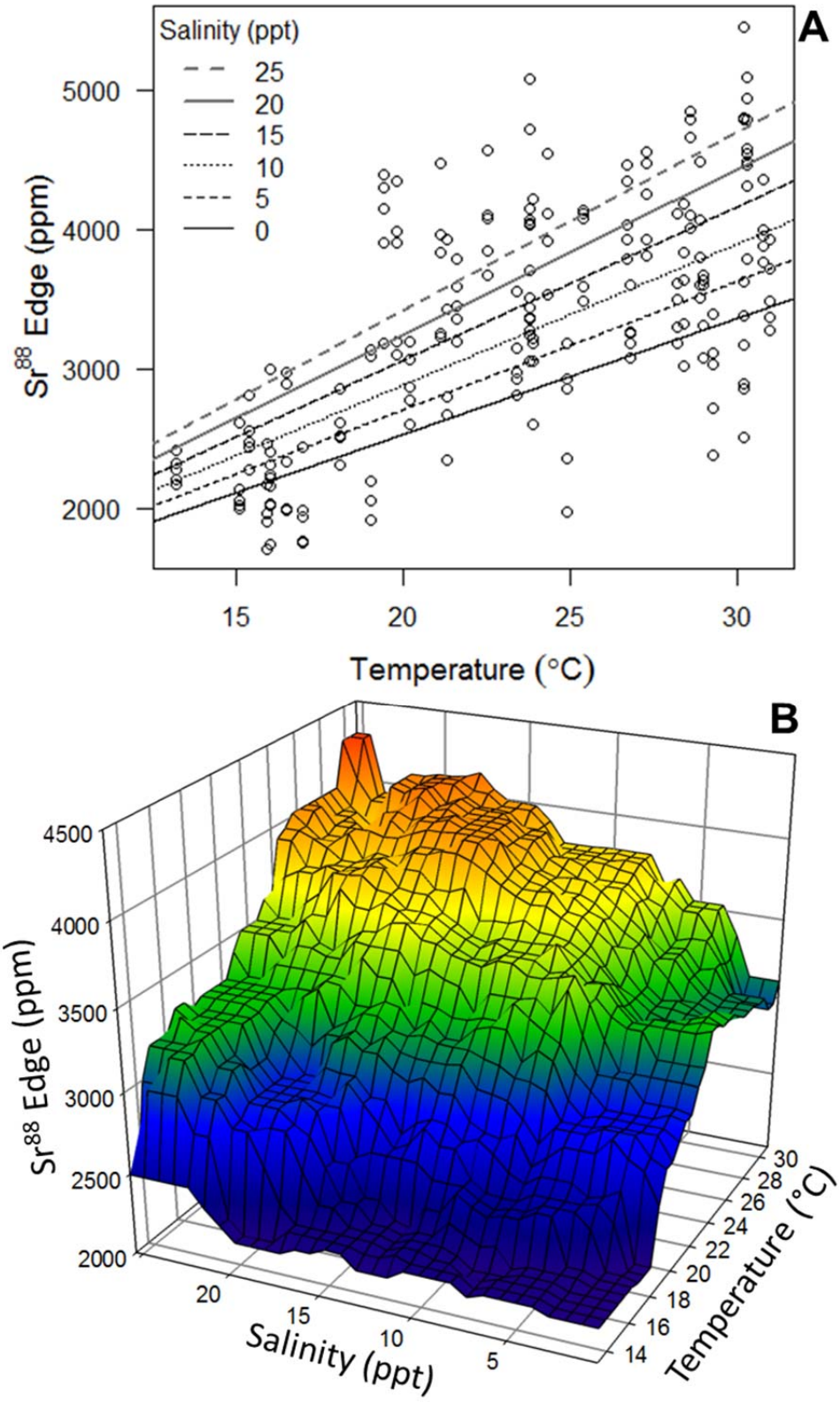
A
Salinity (ppt)
25
20
15
10
5
0
5000
4000
3000
2000
Sr88 Edge (ppm)
15
20
25
30
Temperature (°C)
B
4500
4000
3500
3000
2500
2000
Sr88 Edge (ppm)
20
15
10
5
Salinity (ppt)
30
28
26
24
22
20
18
16
14
Temperature (°C)

Figure 35

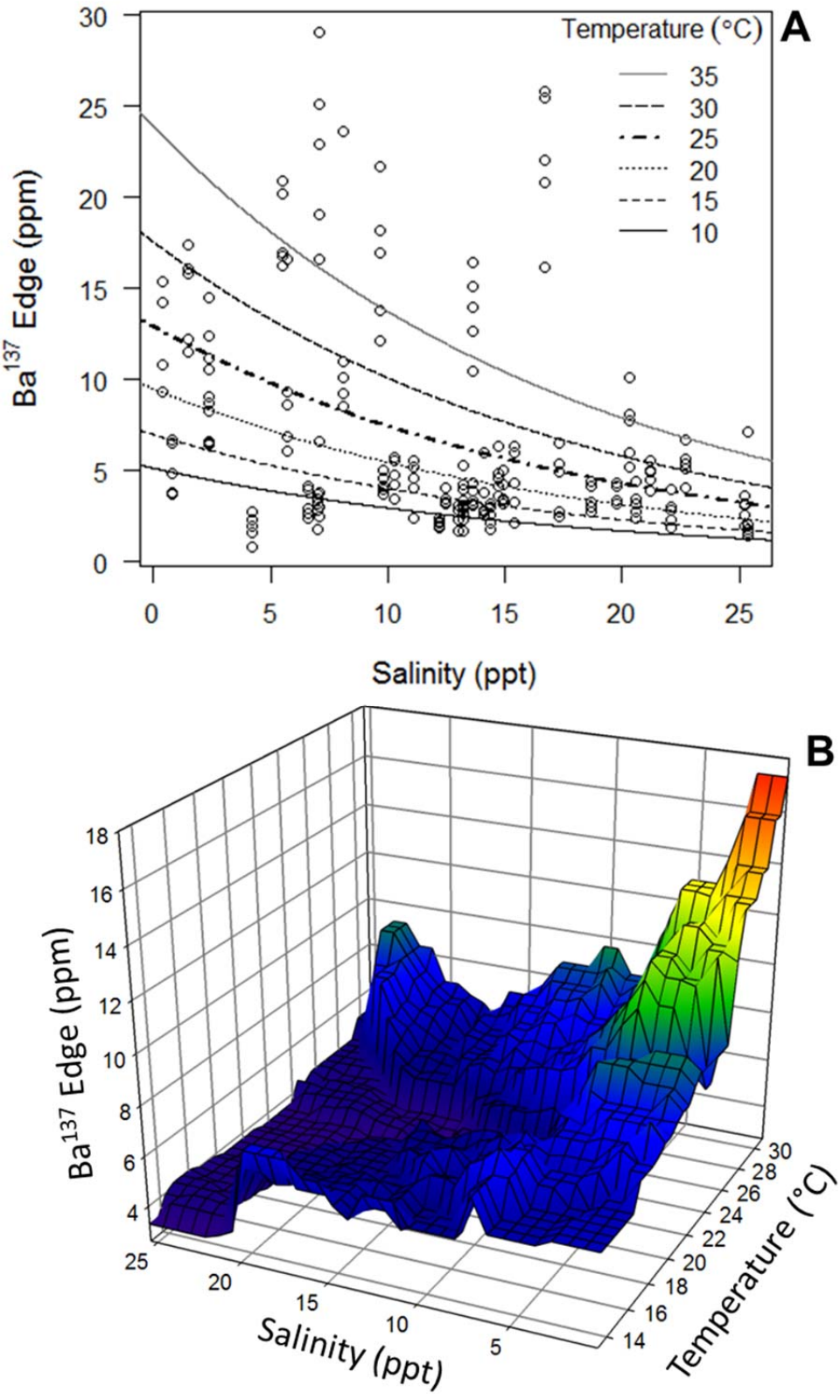
A
Temperature (°C)
35
30
25
20
15
10
Ba137 Edge (ppm)
Salinity (ppt)
B
Ba137 Edge (ppm)
Salinity (ppt)
Temperature (°C)

Figure 36

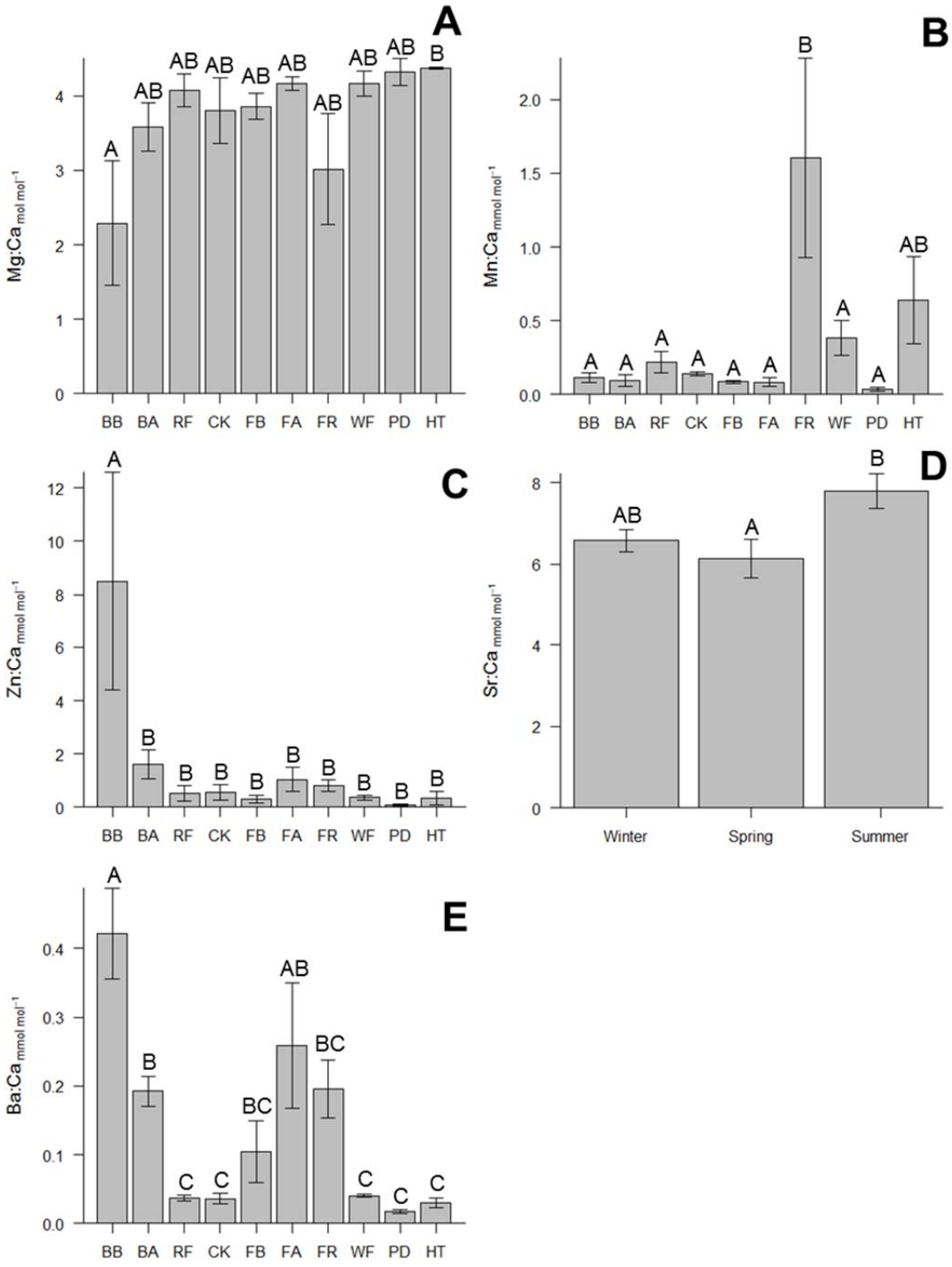
A
Mg:Ca mol mol⁻¹
A AB AB AB AB AB AB AB AB B
BB BA RF CK FB FA FR WF PD HT
B
Mn:Ca mmol mol⁻¹
A A A A A A B A A AB
BB BA RF CK FB FA FR WF PD HT
C
Zn:Ca mmol mol⁻¹
A B B B B B B B B B
BB BA RF CK FB FA FR WF PD HT
D
Sr:Ca mmol mol⁻¹
AB A B
Winter Spring Summer
E
Ba:Ca mmol mol⁻¹
A B C C BC AB BC C C C
BB BA RF CK FB FA FR WF PD HT

Figure 37

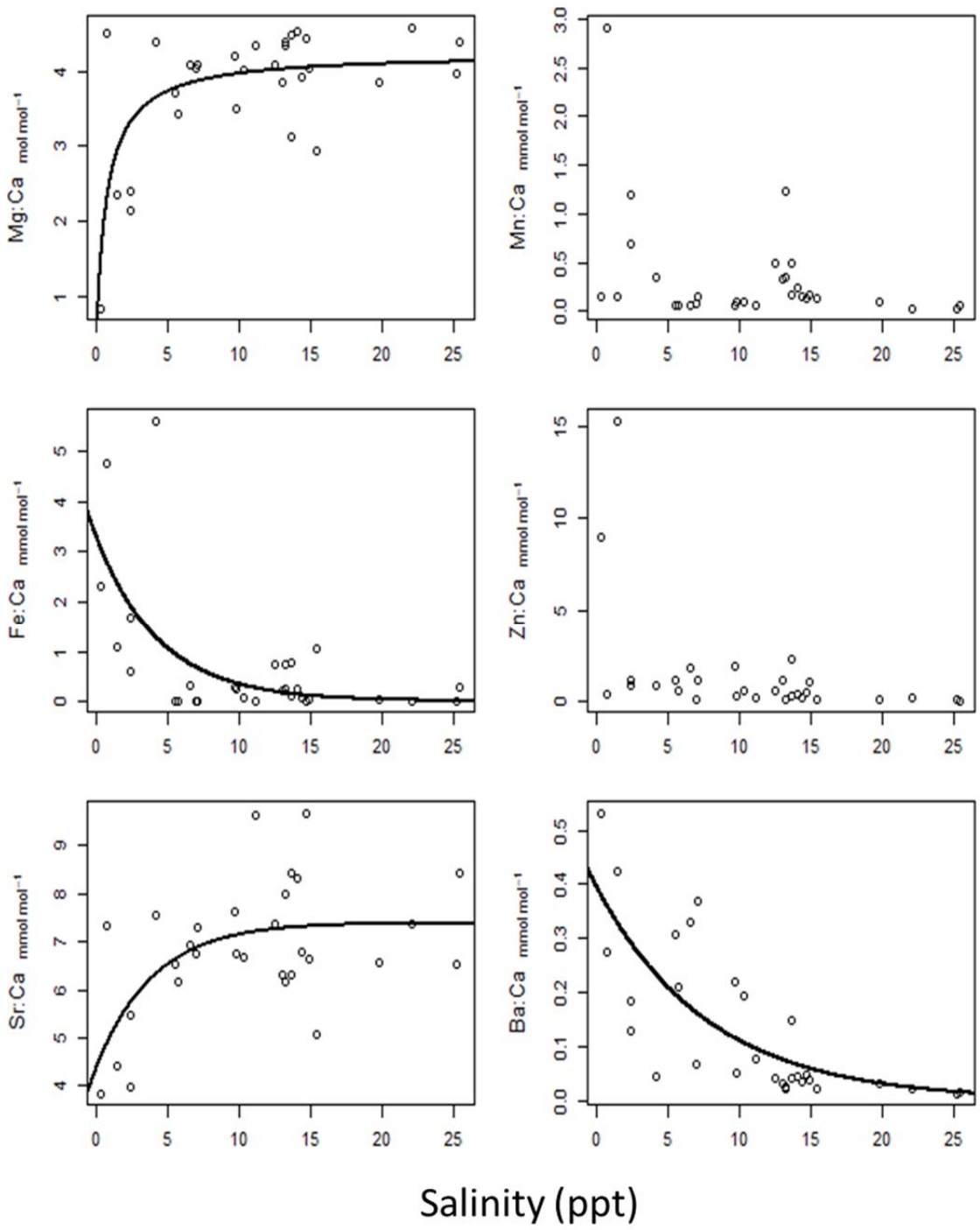
Mg:Ca mol mol⁻¹
Mn:Ca mmol mol⁻¹
Fe:Ca mmol mol⁻¹
Zn:Ca mmol mol⁻¹
Sr:Ca mmol mol⁻¹
Ba:Ca mmol mol⁻¹
Salinity (ppt)

Figure 38

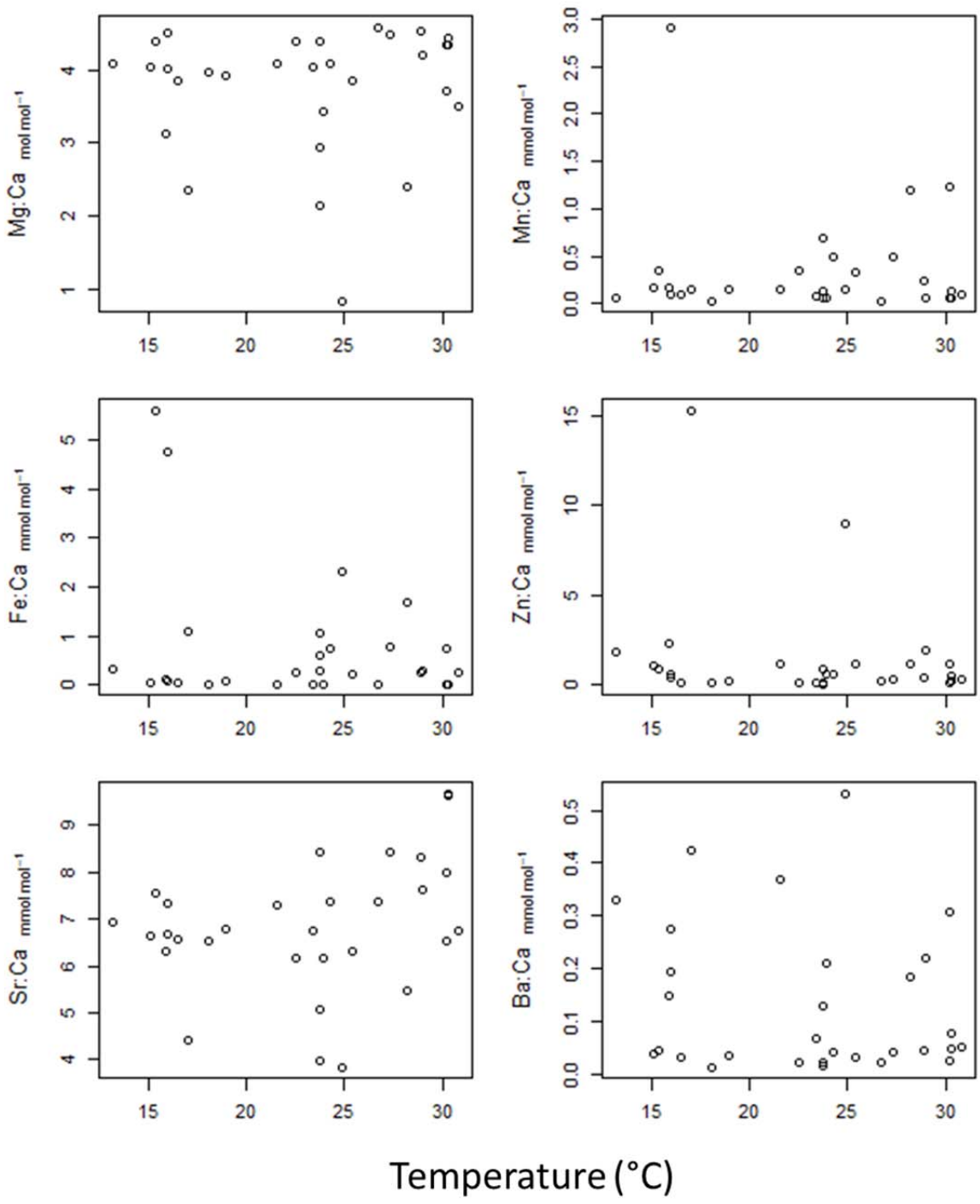
Mg:Ca mol mol⁻¹
Mn:Ca mmol mol⁻¹
Fe:Ca mmol mol⁻¹
Zn:Ca mmol mol⁻¹
Sr:Ca mmol mol⁻¹
Ba:Ca mmol mol⁻¹
Temperature (°C)

Figure 39

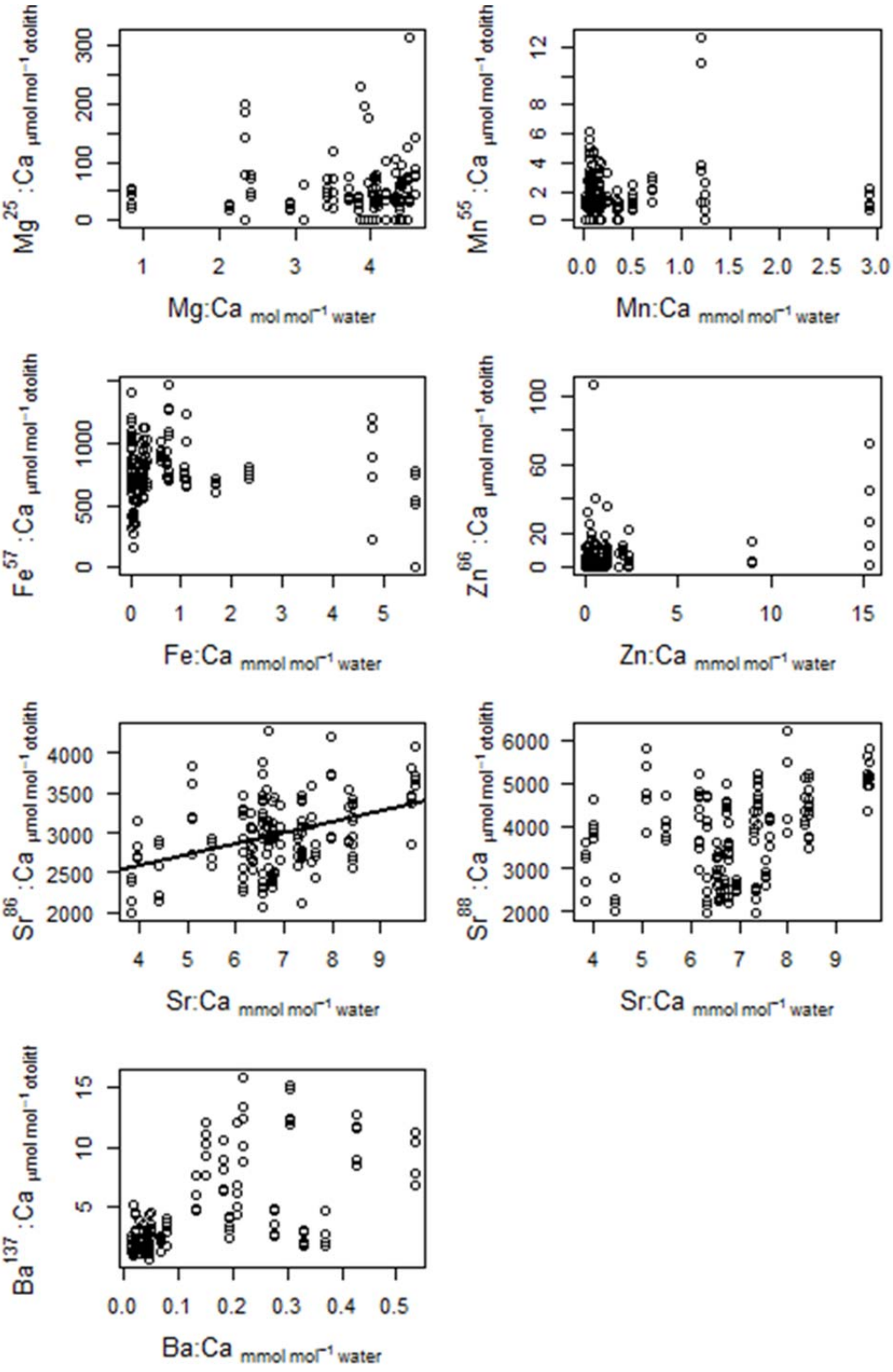
Mg25:Ca µmol mol−1 otolith
Mg:Ca mol mol−1 water
Mn55:Ca µmol mol−1 otolith
Mn:Ca mmol mol−1 water
Fe57:Ca µmol mol−1 otolith
Fe:Ca mmol mol−1 water
Zn66:Ca µmol mol−1 otolith
Zn:Ca mmol mol−1 water
Sr86:Ca µmol mol−1 otolith
Sr:Ca mmol mol−1 water
Sr88:Ca µmol mol−1 otolith
Sr:Ca mmol mol−1 water
Ba137:Ca µmol mol−1 otolitt
Ba:Ca mmol mol−1 water

Figure 40

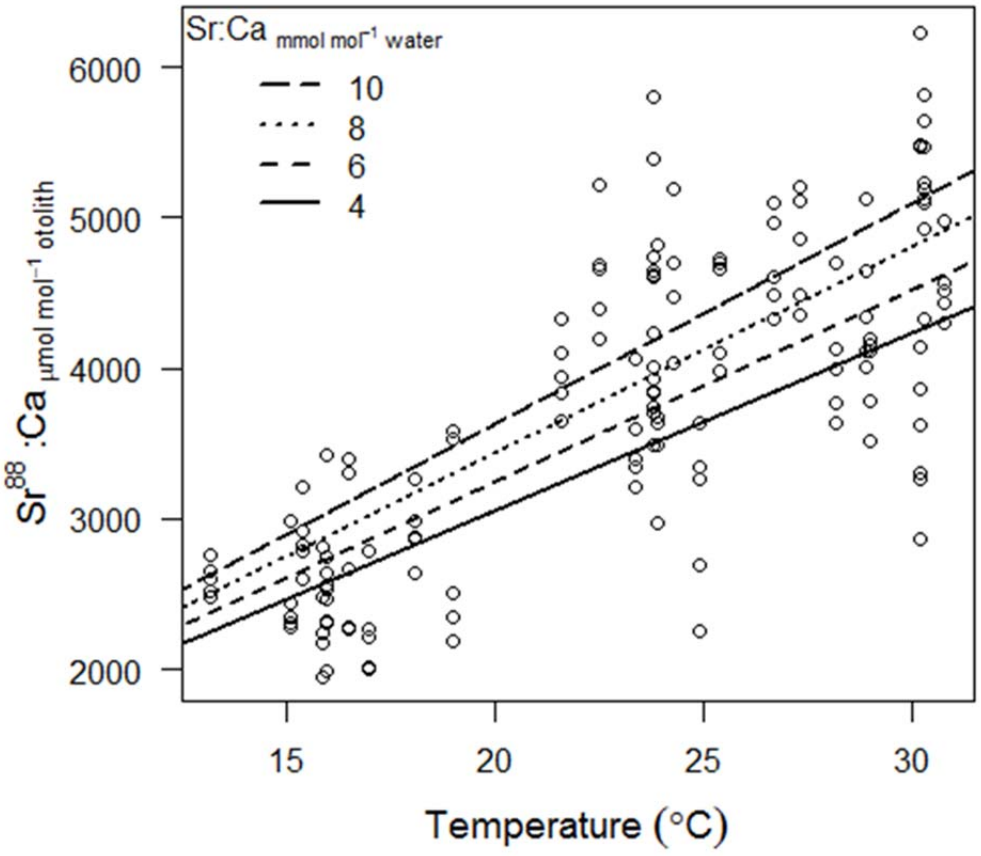
Sr:Ca mmol mol-1 water
10
8
6
4
6000
5000
4000
3000
2000
Sr88:Ca µmol mol-1 otolith
15
20
25
30
Temperature (°C)

Figure 41

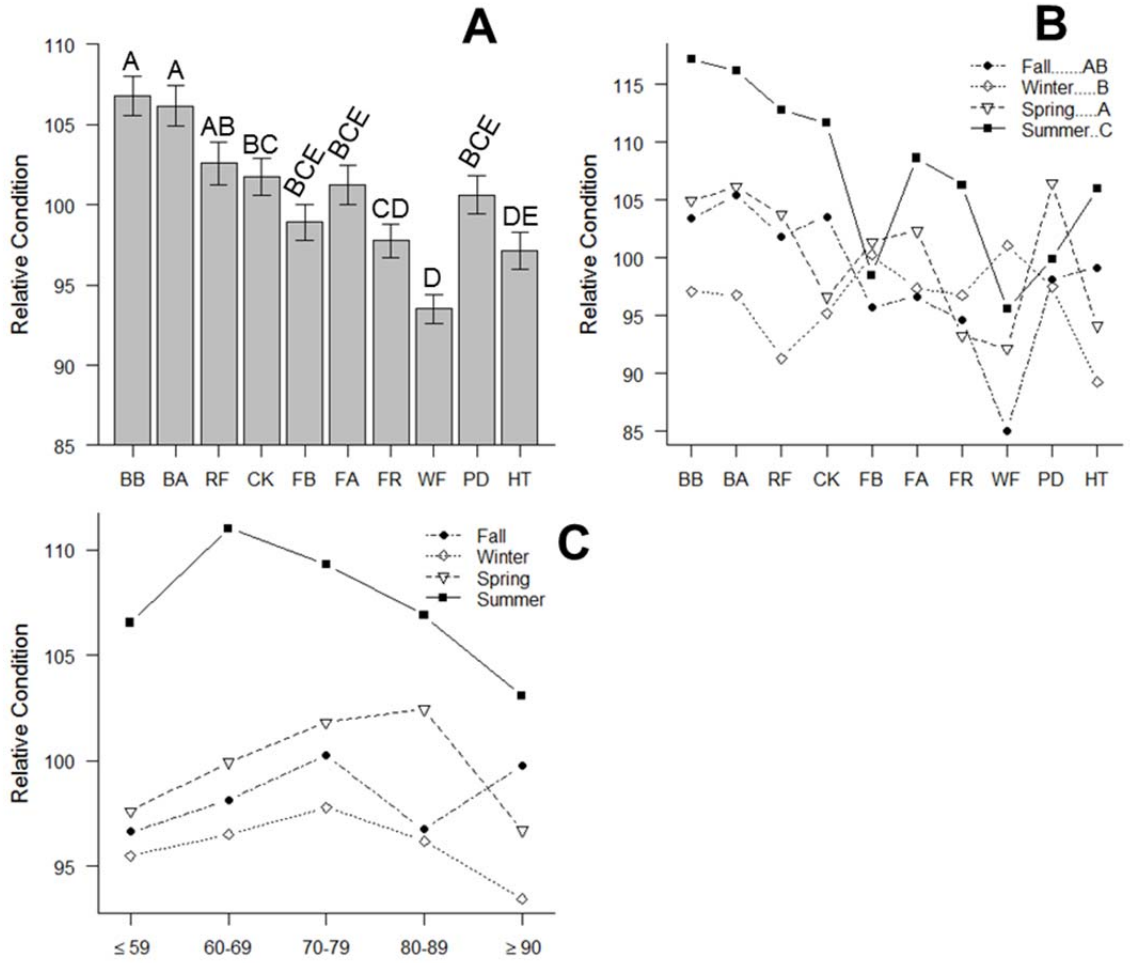
A
Relative Condition
110
105
100
95
90
85
A
A
AB
BC
BCE
BCE
CD
D
BCE
DE
BB BA RF CK FB FA FR WF PD HT
B
Relative Condition
115
110
105
100
95
90
85
Fall.....AB
Winter.....B
Spring.....A
Summer..C
BB BA RF CK FB FA FR WF PD HT
C
Relative Condition
110
105
100
95
Fall
Winter
Spring
Summer
≤ 59
60-69
70-79
80-89
≥ 90

Figure 42